OBSERVATION AND SIMULATION OF ATMOSPHERIC CARBON DIOXIDE IN VANCOUVER

By

Kenneth Howard Reid

B. Sc. (Atmospheric Sciences) University of British Columbia, 1990

A THESIS SUBMITTED IN PARTIAL FULFILLMENT OF

THE REQUIREMENTS FOR THE DEGREE OF

MASTER OF SCIENCE

in

THE FACULTY OF GRADUATE STUDIES

ATMOSPHERIC SCIENCE

We accept this thesis as conforming

to the required standard

THE UNIVERSITY OF BRITISH COLUMBIA

AUGUST 1995

In presenting this thesis in partial fulfilment of the requirements for an advanced degree at the University of British Columbia, I agree that the Library shall make it freely available for reference and study. I further agree that permission for extensive copying of this thesis for scholarly purposes may be granted by the head of my department or by his or her representatives. It is understood that copying or publication of this thesis for financial gain shall not be allowed without my written permission.

Atmospheric Science

The University of British Columbia

2075 Wesbrook Place

Vancouver, Canada

V6T 1W5

Date:

AUGUST 31, 1995

Abstract

Climate change expected from increasing atmospheric CO_2 concentrations has been studied widely (IPCC, 1990). Further, it is recognized that cities are a major source of anthropogenic CO_2. However, few studies of CO_2 concentrations in, or near, cities have been conducted. A LI-COR infrared gas analyzer was operated at the Sunset Tower in a suburban region of Vancouver during different time periods in 1993 and 1994. Sampling revealed important information on seasonal and diurnal variations. The observed summertime concentrations show a clear diurnal signal around the expected upwind background concentration, and are described by a late afternoon minimum, and overnight maximum. The afternoon CO_2 minimum is attributed to the strength of biospheric photosynthesis and strong mixing of local anthropogenic sources within a large mixed layer. Poor nighttime mixing, lower mixed depths, and biospheric respiration account for the observed nighttime maximum, often more than 80 ppmv greater than the background concentration.

A simple numerical multiple-box transport model was developed to simulate the observed diurnal pattern of CO_2 concentration at the suburban site. CO_2 emissions inventories for important mobile sources, stationary sources, and biospheric sources and sinks are calculated as input to the model for upwind fetch areas. Other CO_2 inputs include advection, entrainment from above the mixed layer and determination of the mixed layer depth.

Results of both observations and modelling show large diurnal variation in CO_2 concentrations, and the importance of boundary layer structure (as defined by the mixed layer) on concentrations at a specific location. In terms of CO_2, the role of the city is placed in it global context.

Table of Contents

List of Tables

List of Figures

viii

Acknowledgement

Chapter 1

Introduction

1.1 Carbon Dioxide

Carbon dioxide (CO_2) is recognized to be the most significant contributor to possible anthropogenically induced global climate change scenarios (Houghton *et al.*, 1990). Atmospheric concentrations of CO_2 have been studied extensively over long time periods, to quantify the amount of CO_2 storage in the atmosphere, and rates of change (Bolin, 1986, Houghton *et al.*, 1990, and Boden *et al.*, 1991). Changes in atmospheric CO_2 concentrations are linked to the global biogeochemical cycling of carbon, including pathways to the terrestrial biosphere and the oceans (Appendix A). Globally averaged concentrations of atmospheric CO_2 were 355 ppmv in 1992 (Houghton *et al.*, 1992), and observed to be increasing approximately 1.5 ppmv annually (Conway *et al.*, 1991). Global circulation model results indicate 1.5-4.5°C warming due to a doubling of CO_2 concentrations, and a 1°C global warming by 2030 if CO_2 emissions continue to increase at present growth rates (Houghton *et al.*, 1990).

The lifetime of CO_2 in the atmosphere is estimated to be 50-200 years (Houghton *et al.*, 1990), which ensures that it is well-mixed within the troposphere. However, some gradients exist due to the distribution of surface sources and sinks. The global CO_2 monitoring network (Boden *et al.*, 1991) shows an increase in CO_2 concentrations poleward of the equator in the Northern Hemisphere (Komhyr *et al.*, 1985). Further, influences

1

of surface sources and sinks set up a vertical gradient of CO_2 such that concentrations increase with height in summer, and decrease with height in winter, depending on the seasonal net flux of CO_2 from the surface biosphere (Tanaka *et al.*, 1985).

Temporal variability of local CO_2 concentrations, superimposed on the secular annual increase, are observed primarily at seasonal and diurnal timescales. The role of the biosphere acts to reduce CO_2 concentrations during summertime, and to increase them in winter, due to the cycle of plant growth and net photosynthesis (Keeling *et al.*, 1976; Bolin, 1986). The amplitude of this variability decreases with height up to the tropopause (Tanaka *et al.*, 1983). Also apparent, although more irregular, is synoptic and local scale meteorological variability that affect both the mixing of CO_2 from local sources and sinks, and the trajectories of air parcels over terrain of varying CO_2 source and sink strengths (Halter and Peterson, 1981).

1.2 Anthropogenic CO_2: The Role of Cities

Attempts have been made to quantify the magnitude of anthropogenic perturbations to atmospheric CO_2 at various scales by conducting detailed CO_2 emissions inventories. Global inventories (Keeling 1973; Marland and Rotty, 1984), a national inventory for Canada (Jaques, 1992), and a provincial inventory for British Columbia (B. H. Levelton and Associates, 1990) already exist. Detailed inventories incorporating smaller political jurisdictions, such as cities, are absent.

It is thought that the impetus for reducing anthropogenic emissions of CO_2 is likely to come from urban areas, where high emissions are concentrated, guided by the political power of the city to lead change (Harvey, 1991; Maskell, 1991). Even though the climatic effects of CO_2 are not local, there appears to be a sense of responsibility to the global

community by urban areas, in efforts to curtail emissions (Gilbert, 1991). Initiatives have begun in many cities as part of the Urban CO_2 Reduction Project of the International Council for Local Environmental Initiatives which looks at methods of reducing CO_2 emissions (Lottermoser, 1991; Foute and Andrews, 1991). In Canada, both the Cities of Toronto and Vancouver have adopted resolutions to reduce emissions by 20% of 1988 levels by 2005 (City of Vancouver, 1990; City of Toronto, 1991).

In an effort to reach its emissions target, the City of Toronto undertook a study, which found that significant CO_2 emissions in the urban area come from the combustion of natural gas, combustion of fuels for generation of electricity, and the combustion of fuel from mobile sources. A similar urban inventory, although much more detailed, has been proposed for Vancouver by the B.C. Carbon Project (1992). The Urban Carbon Cycle Model of the B.C. Carbon Project (1992) consists of nine modules to integrate CO_2 storage, uptake, and processes of release.

1.3 Atmospheric CO_2 Flux Processes

Processes acting to augment or reduce the storage of atmospheric CO_2 have been identified. In an urban area, anthropogenic fluxes of CO_2 are primarily from the combustion of liquid, solid, and gaseous fossil fuels (City of Toronto, 1991), most of which is related to space heating and transportation (Berry and Colls, 1991a). In the combustion process, hydrocarbons are nearly completely oxidized to CO_2 and emitted to the atmosphere (Appendix A). More minor sources of anthropogenic CO_2 are associated with cement production, chemical processing, and waste disposal (Griffin, 1987; B. H. Levelton and Associates, 1990). Respiration of CO_2 from humans was calculated to be approximately 3% of anthropogenic CO_2 emissions in Cincinnati (Clarke and Faoro,
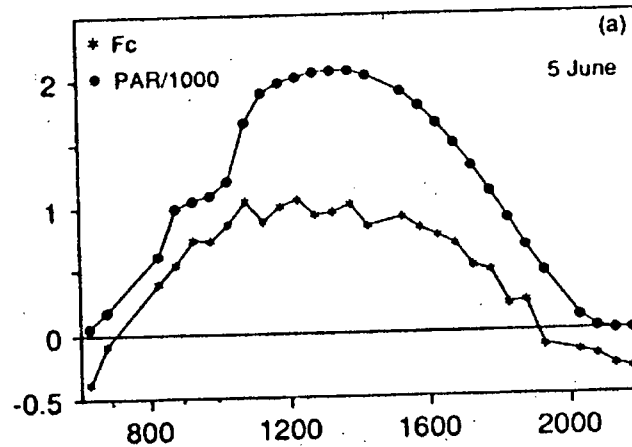
Figure 1.1: Diurnal variation of the daytime CO_2 flux (F_c, mg $m^{-2}s^{-1}$) and photosynthetically active radiation (PAR, μE_i $m^{-2}s^{-1}$) on June 5, 1987 at a height of 2.25 metres above a grass surface. Time is central standard time. Source: Kim and Verma, 1990.

1966).

Natural sources and sinks of atmospheric CO_2 in an urban area are mainly biospheric, due to respiration and photosynthesis by urban parks, lawns, trees and shrubs. A study over temperate grassland (Kim and Verma, 1990) clearly shows the diurnal variation of photosynthesis (Figure 1.1). During daylight there is a net downward flux of CO_2, the magnitude of which is closely correlated to that of PAR (photosynthetically active radiation).

Figure 1.2 shows the CO_2 flux for the nocturnal hours following those of Figure 1.1. As there is no photosynthetic activity, the flux is predominantly due to soil and dark respiration. Diurnal variation in respiration rates are primarily due to temperature and moisture. Generally, respiration is enhanced by higher temperatures (Peterjohn *et al.*, 1993; Raich and Schlesinger, 1992), and inhibited by both excessive moisture, and by a lack of moisture (Dörr and Münnich, 1987; Peterjohn *et al.*, 1994; Raich and Schlesinger, 1992). The effect of soil respiration on nighttime atmospheric CO_2 concentrations is
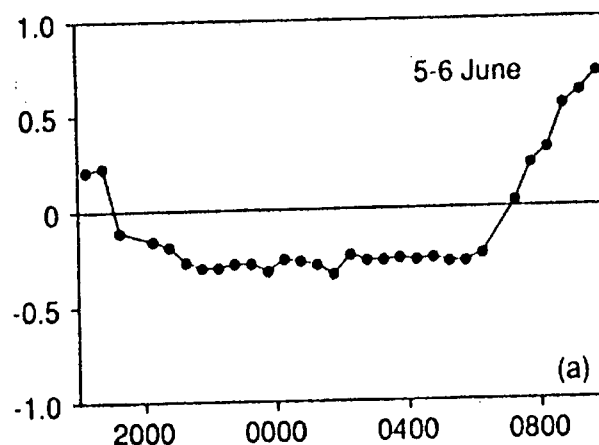
Figure 1.2: Nocturnal CO_2 flux ($mg\ m^{-2}s^{-1}$) on June 5-6, 1987 at a height of 2.25 metres above a grass surface. Time is central standard time. Source: Kim and Verma, 1990.

evident (Figure 1.3) from steadily increasing CO_2 concentrations measured at a rural site near Cincinnati (Clarke, 1969). The measurements of Figure 1.3 were made during a night with light winds and with conditions favourable for the production of CO_2 from soil respiration.

The biosphere has also been identified to contribute to the variation in CO_2 concentrations observed in both urban and suburban areas (Berry and Colls, 1990a,b; Clarke and Faoro, 1966). Concentrations are affected by local photosynthesis and respiration, and by advection of air from rural regions with a strong biospheric CO_2 signature.

1.4 Urban Atmospheric CO_2 Concentrations

The modification of boundary layer CO_2 concentrations by local sources and sinks has not been well interpreted or adequately quantified for diurnal timescales. Studies of atmospheric CO_2 near urban or suburban regions are few (Berry and Colls, 1990a,b;
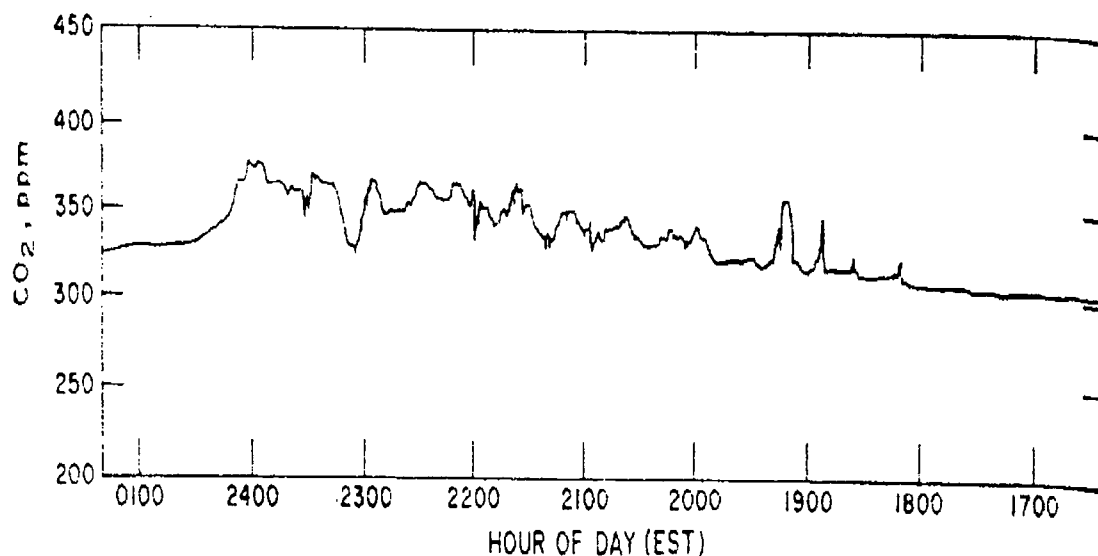
Figure 1.3: Nocturnal trace of CO_2 near Cincinnati, February 10, 1965, recorded at a height of one metre above the surface. Concentrations in ppmv. Note time progresses from right to left. Source: Clarke, 1969.

Clarke and Faoro, 1966; Clarke, 1969; Tanaka *et al.*, 1985), and have involved little analysis to validate heuristic models of expected CO_2 concentration responses to diurnal patterns of local sources and sinks, and wind. They have also neglected to consider the effects of boundary layer structure and have mostly considered only very local source and sinks to be important. This may be a reasonable conclusion for CO_2 concentrations sampled at very low heights, such as 1 metre (Clarke, 1969), and even 4 or 5 metres (Berry and Colls, 1990a, and Enoch, 1977), but perhaps not at higher heights within the well-mixed layer.

An accurate surface inventory for CO_2, such as that of the Urban Carbon Cycle Model (B.C. Carbon Project, 1992), is likely to be important to CO_2 concentrations. An aircraft study at a height of 30 metres indicated that as much as half the variance in
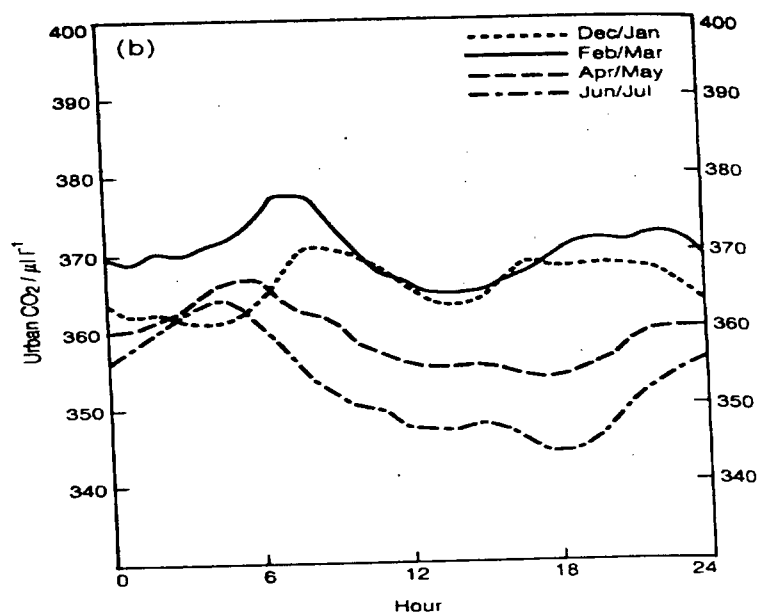
Figure 1.4: Bi-monthly-averaged diurnal variations in the CO_2 concentration at an urban site in Nottingham (December 1984-July 1985). Source: Berry and Colls (1990a).

CO_2 and H_2O fluxes at that height are explainable by surface heterogeneity in the spatial distribution of sources and sinks of CO_2 and H_2O (Mahrt *et al.*, 1994).

Most studies of urban CO_2 describe its diurnal variation in terms of the amplitude between mean daytime and nighttime concentrations, and the deviations from background concentrations. Diurnal variability of CO_2 concentrations is small at remote sites of the global CO_2 monitoring network. Common diurnal concentration ranges are less than 7 ppmv (Keeling *et al.*, 1976; Halter and Peterson, 1981), and often as low as only 1 ppmv at Mauna Loa (Bacastow *et al.*, 1985). Considerably greater variation is seen at both urban and rural sites. Figure 1.4 shows the mean diurnal CO_2 variability at Nottingham, England, to be nearly 20 ppmv in summertime, and about 15 ppmv in winter. CO_2 concentrations tend to follow a pattern with a double peak, due to the typical diurnal
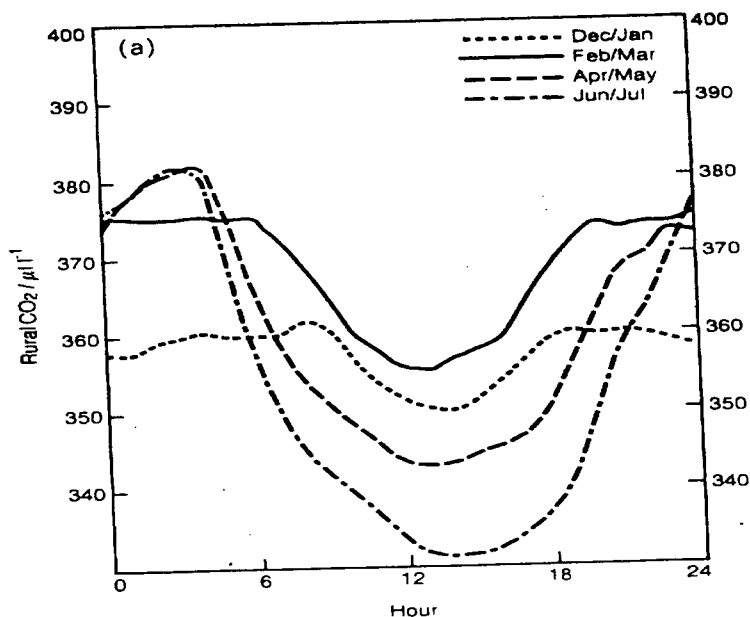
Figure 1.5: Bi-monthly-averaged diurnal variations in the CO_2 concentration at a rural site 15 km south-west of Nottingham (December 1984-July 1985). Concentrations in ppmv. Source: Berry and Colls (1990a).

cycle of human activities, which is most noticeable in winter.

Figure 1.5 shows mean CO_2 traces for a rural site 15 km south-west of Nottingham. The rural traces are characterized by lower concentrations in the afternoon at all times of the year, which is attributed to photosynthesis. Higher nighttime concentrations in the summer months are due to active soil respiration while temperatures are favourable. Consequently the amplitude of diurnal variability, approximately 50 ppmv, is larger than the urban site. The rural site has only one peak due to the dominance of biospheric sources.

Some studies show the amplitude of diurnal variability in summertime CO_2 concentrations at urban sites to reach values as high as those observed in rural regions (Clarke, 1969; Spittlehouse and Ripley, 1977). Diurnal amplitudes in Cincinnati reach 80 ppmv,

while those of New Orleans are slightly less at 60 ppmv (Clarke and Faoro, 1966).

Background concentrations for both Figures 1.4 and 1.5 are estimated to be 345 ppmv (Berry and Colls, 1990a). Summer afternoon rural concentrations can decrease to as much as 15 ppmv below background. At similar times in the city, concentrations reach only 2 or 3 ppmv less than background values. Mean CO_2 concentrations in the cities of Cincinnati and New Orleans are always at least 5 ppmv greater than background concentrations (Clarke and Faoro, 1966). It is likely that the suburban site chosen for this study will have characteristics of both rural and urban CO_2 traces (Berry and Colls, 1990b).

1.5 Objectives

- To describe the CO_2 "climate" of a suburban atmosphere.

Time series CO_2 measurements at a single suburban site in Vancouver will be analyzed primarily to investigate summertime diurnal CO_2 variability. Additional measurements will be used to study seasonal and spatial CO_2 variations, in order to get an overall understanding of atmospheric CO_2 in a suburban environment.

- To identify the principal sources and sinks of CO_2 in a suburban environment.

This study will detail CO_2 flux strengths from both anthropogenic and natural processes.

- To develop a simple multiple-box model to simulate CO_2 concentrations in the atmosphere above the suburban site.

CO_2 concentrations within the well-mixed layer will be interpreted with the aid of a multiple-box model. The structure of the model includes all significant surface sources

and sinks of CO_2, meteorological variables, and the boundary layer structure.

- To assess the applicability of this modelling approach to explain

  observed CO_2 concentrations.

Box models have been used successfully in simulations of other atmospheric constituents. By comparison with observations, this study will evaluate the degree to which diurnal variability of CO_2 concentrations can be resolved by a model of this type.

- To enhance understanding of the interpretation of spot measurements.

  of CO_2, and to place the carbon budget of the suburban atmosphere in

  its global context.

Model results allow the determination of the most significant processes affecting diurnal CO_2 variability, as measured at the suburban site. Concentrations at this site are compared to global values. Application of the modelling approach is addressed.

Chapter 2

Carbon Dioxide in the Greater Vancouver Environment

2.1 Experimental Methods and Observations

The carbon dioxide "climate" of Vancouver is described from examination of carbon dioxide concentration measurements. Measurements of CO_2 were made in various ecosystems within the City of Vancouver and its environs and they are compared with each other, and with values representative of the atmospheric boundary layer below the mixing depth. The bulk of the observational data comprise three time series at a single site. The CO_2 "climate" is explained, in terms of these measurements, at several spatial and temporal scales. There is considerable spatial variability due to the source distribution at ground level (eg. mobile emissions). Thus the diurnal CO_2 description relies heavily on the time series measurements at a single site and the temporal signals found within.

2.1.1 Site

2.1.1.1 General Characteristics of Region

The study was conducted within the Greater Vancouver Regional District (GVRD), located within the Lower Fraser River Valley of British Columbia (Figures 2.1a,b). Topographically the region is bounded approximately 13 km to the north and over 40 km to the south, by mountain chains. The Pacific Ocean lies to the west, separated from
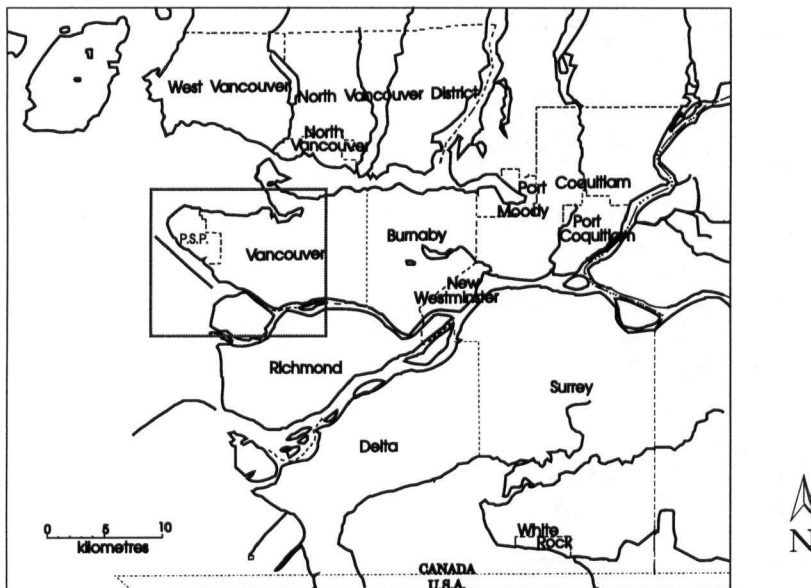
Figure 2.1a: Greater Vancouver Regional District (GVRD) and environs. P.S.P is the region of Pacific Spirit Park, including the University of British Columbia. Boxed region shows the bounds of Figure 2.1b.
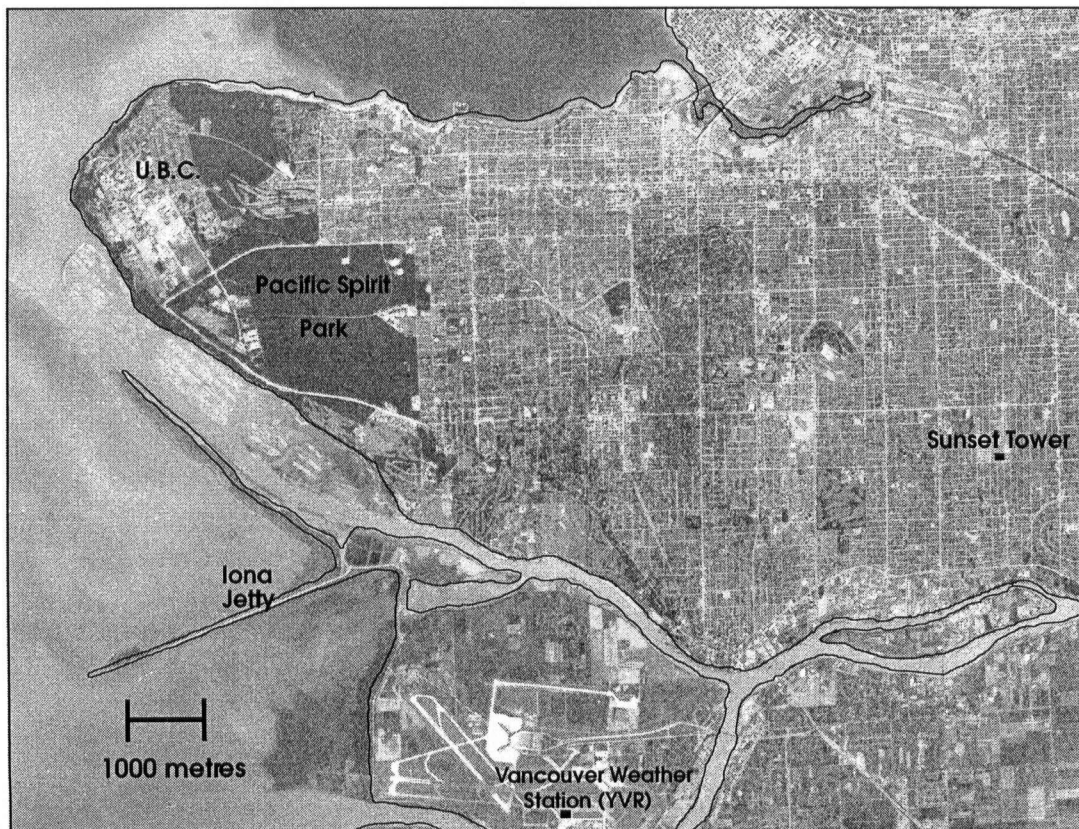
Figure 2.1b: Air Photo of Study Region (National Air Photo Laboratory, Ottawa). Scale - 1:137000.

Vancouver by the Strait of Georgia and Vancouver Island.

Vancouver ($49° 16'$ N, $123° 06'$ W) is situated on the west coast of the North American continent. Predominant upper level westerlies bring air from the Pacific Ocean that is relatively unmodified by continental influences, including anthropogenic emissions. Airflow from that direction is subject only to the influences of Vancouver Island, 35 km across the Strait of Georgia. Atmospheric CO_2 concentrations, then, should be representative of the background concentration reported for that latitude by the global monitoring network.

2.1.1.2 Background CO_2 Concentration

Atmospheric CO_2 concentration observations have not been conducted in this region previously. However there are two stations on the West Coast that are part of the global background CO_2 monitoring network: Cape Meares, Oregon ($45° 29'$ N, $120° 00'$ W) has been operating since 1982, and Cape St. James, B.C. ($51° 56'$ N, $131° 01'$ W) operated from 1978 to 1992. Both stations show a seasonal pattern in CO_2 concentration, with an annual minimum recorded in August, and an annual maximum during the months of January to April. Of note is the considerable variation seen in the global background CO_2 data. Commonly the data show fluctuations of up to 4 ppmv within as little as ten days at a given site. Discrepancies between Cape St. James and Cape Meares at a comparable time can be of similar magnitude. Even monthly averages can differ by as much as 3 ppmv between these sites (Trivett and Higuchi, 1989; Boden *et al.*, 1991).

At Cape St. James the average annual CO_2 concentration increased at the rate of 1.43 ppmv per year from 1979-1989 (Trivett and Higuchi, 1989), while at Cape Meares the increase has been approximately 1.7 ppmv per year from 1979-1990 (Boden *et al.*, 1991). This rate of increase is used to extrapolate Cape St. James data to the concentration

for the months of interest of this study. Within the limitations of the global CO_2 data (Tans and Conway, 1993), the background concentration at Vancouver is assumed to be the average of these two stations. For the three main measurement periods, June 1993, September 1993 and January/February 1994 the background CO_2 concentrations are approximately 360 ppmv, 353 ppmv and 364 ppmv respectively. These are the benchmarks against which the observations from the city of this study can be compared.

2.1.1.3 Climatology

The climate of Vancouver is dominated by a sequence of mid-latitude cyclonic disturbances carried ashore by the predominantly westerly upper level flow. Lower level wind climatology is characterized by planetary boundary influences. Most common under summertime anticyclonic conditions are mesoscale land/sea breeze circulations, with predominantly west and northwest winds during the daytime sea breeze, typically from 1100-1900 PST (Steyn and Faulkner, 1986). Nighttime winds are generally weaker land breezes from the east and southeast, augmented by down valley flow (Oke and Hay, 1994).

2.1.2 Instrumentation and Measurement Uncertainty

Measurements of carbon dioxide concentration were made using a LI-COR 6262 differential, non-dispersive, infrared gas analyzer (NDIR) operating in absolute mode. In this mode gas concentrations (CO_2 and H_2O) are calculated from the difference of absorption between a reference cell of known concentration and a sample cell. The reference cell is held at zero concentration for both gases by continually scrubbing the cell with soda lime and magnesium perchlorate, thereby eliminating CO_2 and H_2O respectively by absorption.

In order to compare the measurements of this study with the existing global network it is necessary to correct for water vapour (P. Tans, NOAA Climate Monitoring and Diagnostics Laboratory, Boulder). Water vapour can influence readings of CO_2 by direct absorption in the CO_2 waveband, by pressure broadening and by dilution. The first is virtually eliminated by choosing a CO_2 absorption band of 4.26 microns. The LI-COR 6262, as it also measures water vapour, can be operated in a mode which automatically corrects for the effects of pressure broadening and dilution. The influence of pressure broadening from water vapour is to increase the value displayed for the CO_2 concentration in the absence of this correction. For water vapour values typical of this study, the correction is on the order of -0.5 to -1 ppmv.

The dilution correction is more important, especially when dealing with time series. It allows the analyzer to display CO_2 concentrations that would exist if water vapour was removed from the sample flow at constant volume. Without a dilution correction the time series show varying CO_2 concentrations attributable to water vapour fluctuations in the absence of sources and sinks of CO_2. Over the range of water vapour concentrations and CO_2 concentrations observed in this study the dilution correction is approximately 2 to 5 ppmv.

Analyzer specifications state the accuracy of the measurements to be $\pm$ 1 ppmv at the CO_2 concentrations of interest, with a noise level of approximately $\pm$ 0.2 ppmv. The zero and span settings of the calibration polynomial are noted to drift over time. For this reason the analyzer was calibrated daily during the study periods. The calibration for CO_2 was accomplished in about 20 minutes using a single calibration gas of 365 ppmv CO_2 in dry air.

Two pressure corrections must be applied to the LI-COR 6262. The first is a result of the measured CO_2 concentration relying on known atmospheric pressure. The magnitude of the correction is approximately -0.47 ppmv/mb, and is linearly applied over all

pressures. Since the instrument was only calibrated once per day, it was only necessary to know the atmospheric pressure for the hour around the calibration time. After all measurements were completed the data were corrected using hourly atmospheric pressure data from the Vancouver International Airport observing site (YVR). At times when the atmospheric pressure changes very rapidly (perhaps 2 mb/hour) the assumption of constant pressure over the whole hour leads to a maximum drift of only $\pm$ 0.9 ppmv. The second pressure correction accounts for the difference in pressure between the reference and sample cells caused by the flow of air through the sample cell. For the flow rates of the sample air in this study (approx. 2.5 litres/min) the flow correction factor was estimated to be 1.069 $\pm$ 0.003. Multiplied by the CO_2 concentration this gives corrections with an error of approximately 1.1 to 1.4 ppmv.

If the aforementioned uncertainties are assumed to be mutually independent, the maximum absolute error on the CO_2 concentration is $\pm$ 1.9 ppmv. However there are errors in calibration, and drift in the zero and span over time, that are harder to quantify.

2.1.3 Tower Site

Measurements for the three main study periods were made from a tower located at the Sunset site in Vancouver (Figure 2.1b). This part of suburban Vancouver is thought to be representative of the majority of the city (T. Oke, Department of Geography, University of B. C.). Located inside the Mainwaring substation of B.C. Hydro, the 30 metre tower is situated in the south-east corner of the substation enclosure, where the base is 5.0 metres below the level of the surrounding terrain. A small instrument trailer located near the base housed the gas analyzer and other equipment.

Air was drawn down the tower to the analyzer by a small DC pump running off a DC voltage regulator, at the constant rate of 2.5 litres/min. Two hoses of equal length were

used to ensure that the two sampling heights have the same flow pressure correction. The first hose, located near the top of the tower, was at a height of 22.5 metres above the surrounding terrain (27.5 metres above ground level). The second was at 5.0 metres above the surrounding terrain (10.0 metres above ground level). During sampling the inlet to the analyzer was alternated between heights, usually for at least one full day at a given height. It is expected that the lower height (H2) will be above the urban canopy layer (Oke, 1976) and within the roughness layer. The upper height (H1) is near the transition from the roughness layer to the surface layer (constant flux layer, Roth 1991). Air, continually drawn down by the pump, was sampled every 20 seconds for 1 second.

The site is situated in a busy suburban neighbourhood with many local sources and sinks of CO_2. As discussed more fully later, the most important sources are mobile and stationary emissions from combustion. The only local sink of CO_2 is that of photosynthesis. The time series integrate these local processes together with the meteorology of the region and the boundary layer processes that affect the horizontal and vertical mixing of CO_2, and the entrainment of CO_2 from above the mixed layer. Depending on the time of day the entrained air contains higher or lower concentrations of CO_2 than the mixed layer. Synoptic processes, such as prolonged anticyclonic conditions, may allow the buildup of CO_2 due to the land/sea breeze circulation extending over a period of days.

Meteorological data observed at the Vancouver International Airport (Figure 2.1b) are used to augment measurements taken at the Sunset site. The distance between the sites is approximately 7.5 km. For typical anticyclonic conditions with a developed sea breeze circulation, it is observed that wind speeds are generally lower at the tower site than at the open coastal site of the airport. The onset of the westerly sea breeze is often lagged by an hour or two at the Sunset Tower.

2.1.4 Sampling Strategy

Background CO_2 concentrations (independent of the global sampling network) were measured upwind of the study area on days with westerly winds, in order to capture undisturbed air approaching the study region. From a shipboard platform about 2 km west of the University of B.C., and from other measurements taken near the Iona Jetty (Figure 2.1b) jutting out into the Strait of Georgia, the mean background CO_2 concentration was estimated to be 369.4 ppmv, and 368.6 ppmv (with sample standard deviations less than 1 ppmv) during the months of June 1993 and September 1993 respectively. Background measurements were not made for the January/February 1994 period, but it is known that the background CO_2 concentration was about 4 ppmv higher than in June period (Boden *et al.*, 1991). The expected mean background CO_2 concentration in January/February 1994 is approximately 373 ppmv.

These measured background concentrations are considerably higher than the undisturbed background concentrations extrapolated from the global sampling network. This is probably because the air near the study area has been modified by the biospheric and anthropogenic sources and sinks of CO_2 near the coast. Longer term circulations caused by synoptic flows, and local circulation, such as the summertime land/sea breeze, may keep modified air within the region for several days. However, the short-term temporal variance in the CO_2 signal is much lower for the background upwind air than that of any other measurements made during the field program. This indicates efficient short term mixing of the background air, although there is still some meandering of the well-mixed CO_2 concentrations about the means listed above. The amplitude of this diurnal variability is about 2 to 4 ppmv, and is an order of magnitude less than the typical diurnal amplitude of more than 20 ppmv observed in this study at the Sunset Tower.

It is the deviation from the mean background values, measured upwind of the study area, that will be discussed, based mainly on temporal data collected at the Sunset site in the following periods: a) June 3 - June 24, 1993, b) September 3 - September 6, 1993, and c) January 12 - February 11, 1994. These measurements give information on temporal scales of variability, including diurnal cycles, as well as synoptic and seasonal changes. The tower measurements are augmented by spot measurements at various locations within the study area, including time series from within the forest canopy of Pacific Spirit Park (Figure 2.1b). Combined with vehicular transects, these *ad-hoc* CO_2 samples indicate the spatial variability of CO_2 in a complex urban environment. The aim is to link CO_2 source and sink processes, and boundary layer processes, with observations of CO_2 concentrations presented here.

2.2 Sampling Results - Temporal Variability

2.2.1 First Sampling Period (June 3 - 24, 1993)

This period was chosen to coincide with the time when the biosphere is particularly active, before summer dry spells and during the time of maximum insolation. The region received above normal precipitation in June, with 72.2 mm recorded at YVR, compared to the normal of 45.7 mm. Cumulative precipitation totals for the year were approximately normal.

Synoptically the whole period was mostly unsettled, and dominated by a weak ridge off the west coast of Vancouver Island giving north-westerly flow to the study region above the surface. Of note were the strong NW winds on June 7 caused by the weak ridge and a low situated near central B.C. Low pressure systems passed through the area on June 9, June 14-15, and June 22, weakening as they moved over the top of the ridge.

Behind the fronts generally cooler, clearer air arrived with some evidence of instability and convection in the form of broken cumulus and towering cumulus. Daytime temperatures were commonly 20-25°C, producing land/sea breeze circulation with winds becoming westerly in mid-morning until late afternoon. Nocturnal flow was generally from the east. Land/sea breeze circulations were observed for the days of June 4, 5, 11-13, 15-17, and 19. The north-westerly flow should minimize the influence of anthropogenic and continental biospheric sources and sinks on the background CO_2 concentration during this period.

CO_2 concentration traces for the period June 3 - June 24 are presented in Appendix B. The diurnal signals appear to be related to wind speed and direction, turbulent mixing, mixed layer depth, and source and sink distribution. Each is not easily resolved, but there are similar features on all days that indicate their importance. Notably, although both tower heights could not be sampled simultaneously, the gross features along with their amplitudes were equally distinguishable at each height, with no significant difference, given the large variability. This indicates good vertical mixing, at least between the heights of 5.0 and 22.5 metres. It is hoped that changes in concentrations at these two heights are representative of those within the mixed layer.

2.2.1.1 Temporal Variability

The major features for all days observed in June (Figure 2.2), are present (with important exceptions - see Case studies, Sections 2.2.1.2 and 2.2.1.3) throughout the whole period and allow the definition of dominant scales of temporal variability. The diurnal cycle of greatest amplitude is shown in Figure 2.3, a smoothed composite of 11 days that show marked similarity in the magnitude and timing of the diurnal CO_2 concentration changes. A concentration frequency distribution shows the concentrations
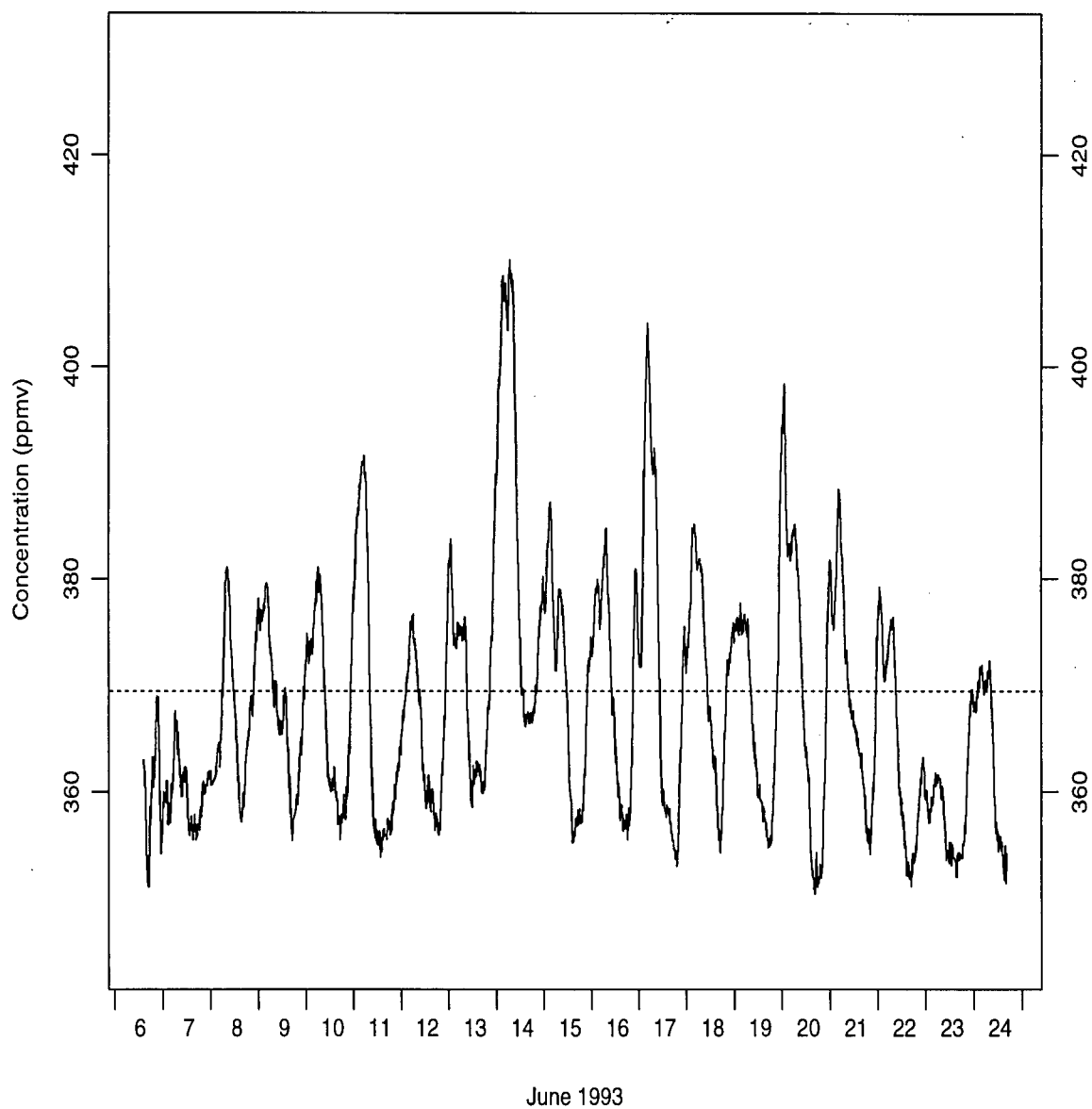
Figure 2.2: Atmospheric CO_2 concentration trace for June 6 - 24, 1993. Sampling at 20 second intervals is smoothed with a 3 hour running mean. The background concentration (369.4 ppmv) is shown as a dotted line.
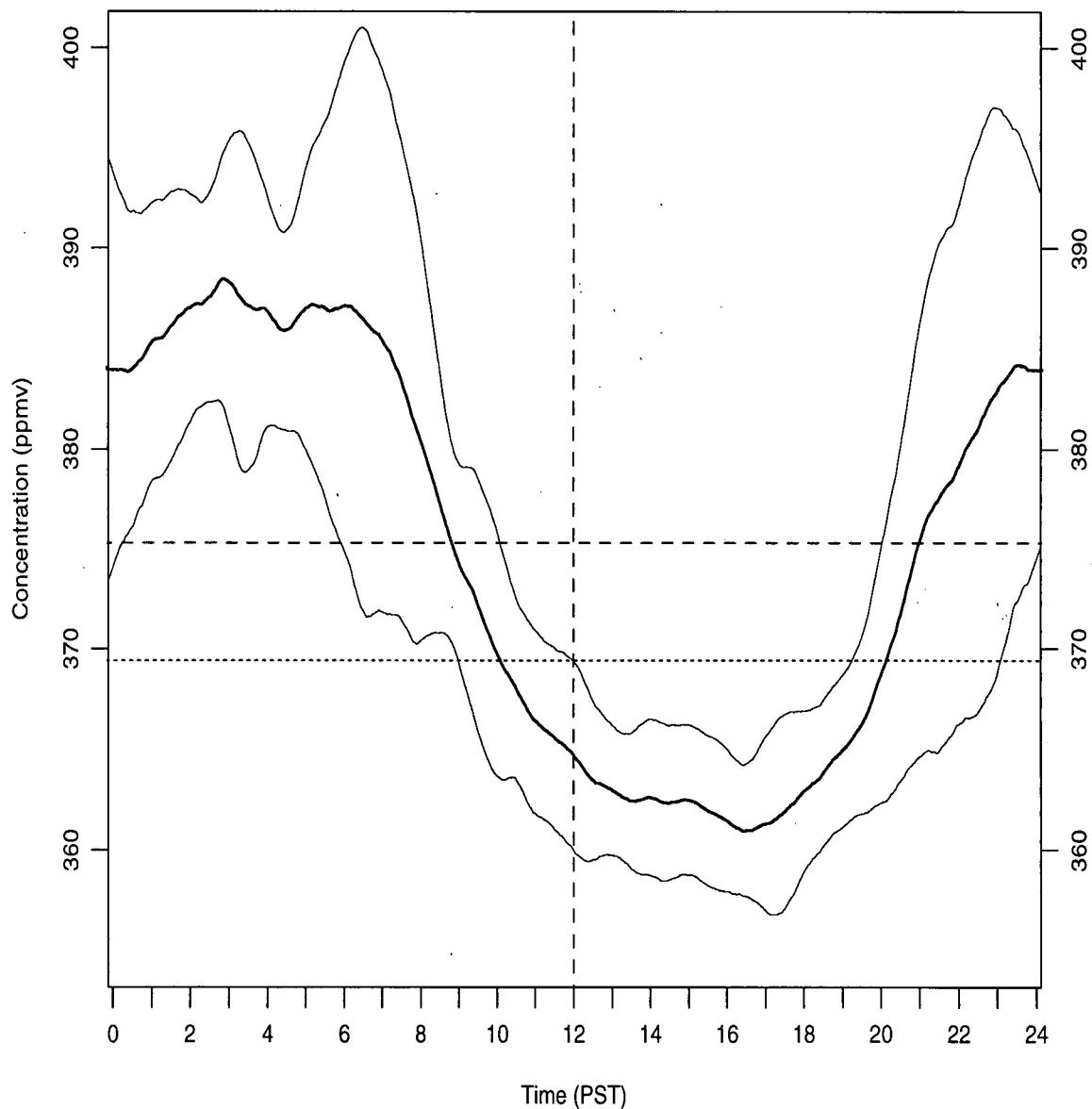
Figure 2.3: Composite atmospheric CO_2 concentration trace smoothed by a one hour running mean, for 11 days in June 1993. Composite CO_2 variance (sample length of 30 minutes) is plotted as σ^2 on either side of the mean, by thin lines. The background concentration (369.4 ppmv) is shown as a dotted line, and the series mean (375.3 ppmv) by the dashed line.

over a day to be bimodal, described by a minimum in the afternoon (1400 - 1700 PST), and a maximum throughout the night, peaking near sunrise. The mean amplitude of this feature is 27 ppmv, although variability about this mean can be as high as 40 ppmv and as low as 13 ppmv (Table 2.1). Deviations from the background CO_2 concentration of 369.4 ppmv are skewed; larger deviations from background concentrations are observed at night. Mean daytime reduction of CO_2 below background is 9 ppmv, with extreme cases of 1 ppmv and 14 ppmv below background. The mean nocturnal value is 18 ppmv above background concentrations, with extremes of 0 ppmv and 39 ppmv above background. The amplitude of the major CO_2 variability observed here is consistent with other diurnal CO_2 studies at urban and suburban sites (Berry and Colls, 1990a; Clarke and Faoro, 1966; Tanaka *et al.*, 1985). The mean of 375.3 ppmv is well above the global average of approximately 357 ppmv (Houghton *et al.*, 1990). As expected (Chapter 1) the mean trace for June at Sunset seems to have characteristics somewhere between those of the rural and urban sampling of Berry and Colls (1990a). This is consistent with the *suburban* surface characteristics of Sunset. Sample extremes of 351.2 ppmv and 444.5 ppmv were recorded during the period.

Superimposed upon the major diurnal amplitude is the CO_2 variance (σ^2) at timescales of minutes. Figure 2.3 shows this as a temporal trace of average 30-minute sample variances for the same 11 days used to calculate the diurnal mean CO_2 signal. Observations show that upwind background concentrations have standard deviations (σ) of less than 0.5 ppmv. Standard deviations of CO_2 observed at the tower are much greater (Table 2.1), reaching values as high as 25 ppmv (for times not shown in Table 2.1). Values are generally higher during nighttime hours (5.5 ppmv average) than for daytime hours (2.2 ppmv average). At the tower, the lowest standard deviations of 0.5-1.5 ppmv (approximately similar to those of background) were observed with strong westerly winds. Daytime variances were commonly 1.5-2.5 ppmv. The variance is noted to decrease under

Table 2.1: Daily mean nighttime and daytime CO_2 concentrations used to evaluate major diurnal cycle for June 1993. All CO_2 concentrations in ppmv. If sampling height was changed after the mid-morning calibration, the sampling height before calibration is indicated first. Standard deviations are calculated for observations 2 hours on either side of the extrema in the mean CO_2 concentrations. Only days with complete observations are shown.

Date Jun/93	Sample Height	Mean Nighttime	σ	Mean Daytime	σ	Amplitude
4	H1	389	7.1	363	0.7	26
7	H1	372	2.5	359	1.1	14
8	H1	386	5.7	360	5.0	26
9	H1	390	4.8	361	1.0	29
10	H2	387	5.2	363	3.6	25
11	H2/H1	395	2.0	359	1.2	36
12	H1	383	1.9	360	3.9	23
13	H1	384	5.3	362	2.9	22
14	H1	408	11.3	368	3.7	40
15	H1	385	5.7	363	1.3	22
16	H1	391	6.3	361	2.0	30
17	H1/H2	396	8.0	358	1.0	38
18	H2	387	4.9	360	4.6	27
19	H2	381	1.3	361	0.7	20
20	H2	392	15.3	357	0.5	35
21	H2	390	5.5	356	4.3	34
22	H2	384	5.4	356	1.1	28
23	H2	368	1.3	355	1.4	13
Avg.		**387**	**5.5**	**360**	**2.2**	**27**

conditions of strong mixing, primarily by high wind speeds, and efficient daytime mixing under a convectively turbulent mixed layer. Consequently, the daytime variance is less than nocturnal values when winds are lighter, as also observed by Enoch (1977).

The composite traces of Figure 2.3 can be used to infer the important processes generating and controlling the amplitude of the diurnal cycle of CO_2 concentrations. As detailed in the following discussion, significant processes are thought to be: 1) temporal and spatial distribution of sources and sinks, and 2) boundary layer parameters, such as mixed layer depth and nocturnal stability that affect the mixing of CO_2 in the atmospheric boundary layer. Processes thought to control the amplitude are: 1) source area of air travelling across the tower (wind direction), 2) ventilation timescale (wind speed) and 3) efficiency of mixing (Berry and Colls, 1990a). Each can have a large effect on the CO_2 concentration, thus creating difficulty in resolving the importance of each at a given time. The above processes will be explained and then used to describe the mean diurnal CO_2 pattern observed in June 1993.

A detailed discussion of the temporal and spatial distribution of sources and sinks is presented in Chapter 3. Briefly, the diurnal pattern of net CO_2 flux at the suburban surface is explained by moderate positive values at night (Kim and Verma, 1990; Price and Black, 1990), peaking before sunrise, in response to augmentation of biospheric respiratory sources by anthropogenic sources. Mid-morning to mid-afternoon surface CO_2 fluxes are dominated by photosynthesis. Photosynthesis increases to a maximum uptake of CO_2 near 1200-1300 PST (Jarvis *et al.*, 1985) then decreases until 1800-1830 PST, at which time the effect of decreased insolation allows soil respiration and mobile emissions to dominate, and to again create a net positive surface flux of CO_2.

Spatially there are variations in source and sink strengths. The dense urban centre of Vancouver lies 6.5 km north of the tower. To the east are tens of kilometres of relatively dense suburban areas. During daytime this area is a large source of anthropogenic CO_2

emissions from mobile sources, but also a significant biospheric sink from urban parks, lawns and trees. Compared to the 9-16 km fetch to the Strait of Georgia to the west, the eastern sector has a more dense concentration of anthropogenic CO_2 sources. Due to the large area of Pacific Spirit Park, less dense housing (and thus more urban lawn), and a greater number of urban trees, as observed from air photos of the region (City of Vancouver, Planning Department, 1989), it is expected that the western half will be a more significant daytime sink for CO_2, and a large source of CO_2 after the cessation of photosynthesis at sunset. Parks appear to be nearly equally distributed in all directions nearby.

The flux "source area" is important because it defines the surface area of sources and sinks which affect the CO_2 concentration in air observed at the tower (Schmid, 1988). Controlled mainly by wind direction and stability, the effect of a changing source area can produce rapid changes in observed CO_2 concentrations. A daytime wind direction change from west to east presents a source area that has greater anthropogenic emissions, often resulting in a significant increase in concentration. Conversely a daytime wind direction change from east to west can create a significant decrease in concentration. An interesting illustration of this is the day of June 9 (Appendix B). Between the hours of 1100-1600 PST the wind changes from east to south-east to west. Near 1100 PST there is a gradual decrease in CO_2 concentration as expected by photosynthesis. A peak in CO_2 concentration at 1300 PST coincides with the south-east wind. Subsequently, a large and rapid decrease in concentration is observed as the wind becomes strong westerly, advecting air more depleted of CO_2 across the tower. "Discontinuities" of this type are explained by wind direction changes, whereas the more general trends are probably explained by temporal distributions of sources and sinks, and mixed layer evolution.

Wind speed defines the distance and areal extent of the source area away from the tower. This is due to the important roles of advection and mixing. Higher wind speeds

promote greater mixing and integrate the emissions of a larger source area to the CO_2 concentration at a point, making contributions to the concentration at the tower less local. Distinctly lower concentrations, caused by greater mixing, are observed at times of wind speed increases . Additionally, the mean wind speed defines the amount of undisturbed background air that is mixed into the boundary layer volume, and the timescale of ventilation for removal of excess CO_2 above the background concentration (Tennekes, 1976). The above processes are important in explaining the composite graph of CO_2 concentrations (Figure 2.2).

Figure 2.2 and Table 2.1 show that mean nocturnal CO_2 concentrations were about 387 ppmv. Nighttime conditions favoured the buildup of CO_2 above background values, primarily from biospheric soil and dark respiration (Appendix A), as winds were generally light easterlies. Shallower mixed depths and poorer vertical mixing under a stable boundary layer at this time may have contributed (Berry and Colls, 1990a). A peak in variance is observed at 0700 PST, coincident with the peak in CO_2 emissions from mobile sources during the morning rush hour traffic (City of Vancouver traffic counts) after a nighttime buildup. This peak is not evident on all days observed, but is subject to influences which allow the increase in mobile emissions at this time to be embedded, as an increase in variance, in the temporal trace of CO_2. June 6, 10, 16 and 24 are examples of days which exhibit increased variance around the time of the morning rush hour. Winds were from the east or south-east for each of these days, and were mostly light. Of importance is the existence of a busy roadway intersection about 125 m to the south-east, which dominates the "source area". Light winds inhibit mixing of vehicular point sources and appear as increased variance on the temporal trace. Variance decreases are often observed when winds become more westerly because there is a much greater fetch to major intersections. If winds remain easterly or light, the variance of CO_2 is often seen to remain high during the day while mobile emissions are high.

The drop in CO_2 concentrations begins near 0700 PST when the biosphere becomes a net sink (photosynthesis dominates over soil and aboveground respiration). The growing importance of photosynthesis coincides with the growth of the daytime convective mixed layer (Steyn, 1980). Mixed layer growth effectively increases the volume of air into which CO_2 from surface sources and sinks is mixed. Mixed layer growth begins soon after sunrise (approximately 0530 PST) and destroys the shallow nocturnal urban boundary layer soon thereafter (Carson, 1973; Oke, 1995). High CO_2 concentrations in the shallow nocturnal mixed layer decrease as CO_2 is mixed vertically by turbulence as the mixed layer grows, and horizontally as the wind speed increases (Berry and Colls, 1990a). Also contributing to decreasing concentrations is the entrainment of air from above the mixed layer which is close to background CO_2 concentrations (R. Desjardins, Centre for Land and Biological Resources Research, Research Branch, Agriculture Canada). Additionally, dominant emissions of CO_2 from anthropogenic sources near the beginning of this CO_2 reduction are diluted into an increasing volume.

Additionally the timing and magnitude of the decrease depends upon wind speed and wind direction. Many days exhibit a sea breeze circulation with moderate westerly winds (4-5 m s^{-1}) starting in mid-morning, with easterly winds at night. Concentrations fall more rapidly with the westerly wind, as it advects air closer to background concentrations from an upwind area with a lesser anthropogenic emissions density, across the tower. Upwind background concentrations are 10-30 ppmv less than CO_2 concentrations observed before sunrise. June 15 and 19 (Appendix B) are both days in which a sea breeze sets up in the wake of a frontal system leaving clearer, warmer air embedded in a north-westerly flow. Evidence of convection is seen in the afternoon reports of towering cumulus. On June 19 the westerly sea breeze begins 2 hours earlier than that of June 15. Consequently mean minimum CO_2 concentrations are reached 2 hours earlier on this day.

Evidence of CO_2 drawdown by photosynthesis below background concentrations is seen in Figure 2.3 after 1000 PST. Typical concentrations after this time are 355 to 363 ppmv, with a mean minimum of 360 ppmv (Table 2.1). Notably the afternoon minimum is observed to occur after the peak in net photosynthesis, and to remain nearly constant from about 1300-1700 PST, rather than follow a curve correlated with the sink strength of photosynthesis. It is likely that ventilation of the region with background air, now higher than observed, is occurring at a rate equal to the rate with which the sum of photosynthesis and anthropogenic emissions are removing CO_2. On days with poorer ventilation, such as June 8 and June 13, the afternoon CO_2 trace follows a curve more closely correlated with the changing afternoon net photosynthetic sink rate.

The mean minimum concentration due to the afternoon drawdown of CO_2 is similar through all days, with only one exception. On June 14 the mean minimum is 368 ppmv, considerably higher than the average. Calm conditions throughout most of the previous night allowed the concentration to reach values as high as 430 ppmv, albeit primarily due to very local emissions. A frontal passage on this day brought moderate easterly winds, advecting air across the tower without the lowering effect of uncontaminated background concentrations.

Rising concentrations are observed after 1700 PST, when the biosphere becomes a relatively constant source of CO_2 (Kim and Verma, 1990), and the mixed layer collapses before sunset. The rise is rapid because anthropogenic emissions are still significant. The mixed layer collapse itself cannot cause a change in concentration, as this process is only the reduction in volume of a uniform concentration layer. An increase in concentration can only be seen if there are significant sources at the surface, such as soil respiration and anthropogenic emissions. The mean CO_2 concentration levels off after the mixed layer has established its nocturnal height, and anthropogenic emissions have nearly ceased, leaving only soil respiration as the major source. Eventually an equilibrium is established

between removal of CO_2 by ventilation and the addition by respiration. Near the time of CO_2 increase the wind often changes direction from westerly to easterly as the sea breeze ends. This enhances the rapid change in concentration seen at this time.

The nighttime situation is clearly different from daytime, as it is generally characterized by low wind speeds, a shallow boundary layer, and poor mixing. Concentrations rise considerably due to biospheric respiration (Table 2.1). Even after the cessation of mobile emissions, large variability is observed in the measurements. It is often observed that the CO_2 concentration will meander in time with an amplitude of up to 25 ppmv. Examples are the mornings of June 4, 11, 13, 15, 20, and 21. This is possibly due to air of lower concentration mixing downwards from above, episodically with a period of 1 to 2 hours (Pales and Keeling, 1965). High and variable nocturnal CO_2 concentrations in a suburban area have also been attributed to the advection of air from nearby rural areas with high biospheric CO_2 fluxes under temperature inversions (Clarke and Faoro, 1966).

These cases differ from the morning of June 14, a day that also shows considerable variability. Notable differences on this day are calm winds and extremely high CO_2 concentrations embedded in a trace of large variance. Unlike mixing from above which brings the concentration down to near background over 1 to 2 hour intervals, the morning of June 14 exhibits changes in CO_2 concentration of up to 65 ppmv over 30 minutes with values much higher than background. A maximum concentration of 444.5 ppmv is observed around a mean of about 400 ppmv. The high concentrations and high variance are indicative of poor mixing of local mobile emissions and soil respiration.

2.2.1.2 Case Study 1: June 10, 1993

This day (Figure 2.4 - Raw data of CO_2 concentrations sampled every 20 seconds is shown in Appendix B) shows many of the dominant features of this summertime period (Figure 2.3) with some exceptions. At 0000 PST CO_2 concentrations are well above background, near 383 ppmv. Variability is high, with standard deviations of up to 5 ppmv. This variability is due to poor mixing as light easterly winds bring air across the tower. The drop in concentration near 0200 PST is possibly explained by a wind shift to the south and thereafter slightly higher easterly winds enhancing mixing in the nocturnal boundary layer. Consequently, with greater mixing, the variance is observed to decrease. A decrease in CO_2 concentrations and variance near this time appears to be a common feature, as it is observed in the composite at 0400 PST (Figure 2.3).

Over the next 5.5 hours concentrations rise steadily due to continued soil and dark respiration into a shallow nocturnal boundary layer. Anthropogenic emissions, albeit low, are nearly constant. The variance in CO_2 concentrations is moderate as expected under relatively unchanging wind conditions. The large increase in CO_2 variance from 0600-0730 PST is attributed to increased vehicular emissions.

A peak in mobile CO_2 emissions occurs near 0700 PST, although emissions begin to rise rapidly from the low nighttime values as early as 0600 PST. The high variance is indicative of poorly mixed air advecting across the tower from these point source emissions local to the tower environment. This effect is enhanced by winds from the east and southeast, the direction of a nearby busy intersection. The morning rise in vehicular activity also produced increases in CO_2 concentrations of a few ppmv. Light winds augment the rise on this day. Peak mean CO_2 concentrations reach about 388 ppmv at 0630 PST. An absolute maximum of 410.3 ppmv was observed during this period.
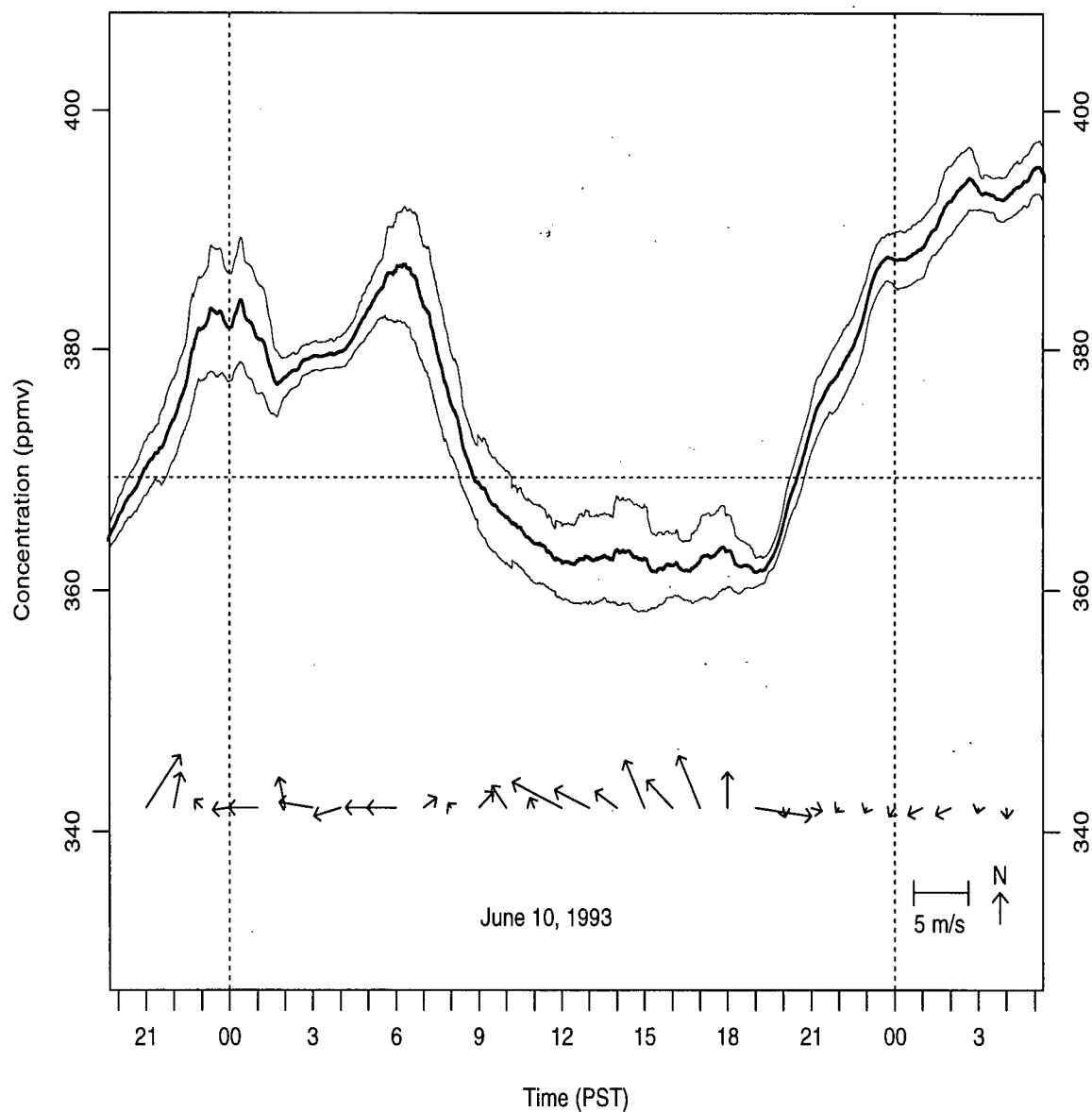
Figure 2.4: Atmospheric CO_2 concentration trace for June 10, 1993. The thick line indicates observations smoothed by a 60 minute running mean. Thin lines indicate one standard deviation on either side of the mean. Hourly wind observations are shown as vectors. The background concentration (369.4 ppmv) is shown as a dotted line.

Near 0730 PST three major processes are acting upon the CO_2 concentration. The two complementary processes of photosynthesis and a developing mixed layer act to decrease the concentration. Instability in the wake of the recent frontal passage is likely to produce a daytime convective mixed layer which increases in height until early afternoon, while entraining CO_2 from above. Turbulent mixing removes CO_2 from the surface layer and mixes it upwards to the growing inversion height, effectively reducing the CO_2 concentration observed at the tower. The third daytime process on June 10 is that of the role of mean winds. Light winds (mostly under 4 m s^{-1}) ensure that contributions to observed CO_2 concentrations are local, and poorly mixed. Winds are primarily southeasterly; thus the tower "sees" air, from an area that is free of low variance background air from the west. As a result, the daytime variance is very high, although mean concentrations clearly decrease as excess nocturnal CO_2 is ventilated under slightly stronger daytime winds.

The CO_2 decrease is steady until nearly 1300 PST, giving mean concentrations of about 363 ppmv, and an absolute minima of 356.1 ppmv, well below background. Daytime concentrations were 3 ppmv higher (Table 2.1) for June 10 than the average daytime concentration for the June period. This may be due to the lack of influence of low concentration background air to the west.

Thereafter the mean CO_2 concentrations remained nearly level until 1900 PST, at which time there was a rapid increase. Important processes are probably the collapse of the daytime mixed layer, and the subsequent decrease in the mixing volume through which CO_2 is assumed to mix relatively uniformly, and the biosphere becoming a net source of CO_2. In response to the strength of the biospheric source, the concentration rose steadily throughout the evening. Notably the variance was seen to decrease after 1900 PST, when winds changed to the west and then to the north, creating a fetch with less vehicular point sources. Generally the nocturnal trace was characterized by rising

concentrations, and a longer period variability than during the day, possibly due to the mixing of lower concentration air from above the inversion height. Irregular nighttime traces similar to this are common in this study (Appendix B), and are likely due also to imperfect mixing of local CO_2 respiration.

2.2.1.3 Case Study 2: June 7, 1993

This day (Figure 2.5) is substantially different from June 10. Mean winds are predominantly westerly at speeds greater than 6 m s^{-1}. Speed and direction changes are small, giving a day without the complexity of a varying source area location.

High westerly winds begin on June 6 after 2100 PST, and before the nocturnal CO_2 concentration has reached its maximum nighttime value. The rapid decrease in CO_2 concentrations is due to effective mixing and a change from winds being light easterly, or calm, to very strong westerlies. The westerlies bring in air that should be close to background, as the ventilation rate is rapid enough to allow little modification from sources and sinks along the fetch to the tower, as evidenced by the low standard deviations (approximately 0.5 ppmv).

After the initial change, the concentration rises slowly until a maximum is reached around the time of rush hour, 0600-0700 PST. The rise, due to soil respiration and anthropogenic emissions, reaches peak mean CO_2 concentrations of 372 ppmv; much lower than for the composite (Figure 2.3). This is attributed to the strong winds allowing background air to reside over soil CO_2 sources for only a short time. An absolute minimum on the previous day of 351.2 ppmv, the lowest concentration recorded, alludes to the possibility of background CO_2 concentrations being less than 369.4 ppmv. Unfortunately both background and tower concentrations could not be measured simultaneously, but it is expected that the background concentration can differ by as much as 4 ppmv over the
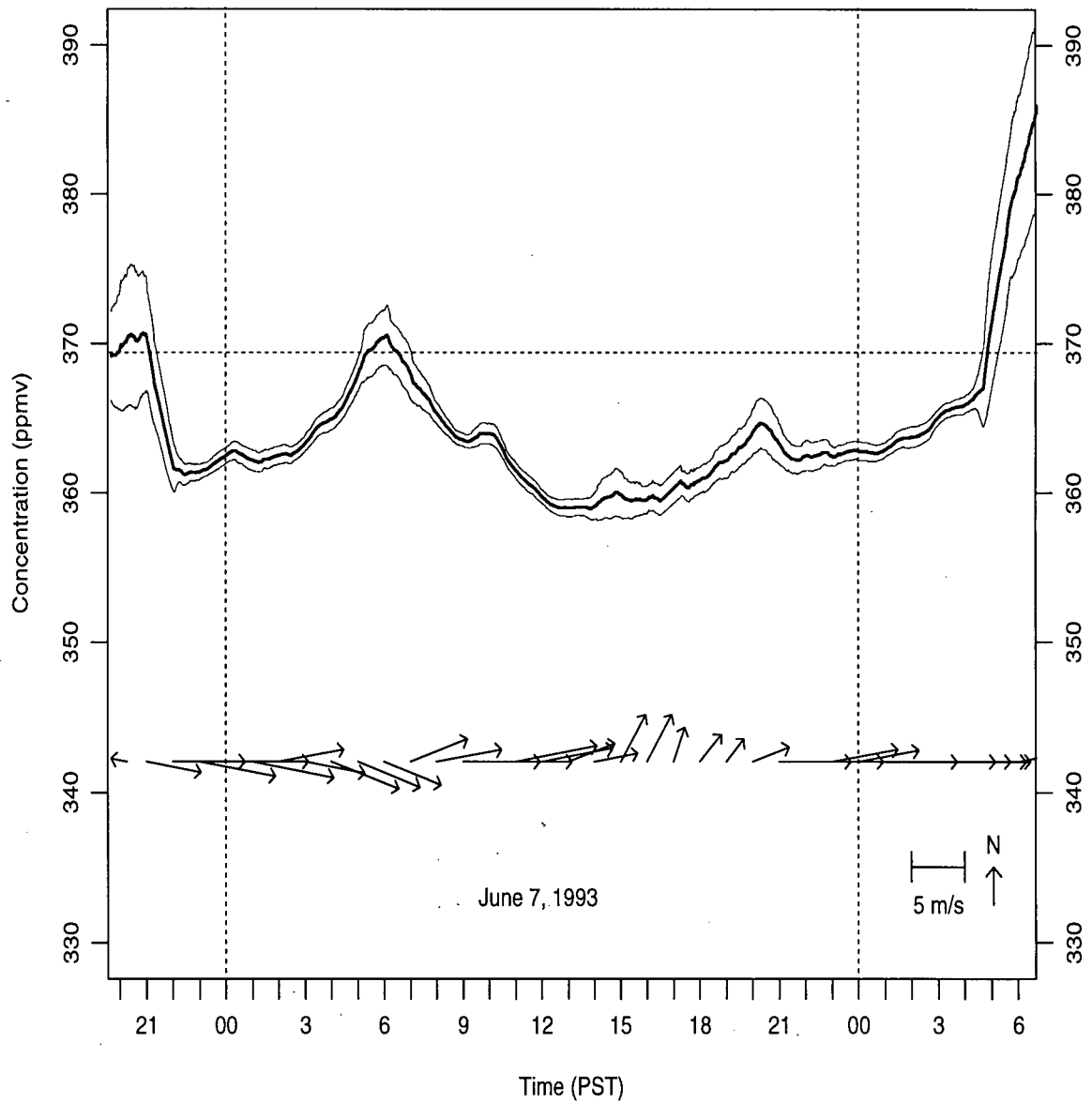
Figure 2.5: Atmospheric CO_2 concentration trace for June 7, 1993. The thick line indicates observations smoothed by a 60 minute running mean. Thin lines indicate one standard deviation on either side of the mean. Hourly wind observations are shown as vectors. The background concentration (369.4 ppmv) is shown as a dotted line.

course of a day.

The overall diurnal pattern is similar to the composite, although decreased in amplitude. After the early morning maximum, the CO_2 concentration decreases under unchanged wind conditions. Afternoon mean CO_2 concentrations are near 359 ppmv. The evening rise in concentration, like the decrease, is at a much reduced rate. At 0400 PST winds become much lighter; thus the trace is influenced much more by local sources. The concentration increases dramatically in less than an hour.

2.2.1.4 Boundary Layer Processes

The role of boundary layer structure and dynamics, specifically the role of mixed layer heights, growth and collapse has already been mentioned. The significance of the mixed layer on boundary layer CO_2 concentrations is difficult to quantify without concurrent observations of both. However, it is suggested that the boundary layer concentration of a pollutant with surface sources is related to the volume of air available for vertical mixing from the surface to the top of the mixed layer (Hosler, 1966; Hanna *et al.*, 1982), especially over an urban surface (Oke, 1995).

Summer daytime variations of mixed layer heights have been studied in Vancouver (Steyn, 1980). Typically the summertime convective mixed layer grows shortly after sunrise and reaches maximum values of about 400 to 600 m near mid-day. The transition to a nocturnal boundary layer has not been well observed in Vancouver. However, it is expected that soon after sunset the daytime mixed layer collapses. Oke (1995) suggests that, unlike rural sites where the characteristic nocturnal boundary layer is a stable one, the urban site is characterized by a shallow mixed layer (100 - 300 m), due to surface heat fluxes caused by the urban heat island effect and increased surface roughness. Nocturnal mixed depths are probably near the lower end of the range at Sunset because it is a

suburban site.

Important for the vertical mixing of CO_2 at this site is the observation that urban mixed layers have particularly intense turbulence (Oke, 1995). Diurnal variation in mixed heights affects diurnal CO_2 concentrations by varying the volume in which emissions of CO_2 are diluted. Thus, the significance of surface CO_2 sources on boundary layer CO_2 concentrations are inversely related to the mixed depth. However, CO_2 sources are not only surface ones. CO_2 has a long atmospheric lifetime, which causes CO_2 to be mixed throughout the troposphere. The concentration is dependent on height and latitude (Boden *et al.*, 1991). This creates an additional boundary layer source of CO_2 above the mixed layer.

A study of vertical CO_2 profiles over parts of North America (R. Desjardins, Centre for Land and Biological Resources, Research Branch, Agriculture Canada) indicates that CO_2 concentrations increase slightly with height within the lower troposphere in summer and that the concentration of CO_2 above the mixed layer differs from that within by ≤ 5 ppmv. Because of this, entrained CO_2 during mixed layer growth is different from CO_2 within the mixed layer. As the mixed layer grows, CO_2 concentrations are affected by entrained CO_2, which may be higher or lower than that of the mixed layer, depending on the time of day.

The importance of mixed layer depths will be examined more closely from analysis of modelling results in Chapter 4. Model design will include explicitly the height of the mixed layer, and a concentration of CO_2 above. Interactions between the two controls of changing mixing volume and entrainment on CO_2 concentrations will be made.

2.2.1.5 Conclusions

The first sampling period shows large changes in CO_2 concentrations on summer days. The changes are due to processes at different scales, with the concentration measured at

the Sunset site depending on turbulence and mixing, boundary layer structure, temporal and spatial distribution of sources and sinks, and meteorology. Also evident is the prominent diurnal pattern shown by a composite CO_2 graph (Figure 2.3)

During this summer period an anthropogenic signal is difficult to distinguish in the observations. Large anthropogenic emissions are overcome by greater mixing, transport, and photosynthesis during the day. The effect of anthropogenic emissions may be to generally raise concentrations above that expected by the global monitoring network (approximately 360 ppmv), but diurnal signals are masked by larger ones imposed by the biosphere and boundary layer processes. High CO_2 variance, especially while mixed layer heights are low, may be evidence of mobile point source emissions.

Generally it was observed that air advecting from the east was higher in CO_2 concentration than air from the west. The south-east direction gave the highest daytime CO_2 concentrations, due to the close proximity of a congested intersection. The highest nocturnal concentrations were observed during light easterly wind conditions.

Although difficult to quantify from the data, it is thought that an accumulation of CO_2 could occur in the study area during particularly stagnant periods. Prolonged anticyclonic conditions allow surface flow reversal at night which tends to bring air from the previous day back across the study area. Many days of such flow, with poor ventilation, could cause CO_2 concentrations to rise. Similarly, the passage of a frontal system with strong winds could flush the area and bring concentrations down to background concentrations (Spittlehouse and Ripley, 1977).

For the above reasons it may be difficult to determine a seasonal trend because of the related decrease in concentration due to the biosphere being a net sink in June. However from Figure 2.2, there is an indication that the mean daytime minima concentrations decrease as expected. This is most clearly seen in the days following June 14.

2.2.2 Second Sampling Period (September 3 - 6, 1993)

This period, near the end of the summer, had many differences compared to the first period. Notably photosynthetic activity of the biosphere had decreased, and continues to decrease as the early stages of senescence are reached (Kim and Verma, 1990; Wofsy *et al.*, 1993). The aggregate summertime effect of biospheric photosynthesis is to draw down background concentrations to about 353 ppmv at this latitude, as reported by the global monitoring network (Trivett and Higuchi, 1989; Boden *et al.*, 1991). The lowest background CO_2 concentrations are recorded in August, suggesting that afterwards the biosphere becomes a net source of CO_2. Temperatures are generally warm, reaching maxima in the mid-twenty degrees Celsius. Precipitation is nil during the period, and was low in the previous weeks.

Synoptically the study area is situated under a dominant high pressure system, bringing a very weak gradient over Vancouver. A weak low off the coast of Vancouver Island produced weak onshore upper level winds from the south-west. With high temperatures on September 3, 5 and 6, a sea/land breeze circulation set up. Poor ventilation, accompanied by prolonged flow reversal at night, appears to bring the mean upwind concentration to levels much above the expected background concentration. At this time when the study region is a net source of CO_2 (from anthropogenic and biospheric emissions) and transport and mixing is weak, concentrations should rise. Measured upwind (westerly) concentrations just before this period gave a background concentration of about 368.6 ppmv, only slightly less than the June period.

The concentration trace for September 3 - 6, 1993 (Figure 2.6) is quite similar to the traces for the June period. The major diurnal cycle is clearly evident and is of a larger amplitude than June (Table 2.2) albeit is derived from a smaller sample. While
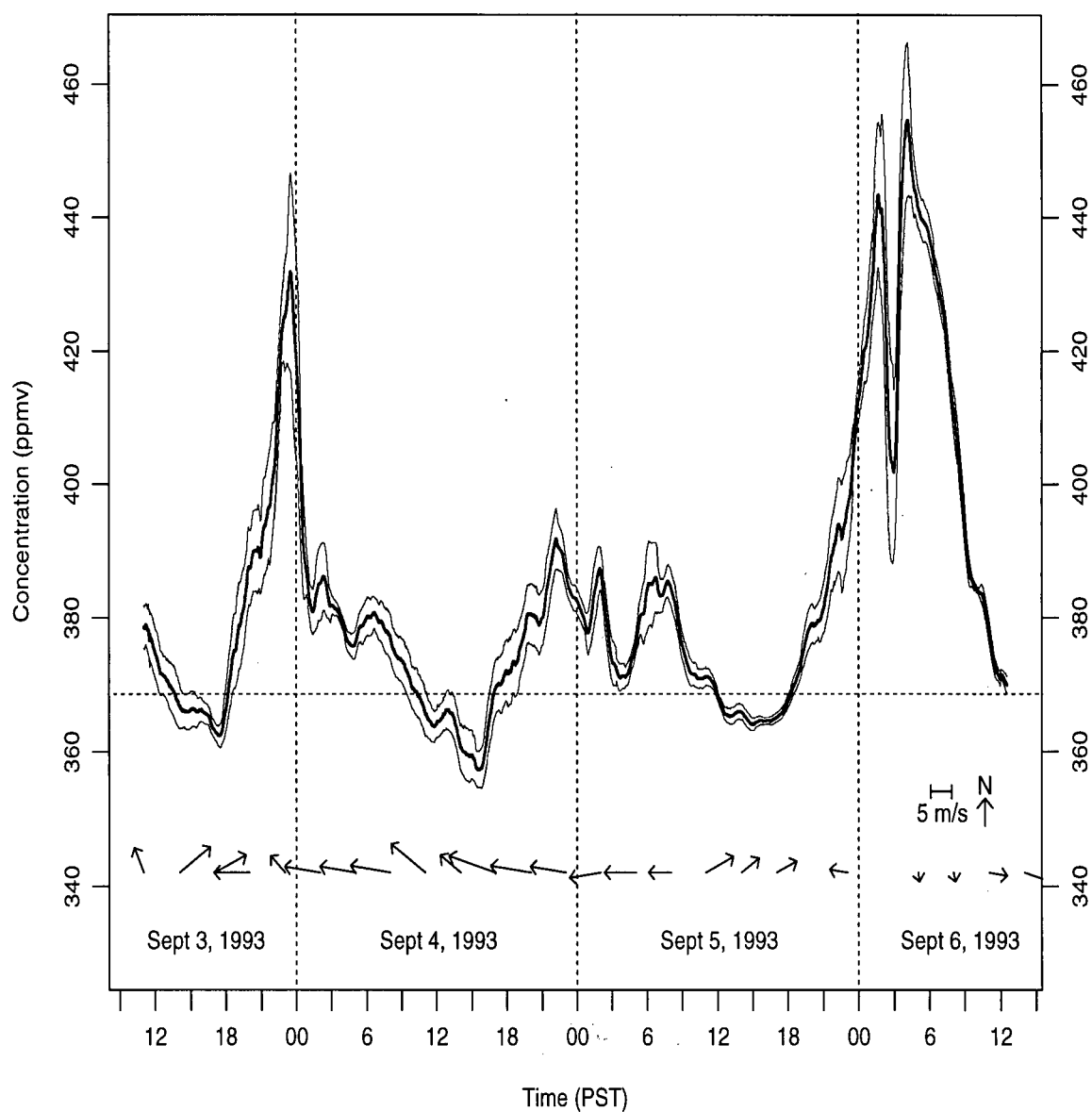
Figure 2.6: Atmospheric CO_2 concentration trace for September 3 - 6, 1993. The thick line indicates observations smoothed by a 60 minute running mean. Thin lines indicate one standard deviation on either side of the mean. Hourly wind observations are shown at three hour intervals. The background concentration (368.6 ppmv) is shown as a dotted line.

Table 2.2: Daily mean nighttime and daytime CO_2 concentrations used to evaluate major diurnal cycle for September 3 - 6, 1993. All CO_2 concentrations in ppmv. Standard deviations are calculated for observations 2 hours on either side of the extrema in the mean CO_2 concentrations.

Date Sept/93	Sample Height	Mean Daytime	σ	Mean Nighttime	σ	Amplitude
3	H2	362	2.6	426	17.0	64
4	H2	357	4.5	389	6.0	32
5	H2	364	1.4	445	24.8	81
Avg.		**361**	**2.8**	**420**	**15.9**	**59**

the daytime mean minimum (361 ppmv) is similar to the average in June (360 ppmv), the mean nighttime maximum is considerably higher (411 vs 387 ppmv). The difference between the extreme CO_2 concentrations is large, with an absolute maximum of 478.3 ppmv and an absolute minimum of 353.2 ppmv. The amplitude of the major diurnal CO_2 variation is 59 ppmv, considerably larger than that of June (40 ppmv).

The reasons for this are twofold. First, it is possible that under anticyclonic conditions the nighttime mixed layer was shallower under a stronger inversion, thus containing the respiratory source within a smaller volume. Secondly the biosphere is a net source at this time of year. The decrease in daytime photosynthesis explains the reduction in the magnitude of the drawdown below background when compared to June. However, nighttime biospheric respiration remains high, because this is the time when soil organic matter from litterfall is high, and temperatures favour decomposition (Peterjohn *et al.*, 1994).

The traces themselves can be explained in the same manner as the previous period and will not be repeated. One notable difference is the V-shaped drawdown of September 3 and 4. On September 4 the wind is primarily east and south-east. Near 0600 PST there is a marked increase in variance in response to the morning rush hour, and remains high

throughout the day. The morning rush hour is followed by a steady decrease in mean CO_2 concentrations, which is unlike most days in June which exhibit a gradual drawdown with a levelling off in mid-afternoon. With photosynthesis becoming less significant, it is possible that the afternoon increase in CO_2 concentration begins earlier in response to the afternoon mobile emissions maximum at 1400-1700 PST, thus reducing the amount of time that the concentration remains level after drawdown.

2.2.3 Third Sampling Period (January 12 - February 11, 1994)

Compared to the summer periods, the observed CO_2 concentrations in the winter show greater variability, and a pattern that is more irregular. The winter diurnal trace is generally characterized by more than one major maximum and minimum in mean CO_2 concentrations. These maxima and minima appear to be readily explained by wind direction and wind speed changes, rather than periodic diurnal processes. The range of concentrations observed over a given day are shown in Table 2.3. The mean maximum and mean minimum are determined from extrema using a running mean of approximately 2.5 hours. For days with more than one maximum or minimum, the more extreme is listed in Table 2.3.

The trace for January 12 - 15 (Figure 2.7) is shown as an example of wintertime CO_2 concentrations. Similarities between these days and most others are: 1) very high concentrations when compared to background, 2) rare occasions when concentrations fall below background, 3) the lack of a repeated diurnal signal, 4) a large diurnal range, and 5) the large concentration changes over short periods.

The very high CO_2 concentrations are probably a result of increased anthropogenic emissions during the winter period. Mobile emissions are similar to those of summer, but stationary emissions (from combustion of natural gas for residential use) increase by as

Table 2.3: Daily mean CO_2 minima and maxima for period of Jan. 12 - Feb. 11, 1994, determined from a 2.5 hour running mean. All CO_2 concentrations in ppmv. Only days with complete observations are shown.

| Date Jan/94	Sample Height	Mean Maximum	Mean Minimum	Range (ppmv)
13	H2	415	380	35
14	H2	460	380	80
15	H2	400	370	30
16	H2	405	365	40
17	H2	445	375	70
18	H2	430	390	40
19	H2	450	368	82
20	H2	530	440	90
21	H2	440	380	60
22	H2	410	380	30
23	H2	405	385	20
24	H2	455	395	60
25	H2	480	405	75
26	H2	450	405	45
27	H2	450	400	50
28	H2	530	420	110
29	H2	590	430	160
30	H2	490	410	80
31	H2	600	410	190
Feb/94				
2	H2	580	420	160
3	H2	570	415	155
6	H2	440	380	60
7	H2	435	395	40
8	H2	465	400	65
9	H2	450	395	60
10	H2	460	385	75
11	H2	430	375	55
Avg.		**469**	**395**	**74**
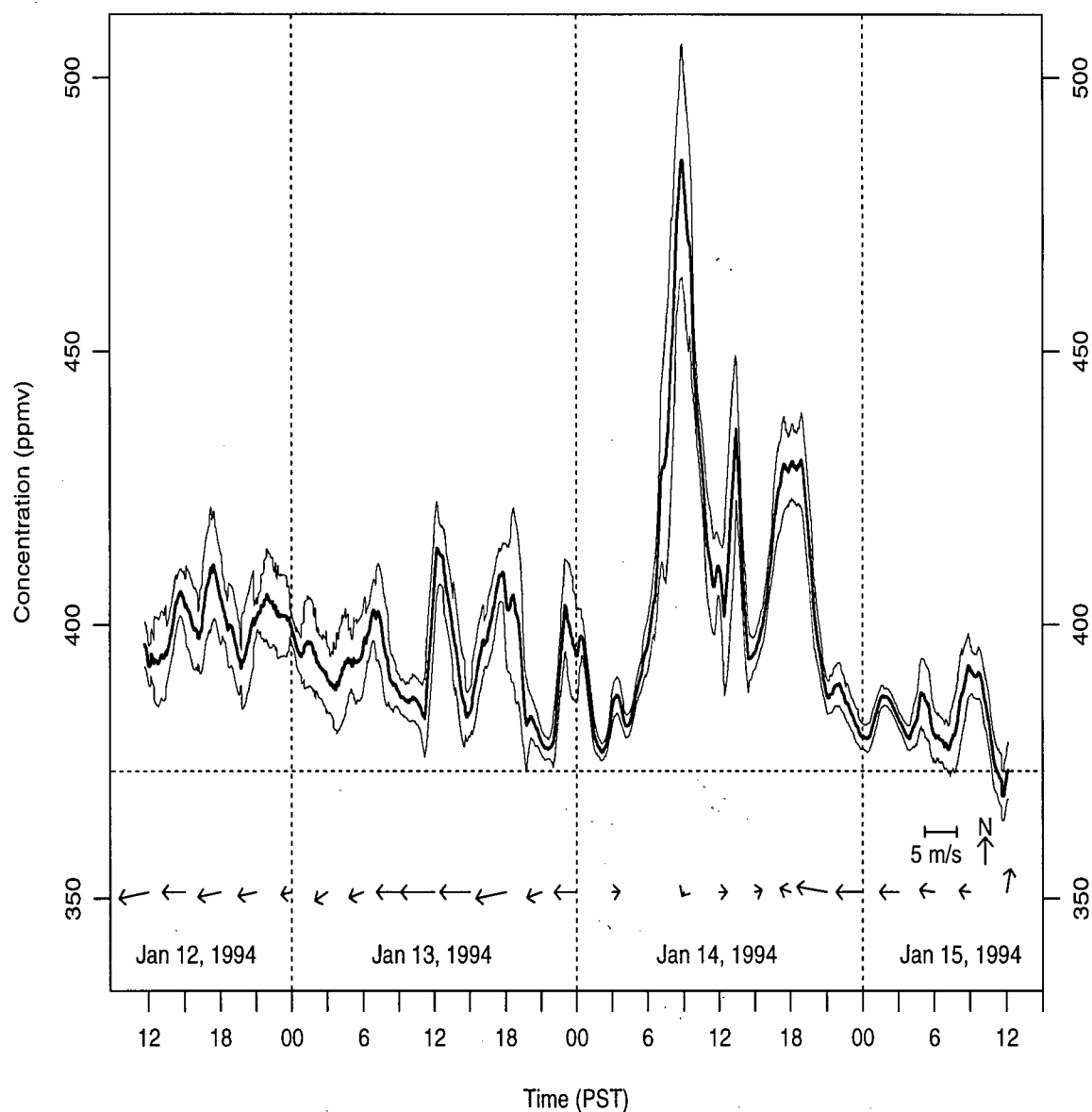
Figure 2.7: Atmospheric CO_2 concentration trace for January 12 - 15, 1994. The thick line indicates observations smoothed by a 60 minute running mean. Thin lines indicate one standard deviation on either side of the mean. Hourly wind observations are shown at three hours intervals. The background concentration (373 ppmv) is shown as a dotted line.

much as five times (Statistics Canada, 1994). In addition the biosphere is a small net CO_2 source at all times. Although respiration decreases with temperature, the photosynthetic sink decreases even more from summertime values (Verma *et al.*, 1992; Dörr and Münnich, 1987; Wofsy *et al.*, 1993). Without a significant sink for CO_2 the net flux is markedly increased. Since this is added to a shallower mixed layer in winter, the resulting CO_2 concentrations can be very high, and are almost entirely above background at this time (373 ppmv).

Under these conditions small changes in wind direction or wind speed have a large effect on the CO_2 concentration. When winds are calm, strong local emissions are able to rapidly bring concentrations up to over 500 ppmv. This buildup can occur at any time of day. On February 1 (Figure 2.8) the highest concentration observed, 748.2 ppmv, occurred under very light wind conditions and during mid-morning when emissions are high. The large changes in concentration observed on January 13 (Figure 2.7) are also typical of poor mixing. Concentration "jumps" of up to 25 ppmv are probably due to the effects of local sources, superimposed on a background of poorly mixed air advected across the tower by light easterlies.

The large diurnal range in concentration (Table 2.3) is in part due to the influence of background CO_2 concentration upon conditions of very high CO_2 buildup. The background concentration is roughly estimated to be 373 ppmv, with some variability. Very high concentrations (400 to 500 ppmv) can be decreased rapidly if westerlies bring in background air. Examples are found on January 30 and 31 (Figure 2.8) when the trace initially exhibits both high variance and high concentrations (over 550 ppmv), but the onset of a moderate westerly wind drops values to about 410 ppmv in as little as two hours. The winds promote mixing of local emissions, reduce the variance, as well as introducing background air. The return to light, or easterly winds results in a sharp rise of concentration. The minimum of 410 ppmv is still well above background. It is likely due
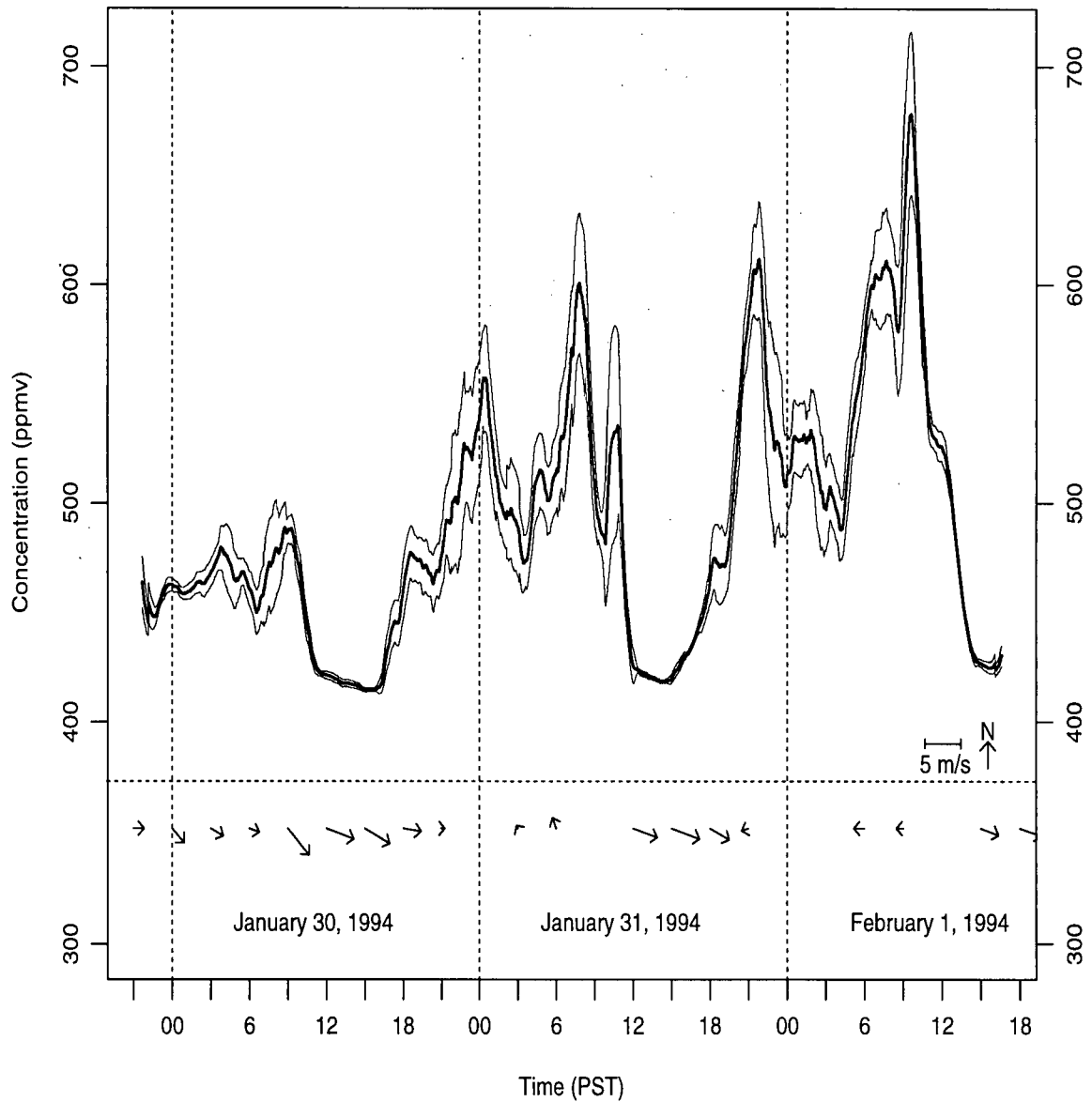
Figure 2.8: Atmospheric CO_2 concentration trace for January 30 - February 1, 1994. The thick line indicates observations smoothed by a 60 minute running mean. Thin lines indicate one standard deviation on either side of the mean. Hourly wind observations are shown at three hour intervals. The background concentration (373 ppmv) is shown as a dotted line.

to the buildup of CO_2 during a period without prolonged westerlies to ventilate the study area. Concentrations approach background on very few days. The lowest concentration observed, 359.4 ppmv, was sampled after a prolonged period of westerly flow on January 16.

The typical winter trace is much more irregular and, in contrast to the summer, there is usually no predominant diurnal cycle. January 14 clearly shows two daytime maxima, and a minimum at night. This clearly indicates the significance of daytime emissions on the CO_2 trace. However, the effects of mixing can dominate over the temporal distribution of emissions, as the observations can show both daytime and nighttime maxima and minima, depending on wind speed and direction. The traces for this period show similarity to the summer period on days when the wind is easterly at night and westerly at some time during the day. Examples of this can be seen in the traces for January 30 and 31 (Figure 2.8). However the magnitude of this feature (approximately 150 ppmv) is much larger than the diurnal amplitude in the summer, and is caused by the mean flow, not photosynthesis.

2.2.4 Discussion of Temporal Variability

The observations show the summer to have a clear diurnal signal with usually only one maximum and minimum. Concentrations can be explained in terms of mixing and the spatial and temporal distributions of sources and sinks. The wintertime observations are harder to explain, in that concentrations can change quickly in a seemingly erratic manner due to changes of wind speed and direction. The effect on CO_2 of wind speed and wind direction is greater during this period, due to the much greater net emissions having raised concentrations well above background. The wintertime mixed layer is expected to be shallower and so may respond more quickly to changes in ventilation, and the effect

of a varying source area. In contrast summertime traces are smoother, suggesting better mixing through a larger volume.

Seasonal differences in the biosphere, the nature of the convective mixed layer, and the presence or absence of a land/sea breeze circulation are important to CO_2 concentrations. The seasonal cycle of the biosphere allows for a seasonal change in background concentration. In winter there is little evidence of reduction of CO_2 below background, indicating that the biosphere is a net source of CO_2 at all times. In summer, large changes in the mixed depth affect CO_2 concentrations due to dilution. In winter the relatively more constant and shallow mixed layer depth (Oke, 1995) allows the role of wind speed and direction to be more important to concentrations. Also, the effect of a periodic land/sea breeze circulation is not evident because this circulation is not readily established in winter (Steyn and Faulkner, 1986).

All periods show the difficulty of interpreting CO_2 measurements. Being virtually inert in the troposphere, CO_2 is long lived and well-mixed. Consequently CO_2 concentrations depend not only on the surface source and sink distribution, but also on the background CO_2 both within and above the mixed layer. Further, it is difficult to resolve the CO_2 advected across the tower into its contributing components. CO_2 concentrations at a site are due to the spatial and temporal patterns of the local sources and sinks, mixing of background air, mixing of air from above the mixed layer, and to flow reversal.

A model is developed in the next chapter to help elucidate the relative importance of these components, and to model diurnal summertime CO_2 concentrations.

2.3 Sampling Results - Spatial Variability

The spatial variability of CO_2 concentrations was studied by conducting brief sampling at locations away from the Sunset Tower site, near areas that were thought to be strong sources or sinks of CO_2. Spatial and temporal CO_2 variability, as measured by time series at the tower, are linked by wind direction and wind speed. CO_2 variability on the temporal trace is, in part, a manifestation of spatial variability of sources and sinks, as CO_2 is advected across the tower from different source areas.

Forest canopy

Measurements were made within the canopy of the forest in Pacific Spirit Park in order to evaluate the temporal variations at this site, and to compare it to the suburban tower traces. A smoothed trace of CO_2 concentrations for a 24 hour period from September 6-7, 1993, within Pacific Spirit Park (at 1.5 m) is shown in Figure 2.9. The shape of the diurnal trace is similar to that seen at the Sunset Tower. However, the diurnal amplitude (83 ppmv) is considerably greater than the average amplitude of all the summer observation periods.

The increase in amplitude at this site is mostly attributable to increases in nighttime concentrations. Daytime CO_2 concentrations are similar to that observed at the tower during all summer periods, but mean nighttime maximum concentrations (approximately 444 ppmv) are as much as 57 ppmv greater than mean summertime nocturnal concentrations.

This nocturnal buildup can possibly be explained by the containment and increased storage of CO_2 below the forest canopy (Woodwell and Dykeman, 1966). Diffusion of CO_2 from soil and dark respiration is inhibited within the roughness elements of the
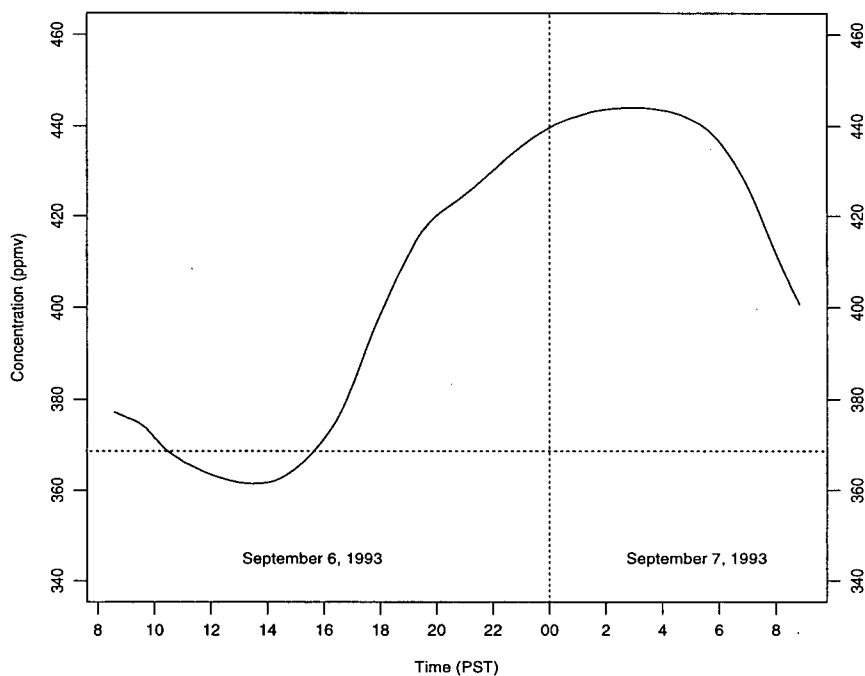
Figure 2.9: Smoothed Atmospheric CO_2 concentration trace for September 6 - 7, 1993, from within forest canopy of Pacific Spirit Park. Sampling height is 1.5 metres. The background concentration (368.6 ppmv) is shown as a dotted line.

forest canopy. Further, the exchange of air from within the canopy with that above is reduced, especially under calm nighttime conditions. Another sampling site, still within the forest canopy of Pacific Spirit Park, indicated similar nocturnal CO_2 buildup with concentrations near 450 ppmv on the same night.

Street canyon

Measurements were made adjacent to a major downtown Vancouver roadway subject to high CO_2 emissions from combustion from numerous point sources. This site exhibited some of the highest concentrations observed, with a maximum of 721.2 ppmv, observed

at 1.5 metres. The average concentration, measured during the daytime on June 2, 1993, was 420 ppmv, with a standard deviation of 29 ppmv. Compared to the summertime tower measurements the daytime mean and temporal variability at this site was very high. Standard deviations at the tower during the daytime were typically only 1 to 5 ppmv. Background concentrations had a standard deviation of less than 0.5 ppmv.

Mobile transect

A relatively crude look at spatial variability on a short timescale was made by mounting the inlet hose at 1.5 metres above the road near the front of a moving vehicle. Transects at the western end of the study area were made near 2000 PST so as to reduce contamination from automobile emissions. The route of one such vehicle traverse is shown in Figure 2.10. Sampling results along this route (Figure 2.11) are matched by letters to the location of the sample in Figure 2.10. The time from point A to point G is 30 minutes. Winds during this period were light easterlies, or near calm.

The trace indicates that there is considerably more spatial variability of CO_2 concentrations than the temporal variability observed at the Sunset Tower. Standard deviations for CO_2 time series of 30 minutes at the tower are below 8 ppmv. For the transect in Figure 2.10, one standard deviation is 28 ppmv. Similar transects indicate that standard deviations for mobile sampling is commonly near 28 ppmv. Low standard deviations of CO_2 concentrations at the tower indicate that the spatial variability of CO_2 near the surface is relatively well-mixed at the tower sampling heights. The large concentrations near 2010 PST are attributed to sampling within close proximity of a vehicle.
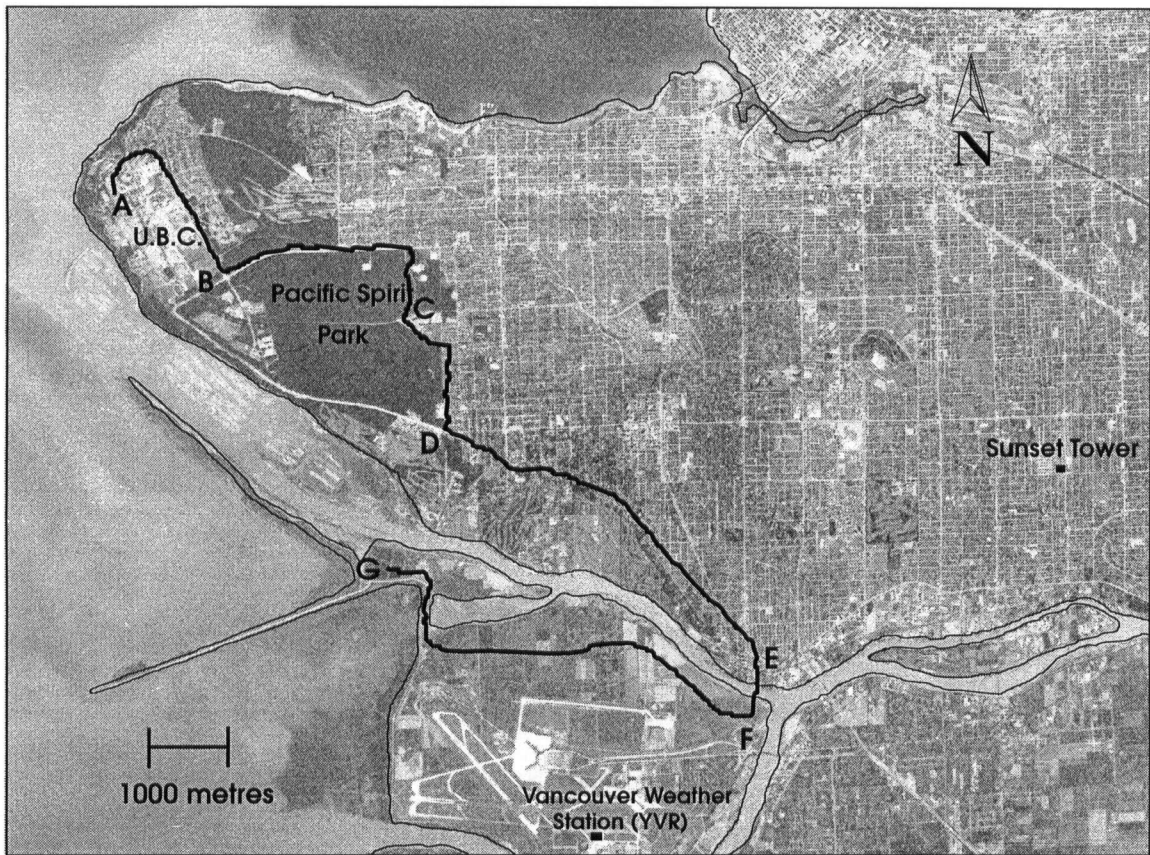
Figure 2.10: Route of mobile sampling on September 7, 1993.
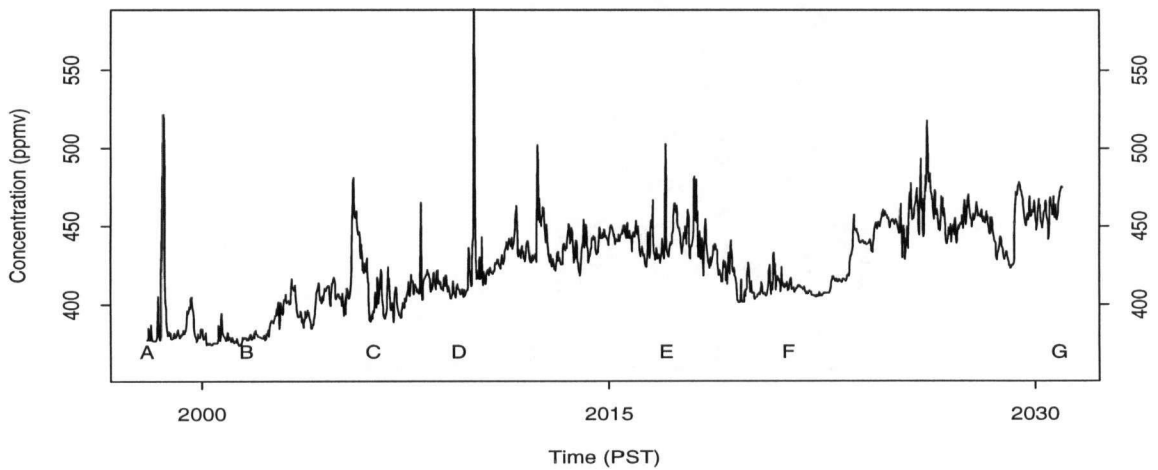
Figure 2.11: Atmospheric CO_2 concentration transect for September 7, 1993, collected from a vehicle at a height of 1.5 metres.

Chapter 3

Multiple Box Model for CO_2 in the GVRD

3.1 Introduction

The model described here is designed to simulate gross features of the observed diurnal CO_2 concentration variation (Chapter 2). A multiple-box model, which is ideal for the description of temporal variability (diurnal in this case) but is not necessarily appropriate to a reasonable (or realistic) realization of spatial detail (Lettau, 1970) is considered appropriate. Assumptions of rapid and uniform mixing, and homogeneous areal sources and sinks across the large surface area of each box reduces the spatial resolution of the model. Boundary layer effects are incorporated by bounding the model vertically by a variable height convective mixed layer, which has been studied and modelled in this region (Steyn, 1980; Steyn and Oke, 1982), giving good temporal resolution for the model.

Box models have been widely used to simulate mean concentrations of atmospheric pollutants, including ozone (Demerjian and Schere, 1979), sulphur dioxide (Randerson, 1970; Jensen and Petersen, 1979; Giovannoni and Swan, 1988), and suspended particulate (Reiquam, 1970). Simplicity is a primary feature of box models. They illustrate that if the significant processes are adequately modelled, important information on concentrations can be obtained using little more than mass balance considerations. Although most models of this type involve similar assumptions and limitations, the actual layout and design of the model is specific to the problem at hand, and often to physical or

53

topographical constraints (Giovannoni and Swan, 1988).

Previous studies illustrate the successful use of box models with very different structures. Simulations of ozone have been successfully obtained using a single box model, with horizontal dimensions 32 km square, bounded vertically by the height of the inversion base (Demerjian and Schere, 1979). The model included emissions of ozone precursors, advection, entrainment, dilution, and chemical reactions. Computed ozone concentrations within the box are similar everywhere, due to the assumption of instantaneous vertical mixing to the top of the variable mixed layer.

In contrast, a more complex two-dimensional box model was developed by Ragland (1973). It includes 24 boxes in the vertical (of varying height) to the top of the mixed layer, and 40 boxes in the horizontal, each 300 metres long. Mass conservation equations were solved for each box, accounting for pollutant emissions, advection, and vertical mixing. Vertical mixing between boxes was defined by a height dependent turbulent eddy diffusivity. The model of Demerjian and Schere (1979) relies on near surface wind observations, while the model of Ragland (1973) calculates mean planetary boundary layer winds dependent upon stability. Both models require mean winds to be from a relatively constant direction during model simulation. This chapter will discuss assumptions involved in box modelling of CO_2, the structure of the model developed for CO_2 at the study site for this research, and the inputs to the model necessary to successfully simulate diurnal CO_2 concentrations.

3.2 Assumptions

The major assumptions of the box model developed here are that:

- CO_2 source and sink terms (Q) are primarily of an areal nature, whereby the source or sink strengths are distributed uniformly across the lower surface of the box ($\frac{\partial Q}{\partial x}, \frac{\partial Q}{\partial y} = 0$), and
- CO_2 is mixed rapidly and uniformly throughout the box, giving uniform CO_2 concentrations (C), ($\frac{\partial C}{\partial x}, \frac{\partial C}{\partial y}, \frac{\partial C}{\partial z} = 0$).

The first assumption is necessary in order to rationalize a part of the second assumption, namely that mixing in the horizontal (independent of vertical mixing) is complete. The areal source/sink assumption is an interpretation of the degree to which surface homogeneity is achieved for a given horizontal scale. Although, for example, automobiles are actually point source emitters of CO_2, for a box of sufficient dimensions the CO_2 emissions, essentially following a gridded road structure, become regular line sources, and at even larger scales can be merged to form a relatively homogeneous distribution of area sources.

Box dimensions for this study vary, with the smallest boxes being 1.9 km square. Justification for concluding that small scale surface heterogeneity is a homogeneous distribution of sources and sinks at this scale is difficult, although intuitively it appears reasonable, because there is regular spacing of roads (approximately 14 roads across one horizontal dimension of the box), suburban dwellings, suburban lawn, and suburban trees. This assumption allows the source/sink strength to remain spatially constant across the lower surface of the box, leading to the assumption that CO_2 is mixed uniformly throughout the box. Thus, diffusion from point sources need not be considered,

as the very large number of point sources within each box can be treated as a single areal source or sink. The only major surface heterogeneity observed is in the distribution of large parks throughout the study region.

The second assumption, that of uniform mixing throughout the box, can be divided into horizontal and vertical components. Uniform mixing in the horizontal is achieved if the assumption of homogeneous areal sources and sinks is good. The assumption of uniform vertical mixing is more difficult to justify. The multiple-box CO_2 model of this study assumes that vertical mixing efficiency is sufficient to ensure that CO_2 is well-mixed up to the height of the inversion base. A timescale for full vertical mixing in a convective boundary layer can be defined by:

$$t_c = \frac{z_i}{w_*} \tag{3.1}$$

where z_i is the height of the inversion layer defining the top of the mixed layer, and w_* is a convective velocity scale and,

$$w_* = \left(\frac{g z_i}{\overline{\theta_v}} (\overline{w'\theta_v'})_s\right)^{\frac{1}{3}} \tag{3.2}$$

For typical midday summertime mixed layer depths near 500 m (Steyn and Oke, 1982), surface heat fluxes $(\overline{w'\theta_v'})_s$ near 0.30 K m s^{-1} and virtual potential temperatures near 300 K, t_c is about 5 minutes.

For each box, the model deals with a single CO_2 concentration within the mixed layer, constrained by a surface CO_2 mass budget applied to an atmospheric volume bounded by the variable top of the mixed layer. Evidence for efficient horizontal and vertical mixing can be found by comparing CO_2 concentrations measured during the transect at 1.5 m (Figures 2.10 and 2.11) with the tower observations at 5.0 and 22.5 m above ground.

The spatial CO_2 variability is high, with concentrations varying by as much as 70

ppmv over less than 5 km. If CO_2 concentrations are stationary, then similar variability should be seen on a temporal trace observed at the tower, as CO_2 is advected across the tower by the mean wind. Mean wind speeds of 2.5 m s^{-1} give a timescale of approximately 30 minutes over which to observe similar CO_2 variability as that observed during the transect. However, variability of this magnitude is not observed at either of the two tower measuring heights. Standard deviations of CO_2 time series are about 4 times less at the tower.

This analysis gives confidence to the assumption that CO_2 variability from small scale surface heterogeneity is efficiently mixed horizontally between the surface and, at least, the tower measuring heights. As mentioned previously, there were no discernible differences in measurements of CO_2 at 5.0 m and 22.5 m on the tower, indicating that there was no significant source or sink (as atmospheric storage) of CO_2 between the two measuring heights. To infer from this that CO_2 is mixed uniformly throughout the mixed layer is tenuous. Such a bold assumption is valid only if the vertical mixing of CO_2 is not limited by vertical diffusion, but only by the inversion at the top of the mixed layer. This is not likely to be the case (Tennekes, 1976), but the depth of the convective mixed layer may be a surrogate for the effectiveness of CO_2 transport in a turbulent planetary boundary layer (Gifford and Hanna, 1973), and thus a measure of the extent to which CO_2 is mixed uniformly. The model, as does the discussion throughout this chapter, assumes that daytime mixing is achieved quickly, and a uniform CO_2 concentration is established vertically and horizontally within the bounds of each box.

There is a strong photosynthetic sink for CO_2. Surface sink mechanisms are not fully addressed in the literature, though there may be an analogy to the destruction of ozone through chemical reactions (Demerjian and Schere, 1979). This study treats surface sinks similarly to surfaces sources, in that removal of CO_2 is extracted from the box surface, with uniform concentration reduction throughout the box volume.

3.3 Model Description

The computational grid layout of the model is designed to simulate observed CO$_2$ concentrations at the Sunset Tower from the summer field period of June 1993. A plan view of the spatial limits of the box model within the study region is shown in Figure 3.1. The series of boxes numbered one to eight are aligned with the predominant wind directions observed during the June 1993 study period. Dominant boundary layer winds for this location are generally on a W-NW to E-SE axis (Oke and Hay, 1994), and an examination of winds for June 1993 indicate a prominence of W-NW daytime winds, often due to onset of a sea breeze circulation, with nighttime return flow commonly from the E-SE. The model runs are restricted to days on which this common wind pattern is observed, or to days with very light winds.

The Sunset Tower measurements are most readily modelled when the mean wind is from 280°, parallel to a line drawn from Georgia Strait through each box to the tower site. As there is some variance in mean wind direction, the boxes furthest west from the tower (boxes 1 to 5) are increased in size in the crosswind direction to allow the model fetch to encompass an arc of 10° on either side of 280° (Figure 3.1). The restriction to predominantly westerly daytime flow also ensures minimal contamination of background air by the urban region.

Box dimensions were determined by two important, but conflicting, criteria. The necessity for homogeneity of areal sources and sinks required large boxes, while a high resolution of the mixed layer, and its change in depth from the westward edge of the study area to the tower site, required boxes of smaller dimension along the mean wind direction. Box lengths of 1.9 km in the along-wind direction appear to adequately fulfill both demands.
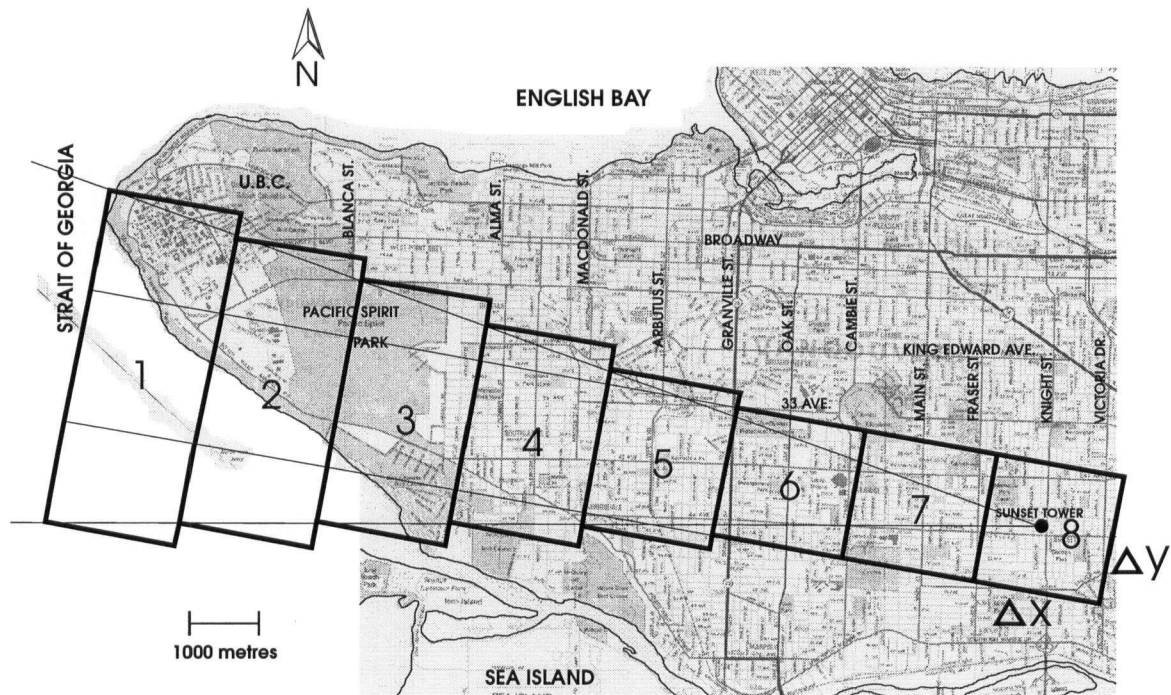
Figure 3.1: Plan view of box model within study region.

If the assumptions of Section 3.2 are met, then the numerical simulation of CO_2 concentration at the Sunset site can be explained by the following CO_2 mass balance equations, based on similar box modelling techniques (Lettau, 1970; Tennekes, 1976; Hanna *et al.*, 1982):

$$
\text{Rate of change of mass of } CO_2 = \text{Sources } - \text{ Sinks} \tag{3.3}
$$
$$
+ \text{ Advection of background } CO_2 \text{ into box}
$$
$$
- \text{ Advection of } CO_2 \text{ out of box}
$$
$$
+ \text{ Entrainment of } CO_2 \text{ from above mixed layer}
$$

$$\frac{d(C\,\Delta x\,\Delta y\,h)}{dt} =$$

$$Q_C\,\Delta x\,\Delta y + \overline{u_j}\frac{\partial(C\,\Delta x\,\Delta y\,h)}{\partial x_j} + C_h\frac{\partial h}{\partial t}\Delta x\,\Delta y \qquad (3.4)$$

Equation 3.4 applied to each box of the model domain, bounded vertically by the height of the inversion base, gives,

$$\frac{\partial C_j}{\partial t} = \frac{1}{h_j}\sum_{i=1}^{n}Q_{ij} + \frac{\overline{u}C_{j-1} - \overline{u}C_j}{\Delta x} + \frac{1}{h_j}(C_h - C_j)\frac{\partial h_j}{\partial t} \qquad (3.5)$$

$$j = box\ number$$

$$i = source\ or\ sink\ type$$

if the source and sink terms are the areally-averaged flux strengths over the lower surface of the box, rendering essentially a two-dimensional mass conservation equation.

In Equation 3.5, C_j is the density of CO$_2$ ($kg\,m^{-3}$) within each box j ($j = 1$ to 8), h is the height (m) of the inversion base, Q_{ij} are source and sink terms ($kg\,m^{-2}\,s^{-1}$) of CO$_2$ in each box, $\frac{\overline{u}C_{j-1} - \overline{u}C_j}{\Delta x}$ is the difference ($kg\,m^{-3}\,s^{-1}$) of advection of CO$_2$ from the adjacent upwind box and CO$_2$ lost through ventilation out of the downwind edge of the current box by $\overline{u}$, the mean wind speed ($m\,s^{-1}$), Δx is the along-wind dimension of the box (in this case 1.9 km), and $\frac{1}{h_j}(C_h - C_j)\frac{\partial h_j}{\partial t}$ is a volume entrainment of CO$_2$ ($kg\,m^{-3}\,s^{-1}$) from above the mixed layer during mixed layer growth. C_h is the density ($kg\,m^{-3}$) of CO$_2$ (assumed constant) above the height of the inversion base.

Lateral (or crosswind) diffusion into or out of the sides of the model boxes is neglected in the conservation of mass equation (Equation 3.5), because it is small compared to the magnitude of the advective (or alongwind) components (Ragland, 1973; Demerjian and Schere, 1979). Furthermore, the array of areal source and sink strengths generally does

not change significantly from within the confines of the box to the immediate surroundings. Diffusion into and out of the box should be of similar magnitude, because the gradient of source or sink strengths is small across the box limits, so that net lateral diffusion is insignificant.

Equation 3.5 relies on accurate specifications of the boundary conditions of background CO_2, entrainment CO_2, and initial CO_2 concentrations for each box, expressed in dimensionless units of ppmv. However, the expression of source and sink strengths as an areal mass flux ($kg\,m^{-2}\,s^{-1}$) necessitates the conversion of constant CO_2 concentrations (C_h, C_0), as well as initial concentrations, from ppmv to kg m^{-3}, and back to ppmv, for comparison of model results to diurnal observations of CO_2 concentrations. The conversion was simply,

$$CO_2\ density\ [kg\,m^{-3}] = CO_2\ [ppmv]\frac{1}{10^6}(\frac{M_{CO_2}}{M_d})\rho_d \tag{3.6}$$

ρ_d, the density of dry air, is used, since the CO_2 concentrations (ppmv) are expressed as a molar ratio in dry air and,

$$\rho_d = \frac{P - e}{R_d T} \tag{3.7}$$

where e, the vapour pressure, is a function of water vapour and atmospheric pressure.

Hourly observations of atmospheric pressure (P), temperature (T), and relative humidity from Vancouver International Airport were used to calculate the density of dry air, which is assumed to be constant below the top of the mixed layer. This assumption is not likely to significantly affect model results, as air density affects only the change in CO_2 caused by the influence of CO_2 fluxes into or out of a box during a given timestep. Compared to the mass of CO_2 in each box, the fluxes are relatively small. Separate

model runs using; a) air density calculated from equations 3.6 and 3.7 with the assumption noted above, and b) an unvarying air density throughout the simulation time period, show differences in modelled CO_2 concentrations of less than one tenth of one ppmv.

Equation 3.5 is coupled to an advective model for the growth of the daytime turbulent mixed layer ($\frac{\partial h_j}{\partial t}$). The mixed layer model, which simultaneously determines mixed layer depth (h), mixed layer potential temperature ($\overline{\Theta}$), and the temperature "jump" across the inversion base (Δ), is fully explained by Steyn (1980), and Steyn and Oke (1982). The addition of a diagnostic equation for CO_2 to the other model variables in the mixed layer model in no way changes its function. A discussion of the meteorological variables necessary for the determination of h, using this model, are presented separately in Section 3.5, as a prelude to an evaluation of the mixed layer depth determined for the CO_2 model discussed here. Suffice to say that the differential equation (Equation 3.5) can be adequately solved when coupled to this model, and is solved numerically using a fourth-order Runge Kutta method (Press *et al.*, 1992). The model time step of 6 minutes remained constant throughout, and is consistent with the timescale for full vertical mixing (t_c).

The other unknowns in Equation 3.5, Q_{ij} and C_h, are discussed in Sections 3.4 and 3.6 respectively. Model wind speeds $\overline{u}$, are hourly observations (at 10 m) from the Vancouver International Airport observing site (Figure 2.10). It is expected that the wind at the airport site is representative of the mean wind within the airshed of the model region from the surface to the top of the mixed layer. Observation of 20 m wind speeds at Sunset tower show close agreement to mean mixed layer wind speeds (Steyn, 1980). However, 10 m winds from the Airport might be different in both speed and direction.

Model wind speeds are significant as a strong controlling mechanism on the degree to which local sources and sinks affect CO_2 concentrations within the final box (number 8). A simple area source formula, from a simplification of Equation 3.5,
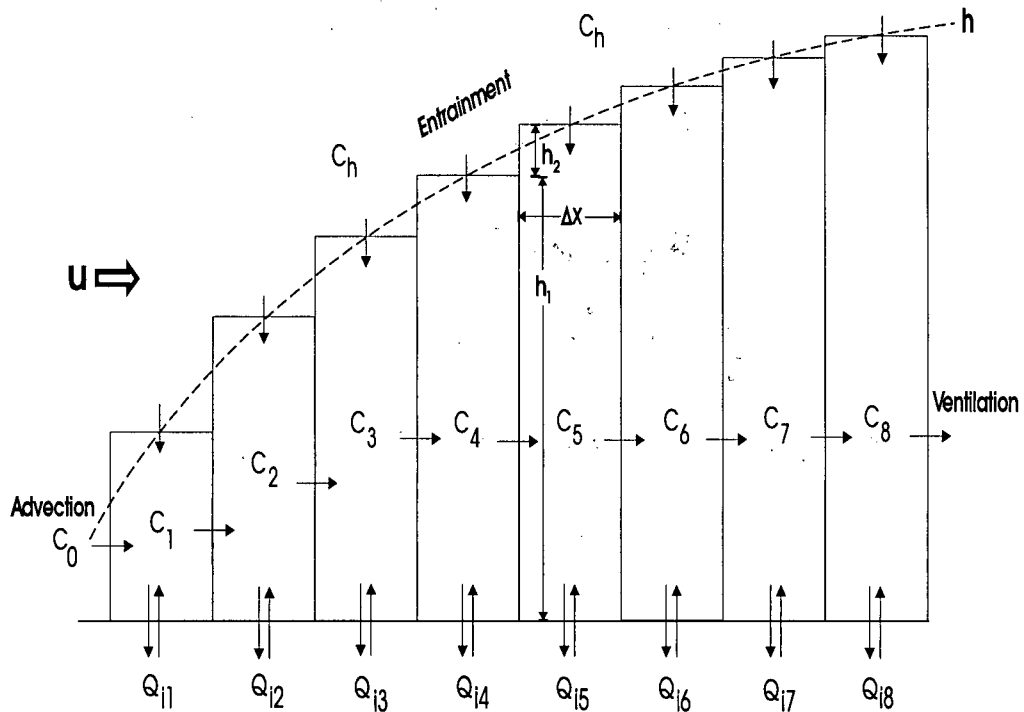
Figure 3.2: Side view of model, showing mixed layer structure.

$$C_j = \frac{cQ_j}{u_j} \qquad (3.8)$$

shows good results compared to more complex models (Gifford and Hanna, 1973). Lower wind speeds allow the air in the box to be affected for a longer time by sources and sinks of CO_2 located within the box. Higher wind speeds both bring in more background air or disturbed air from upwind boxes, and remove CO_2 from the downwind edge of the box at a greater rate.

Figure 3.2 shows a side view of the model structure, with vertical exaggeration of approximately 20 to 30 times. The mixed layer depth is determined independently for each box, giving a physical structure similar to that depicted in Figure 3.2 under ideal conditions (Steyn, 1980).

The consequence of a constant wind direction during model simulation is that the advective component of the mass balance for any given box is dependent only on the concentration of CO_2 within the next upwind box at any given time (C_{j-1}), the concentration within a given box (C_j), and the background concentration (C_0). In the case of box 1 $(j=1)$ then,

$$C_{j-1} = C_0 = \text{background } CO_2 \text{ density } (kg\, m^{-3}) \tag{3.9}$$

The background CO_2 concentration, as discussed in Chapter 2, is 369 ppmv during the simulation period.

At each time step, and for each box, CO_2 advection can occur across the upwind edge of the box, through the faces h_1 and h_2 (Figure 3.2). Background CO_2 is advected through h_2, and well-mixed CO_2 from the adjacent upwind box through h_1. If the depth of the mixed layer decreases in the downwind direction, the advective component will consist solely of C_{j-1}, with no direct contribution from the background concentration.

3.4 Inventory of CO_2 Sources and Sinks

The Urban Carbon Cycle Model (B.C. Carbon Project, 1992) is designed to examine emissions of CO_2 to the atmosphere from activities within the urban area of Vancouver, and to perform an inventory of fixed carbon in both living and non-living form. Included are the emissions of CO_2 categorized by fuel type, emissions of CO_2 through longer timescale oxidation of fixed carbon such as that contained in building materials (Marceau and Lau, 1992), and the role of urban vegetation in both respiring and sequestering CO_2. In this manner the complete impact of the urban area on atmospheric CO_2 can be quantified in terms of CO_2 emissions. Furthermore the Urban Carbon Cycle Model is

part of a plan to construct a mass balance model of carbon for B.C. Other modules in this larger model include a forest carbon cycle model based on a comprehensive budget of carbon within Tree Farm License 44 near Port Alberni, B.C. (Wellisch, 1992), and a waterbodies (reservoirs and lakes) carbon cycle model (B.C. Carbon Project, 1993).

Major anthropogenic sources of CO_2 already determined to exist within the GVRD include emissions from mobile sources, stationary sources (natural gas combustion, fuel combustion for power generation, and fuel wood combustion), process sources (Petroleum refining, and cement production), and solid waste disposal (landfill gas emissions, and solid waste incineration), (B. H. Levelton and Associates, 1990; Jaques, 1992). However, the model region (Figure 3.1) has significant anthropogenic CO_2 emissions from only mobile sources and from the combustion of natural gas, primarily through residential use. The biosphere is known to be a significant nighttime source of CO_2 through the processes of soil, root, and leaf respiration, and a significant daytime sink of CO_2 by photosynthesis (Appendix A). The oxidation of CO to CO_2 is thought to be an important global atmospheric source of CO_2 (Tans *et al.*, 1990), and may be significant near an urban region, where the CO concentrations are high. However, for this study CO is ignored, because the model timescale ($\approx$ 1 day) is much less than the lifetime of CO in the atmosphere (approximately 3 to 4 months, McConnell and McElroy, 1971).

An accurate determination of diurnal CO_2 fluxes to and from anthropogenic and biospheric sources, and biospheric sinks, is crucial to the accuracy of the simulation, before the meteorology is applied. Without accurate flux strengths, model results will be poor, and at best only illustrative of trends in CO_2 concentration, without reasonable reproduction of the magnitudes of such changes. A time-dependent inventory has been carefully prepared for each of the source and sink strengths (Q_{ij}) in Equation 3.5, for each of the 8 boxes and are discussed in the following order: Q_{1j}, mobile CO_2 emissions, Q_{2j}, emissions from natural gas combustion, and Q_{3j}, net biospheric CO_2 fluxes.

3.4.1 Anthropogenic Mobile CO$_2$ Emissions

CO$_2$ from mobile sources accounts for emissions due to fuel combustion from all vehicles operating on the roads of each box, based on vehicle distributions for British Columbia as a whole, including both diesel and gasoline operated vehicles. Most abundant are light duty gasoline vehicles (69% of all vehicles), followed by light duty gasoline powered trucks (22% of all vehicles)(B.H. Levelton and Associates, 1990). Vehicle distributions within the model boundaries may be slightly different.

CO$_2$ emissions from the combustion of hydrocarbons by mobile sources (Q_{1j}) are a function of fuel efficiency (by vehicle type), fuel type (of a known carbon content), completeness of combustion, and distance travelled. Q_{ij} ($kg\,CO_2\,m^{-2}\,s^{-1}$) was calculated as a function of time for each box, j, by:

$$Q_{1j}(t) = \sum_{i=1}^{8} D_{ij}(t)(Eff_i)(Em_i)(Ox)/(3600)(Ar_j) \qquad (3.10)$$

where D_{ij} is the distance in metres travelled by vehicles in each box, sorted into eight vehicle classes i. Vehicle class is defined by vehicle and fuel type, and,

$$D_{ij}(t) = \sum_{roadway} N_{ij}(t)(Rd_j)X_i \qquad (3.11)$$

where $N_{ij}(t)$ is the number of vehicles of each type on a given roadway for a given hour, Rd is the road distance (m) of the particular roadway, X_i are the % weightings of abundance of each vehicle class, and Ar_j is the box area (m^2). Eff_i is the fuel efficiency (l/m) by vehicle class;

Em_i is an emissions factor for mass of CO$_2$ emitted per litre of fuel combusted ($kg\,CO_2\,l^{-1}$) by fuel types;

$$Em_i = (745.75 \frac{g\,C}{l})(\frac{44\,g\,CO_2}{12\,g\,C}) = 2.73 \frac{kg\,CO_2}{l} \quad \text{for diesel} \qquad (3.12)$$

$$Em_i = (642.60 \frac{g\,C}{l})(\frac{44\,g\,CO_2}{12\,g\,C}) = 2.36 \frac{kg\,CO_2}{l} \quad \text{for gasoline} \qquad (3.13)$$

Ox is a measure of completeness of combustion. It is estimated that approximately 99.0% of the carbon content of liquid fuels undergo complete oxidation in modern combustion engines (Marland and Rotty, 1984). For this study Ox is 0.99.

Vehicle counts at 180 locations within the model area were obtained from the Traffic Management Branch of the City of Vancouver. These locations cover virtually all of the main roads, and nearly 33% of the total road distance over the region. Data on vehicle counts were tabulated hourly for the hours from 0500 PST to 2000 PST. This gives sufficient resolution for inclusion to the CO_2 model. Roads without counters were all secondary roads (near major arterials) with approximately 2600 vehicles/day, or local streets with approximately 500 vehicles/day (City of Vancouver, Traffic Management Branch). To obtain a diurnal pattern for the non-major roads without counters, the hourly averages were normalized to the daily total, based on averages of all roads with counters. Consequently the total number of vehicles of a given type travelling a given road distance through each box within each hour (N_{ij}), was calculated.

The resulting anthropogenic CO_2 source strength from mobile sources is displayed in Figure 3.3, as a function of box number and time. It is important to note that the rapid changes near 0600, 1400 and 1800 PST, and the peaks in emissions strength at 0730 and 1600 PST, are related to the morning and afternoon rush hours, with the latter of greater magnitude and duration. Between peaks, emissions remain high throughout the day. Boxes with most significant emissions are generally those at the eastern extent of the model region. Box 8 has the second largest emission strength throughout the day.
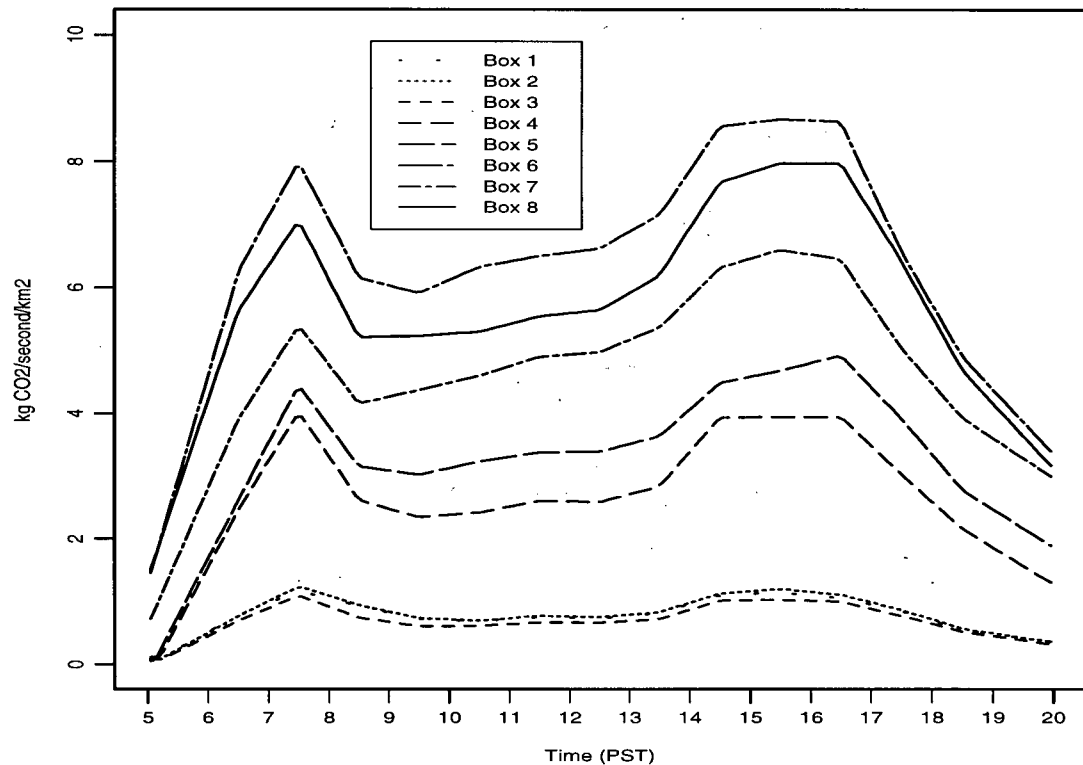
Figure 3.3: Diurnal CO_2 emission strengths from mobile sources for each box of the model.

It is expected that under low wind conditions and poor ventilation, the closest boxes to the tower (those with largest mobile emissions) will most strongly affect the diurnal CO_2 concentration modelled for box 8, while under stronger wind conditions, the influence of local sources will be diluted somewhat by the low emissions upwind in boxes 1 to 3. Nocturnal emissions (not shown on Figure 3.3) are extremely low.

3.4.2 Anthropogenic Stationary CO$_2$ Emissions

Emissions from stationary sources are limited to combustion of natural gas and oil. Other stationary sources within the study area are thought to be negligible. Natural gas sales in this region are primarily for residential use, and indicate that, for the month of June 1993, consumption was only 3% of the annual total (Statistics Canada, 1994). Monthly CO$_2$ emissions from the combustion of natural gas and oil are determined by,

$$Q_{2j\,(month)} = N_{ij}(Eu_{ij})(Em_i)Ox \qquad (3.14)$$

where N_{ij} is the number of users of a given fuel type i (natural gas or oil), per month for each box, and,

Eu_i is the average energy use per month for each fuel type ($GJ/month$),

Em_i are emissions factors for mass of CO$_2$ emitted per GJ of fuel during combustion, by fuel type.

Ox is a measure of completeness of combustion. It is estimated that approximately 1.5% of the carbon content of natural gas and oil remain unoxidized after combustion (Jaques, 1992; B.H. Levelton and Associates, 1990).

N_{ij} was determined for each box from census tracts (Statistics Canada, 1988), and updated to expected 1993 values from trends of energy conversion documented in the *1990 Residential End Use Survey for B.C.* (Campbell and Paull, 1991). Primary fuels were natural gas and oil, which accounted for primary energy use in 80%-88% and 3%-7% of total dwellings respectively, within each box. Emissions from the combustion of propane and wood were considered negligible, as were emissions attributed to combustion of fuel by lawnmowers which was estimated to be an order of magnitude less than natural gas emissions. Space heating, water heating, and cooking appliances account for most of

the energy use from natural gas (Campbell and Paull, 1991).

The average energy use based on sales of natural gas is 4.2 GJ/month per customer for the month of June, 1993 (British Columbia Gas). This value is assumed to be the same for the average energy use of oil by dwellings where oil is the primary fuel. CO_2 emissions are related to energy use through emissions factors by;

$$Em_{nat.\,gas} = C_g(\frac{44\,g\,CO_2}{12\,g\,C}) = 50.93\,\frac{g\,CO_2}{MJ}\,, \tag{3.15}$$

where C_g is given by (Marland and Rotty, 1984) as:

$$C_g = 57.357 + 1.459 \times 10^{-3}(\Delta H_H - 8898) \tag{3.16}$$

and the energy content of natural gas, ΔH_H, is estimated from *Gas Utilities* (Statistics Canada, 1994) to be about 9433.96 kcal/m^3 (39.5 MJ/m^3) for B.C.

For oil (Jaques, 1992),

$$Em_{oil} = 73.11\,\frac{g\,CO_2}{MJ} \tag{3.17}$$

Q_{2j} is shown in Figure 3.4 as a function of time and box, where,

$$Q_{2j}(t) = \frac{Q_{2j\,(month)}}{720 \times 3600}(Df)(Ar_j) \tag{3.18}$$

Df is a diurnal factor relating monthly energy consumption to the rate of consumption at a given time of day (Grimmond, 1988). Ar_j is the box area (m^2).

Absent in the above calculations are a) the use of energy by commercial consumers, approximately 28.8 GJ for the month of June 1993, per customer, and b) correction for the practice of billing a customer which may actually represent more than one "dwelling" as defined by census tracts. These omissions would affect the emissions calculations in opposite directions and were ignored.
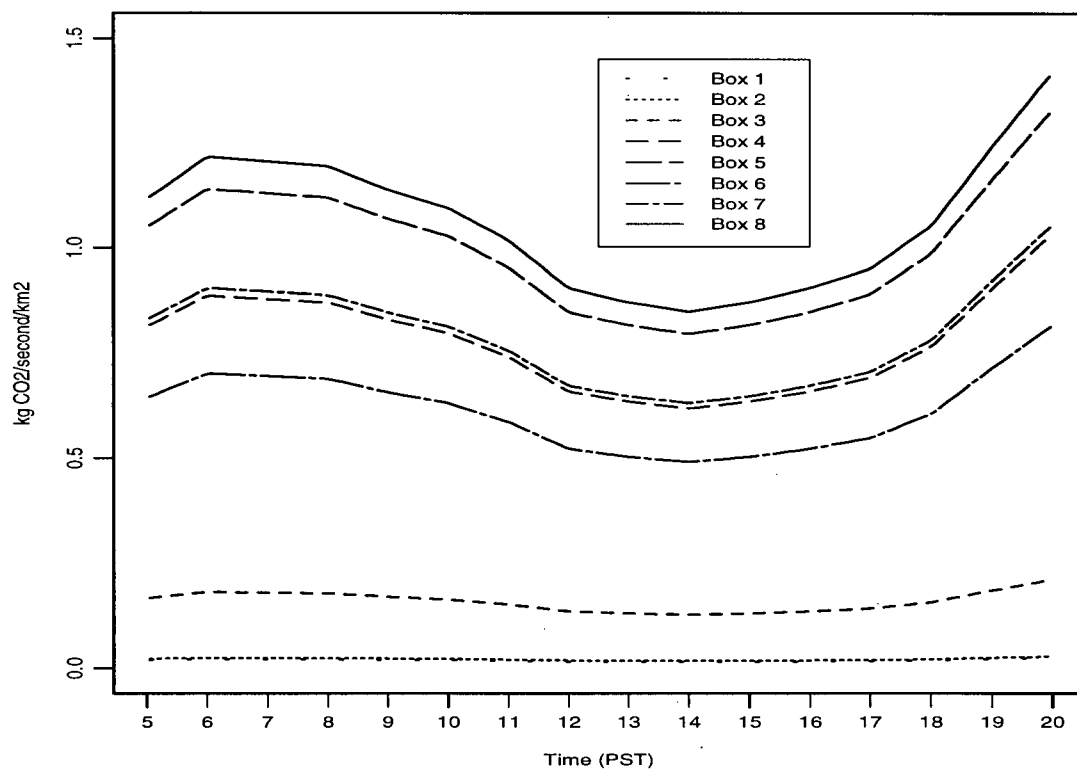
Figure 3.4: Diurnal CO_2 emission strengths from stationary sources for each box of the model.

Similarly to mobile CO_2 emissions, emissions from stationary sources (Figure 3.4) have two maxima, separated by an early afternoon minima. The morning maximum occurs near 0600 to 0700 PST, slightly earlier than the morning peak of mobile emissions. However, this first maximum is of sufficiently long duration to augment the peak in mobile emissions at that time. The evening maximum clearly peaks later than the second maxima of mobile emissions, with the intervening minima acting counter to the second mobile emissions peak near 1600 PST. Cumulative totals of emissions for each box indicate that stationary emissions are approximately 15% of mobile emissions over the model area, and show smaller diurnal variation. Generally the same spatial pattern

of significance of mobile sources is seen for stationary sources, with greatest stationary emission strengths in box 8.

3.4.3   Biospheric CO$_2$ Fluxes

The role of the biosphere is the product of the opposing processes of photosynthesis and respiration. There are two methods by which the net CO$_2$ flux can be modelled; a) a mechanistic or process oriented approach, and b) an ensemble approach. Process oriented modelling is complex and difficult. Net CO$_2$ fluxes above an ecosystem are sensitive to many environmental variables, such as temperature, soil moisture, vapour pressure deficit, stomatal conductance, leaf area index, canopy resistance and incident photosynthetically active radiation (Kim *et al.*, 1992; Leverenz, 1981; Verma *et al.*, 1992). Measurements of these variables are, for the most part, not routine, and were not made at the time of the CO$_2$ observations. Process oriented modelling of CO$_2$ fluxes over a coniferous stand has been attempted by Price and Black (1989) with the flux magnitudes poorly resolved, although the diurnal variation is similar to that observed. Uncertainties involved in physiologically modelled components of biospheric CO$_2$ fluxes (soil respiration, live root respiration and photosynthesis) is large.

Additionally there is large spatial variability of CO$_2$ fluxes *between* surfaces of different vegetation types, and *within* surfaces of similar type. Modelled fluxes at a specific site may not be representative of the ecosystem as a whole. The aggregation of many modelled sites could eliminate some of this site specificity. Because of this, and the difficulty mentioned previously of measuring flux sensitive variables for CO$_2$, the ensemble approach was chosen.

The ensemble approach averages many previous studies of net CO$_2$ exchange over grass, coniferous, and deciduous ecosystems that are prominent within the study region.

This, in a sense, "smooths" the spatial variability, giving a reasonable aggregate CO_2 flux for each ecosystem type. Selection of previous CO_2 flux studies was limited strictly to studies conducted in areas for which there existed diurnal measurements in similar climate, latitude, and moisture regime, at a similar time. Seasonal changes of net above-canopy CO_2 fluxes can be large. Maximum uptake occurs in late June to early July (Ripley and Redman, 1975). Since precipitation for the month of June was well above normal, a further criterion for selection was that the site not be subject to moisture stress. This method should give a good spatial average, albeit with less scientific rigour than the process approach. Net CO_2 fluxes have not been observed at sites within the study region, although respiratory flux measurements have been performed over the forest floor in a coniferous region of Pacific Spirit Park (Lee *et al.*, 1994).

Appendix A details carbon storage and the many pathways of CO_2 exchange. Here it is necessary only to consider CO_2 exchange above the level of the canopy. Above this, CO_2 is considered to be mixed uniformly below the inversion height. The studies chosen for net exchange (respiration - photosynthesis) are for grassland: Desjardins *et al.* (1992), Kim and Verma (1990), Verma *et al.* (1989), Volkov *et al.* (1988), Ripley and Saugier (1974), and Ripley and Redman (1975); for coniferous trees: Lee *et al.* (1994), Leverenz (1981), Jarvis *et al.* (1985, 1975), and Price and Black (1991, 1990, 1989); and for deciduous trees: Baldocchi and Meyers (1991), Verma *et al.* (1986), and Wofsy *et al.* (1993). The aggregate net flux strength of biospheric CO_2, Q_{3j}, summed for grass, coniferous, and deciduous vegetation for each box is shown in Figure 3.5, where

$$Q_{3j}(t) = \sum_{i}^{G,D,C} F_i(t) \frac{A_{ij}}{Ar_j} \qquad (3.19)$$

and for each vegetation type i;
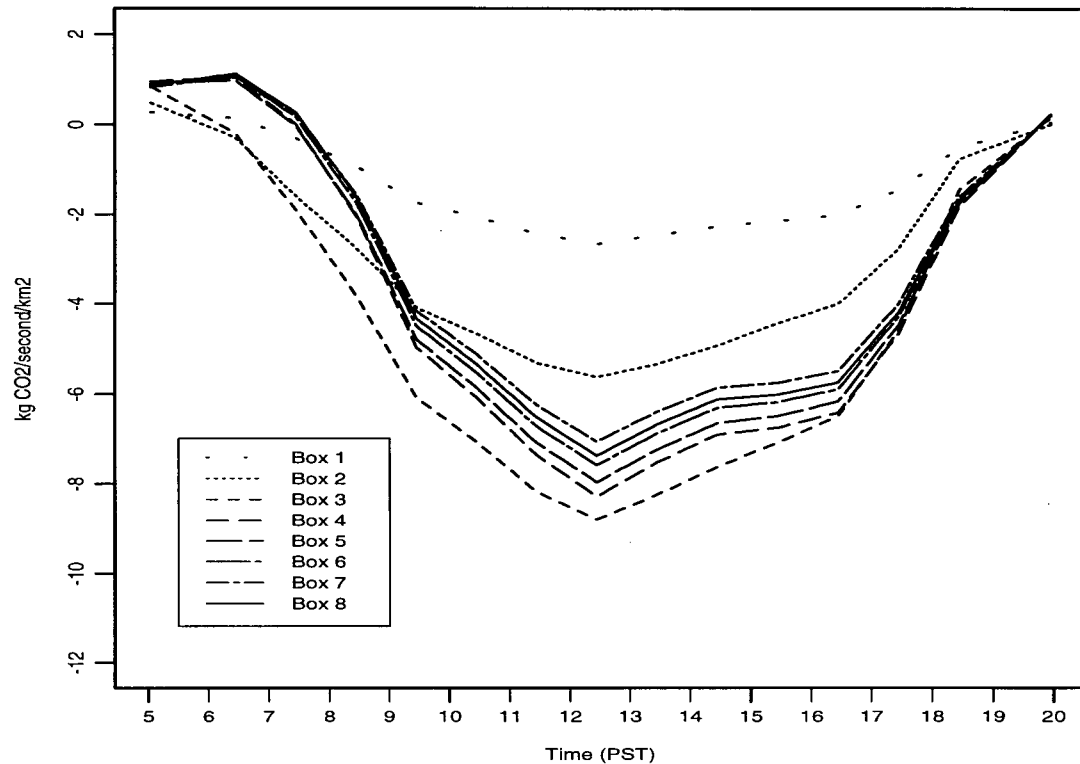
Figure 3.5: Diurnal net CO_2 flux strengths from biospheric respiration and photosynthesis for each box, summed for contributions from grass, deciduous, and coniferous ecosystems.

F_i is the average CO_2 flux strength $(kg\,CO_2\,m^{-2}\,s^{-1})$ of each vegetation type, determined hourly as described by the ensemble approach,

A_{ij} is the area of each vegetation type within each box, and

Ar_j is the area of the particular box.

The area of each vegetation type (grass, coniferous and deciduous) within each box was determined from aerial photographs (City of Vancouver, Planning Department, 1989), a database of vegetation within 5 km of Sunset Tower (Grimmond, 1988), and a detailed study of vegetation classification in Pacific Spirit Park (Thompson, 1985). Table 3.1 indicates the fractional coverage of each type within each box $(\frac{A_{ij}}{Ar_j})$, based on surface

Table 3.1: Abundance of coniferous, deciduous, and grass vegetation as a fractional coverage of model surface area for each box.

Box	Grass	Coniferous	Deciduous	Total Veg.
1	0.10	0.06	0.04	0.20
2	0.09	0.28	0.08	0.45
3	0.23	0.27	0.21	0.71
4	0.42	0.07	0.09	0.58
5	0.40	0.07	0.09	0.56
6	0.40	0.06	0.05	0.51
7	0.38	0.05	0.05	0.48
8	0.40	0.05	0.05	0.50

area.

Grass, from urban lawn and parkland, is the most abundant vegetation type, and is especially dominant in boxes 4 to 8. Domestic grasses in this region are virtually all temperate cool season C_3 plants (B. Holl, Department of Plant Sciences, University of British Columbia). At the western side of the model area, the vegetation of Pacific Spirit Park is composed primarily of coniferous Douglas fir and Western Hemlock, and deciduous Red Alder.

The diurnal behaviour of net biospheric CO_2 exchange is evident in Figure 3.5. The peak uptake is near midday (1230 PST), mostly due to the relationship of photosynthesis to PAR, and by moderate CO_2 emissions by soil and dark respiration before sunrise and after sunset. Soil respiration is more constant than photosynthesis throughout the day, and less extreme in magnitude (Kim and Verma, 1990). However its positive dependency on temperature leads generally to moderate increases during the day, ameliorating some of the intensity of photosynthesis at that time.

Unlike net anthropogenic CO_2 fluxes, the biosphere acts as a net sink. Spatially, the dominant photosynthetic sink strength is not close to the tower, but in boxes 2 and 3,
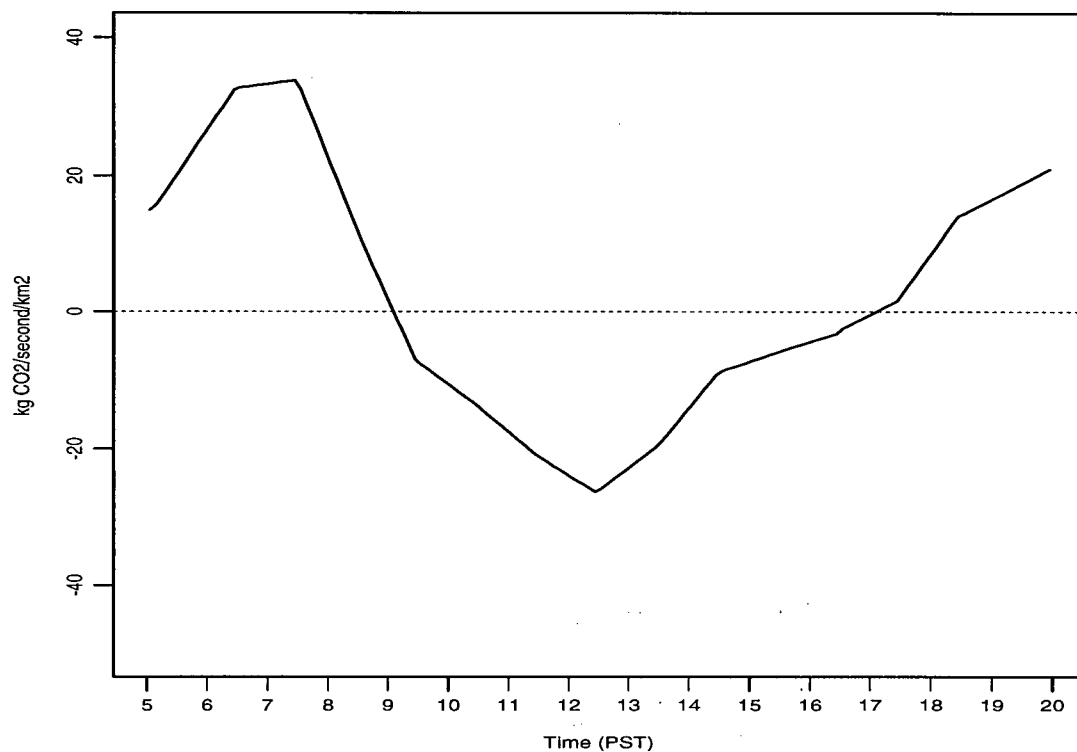
Figure 3.6: Diurnal aggregate net CO$_2$ flux strengths from all major sources and sinks within the model region.

due to the forest of Pacific Spirit Park.

3.4.4 Net CO$_2$ Exchange

Diurnal net CO$_2$ exchange (Figure 3.6) is the net CO$_2$ flux summed over all boxes of the model, and the net CO$_2$ flux within each box is given in Figure 3.7. As a whole, the model surface is a net source until 0900 PST, a net sink until 1700 PST, after which it again acts as a net source. Spatially the interaction of anthropogenic sources and net biospheric sinks do not act to maximize their ability to cancel each other. This
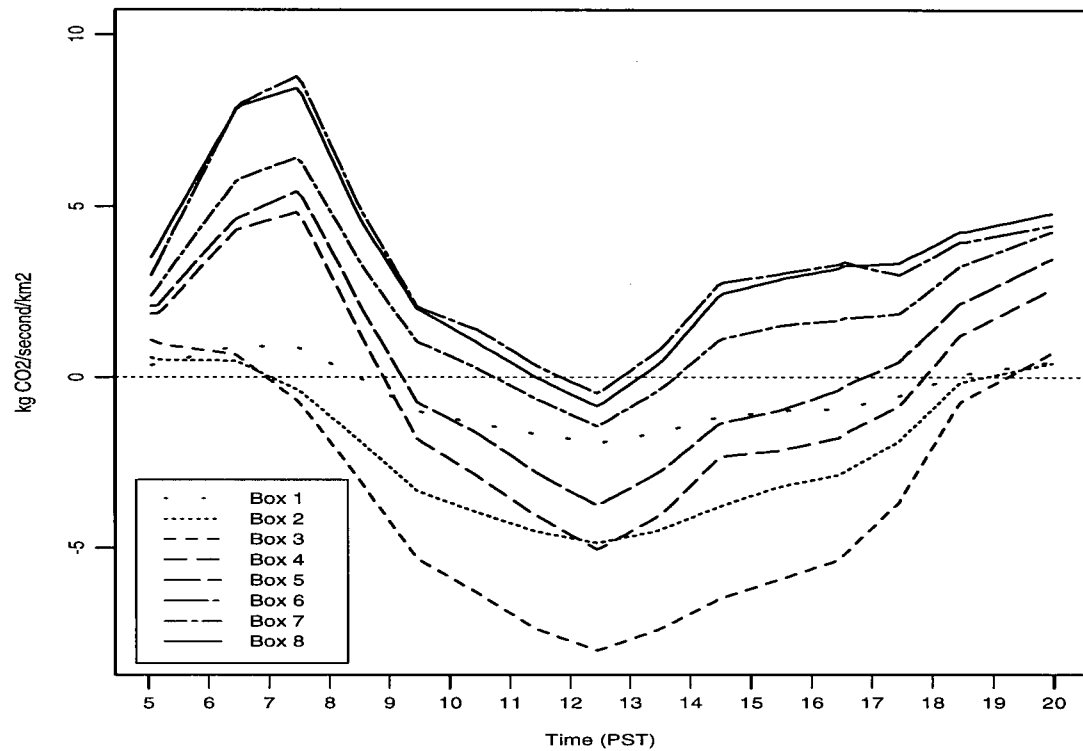
Figure 3.7: Diurnal net CO_2 flux strengths from all major sources and sinks for each box in the model region.

spatial pattern allows wind speed to influence the CO_2 signature of air advected through the model region to box 8. Figure 3.7 indicates that boxes 6, 7, and 8 are diurnally dominant as sources of CO_2, boxes 4 and 5 are both sources and sinks, and boxes 1, 2, and 3 are sinks. Additionally, Figures 3.6 and 3.7 indicate that on timescales as short as t_c (approximately 5 minutes for full vertical mixing), net CO_2 fluxes are relatively unchanged.

3.5   Mixed Layer Depth

The varying depth of the mixed layer, h, acts as both a source of CO$_2$, through volume entrainment from above when the mixed depth is increasing, and as a regulator which allows surface source and sink strengths to have a diurnally varying importance on CO$_2$ concentration, by changing the volume into which CO$_2$ is mixed. Larger mixed depths decrease the effect of surface sources and sinks in setting CO$_2$ concentrations within each box, while increasing the relative importance of the advection of background concentrations. Two regimes of mixed layer depth are used in the model:

1) convective daytime regime (0500 - 1900 PST), and

2) mechanical nocturnal regime (1900 - 2100 PST).

Daytime mixed layer depths are incorporated into the model using a model of convective mixed layer evolution (Steyn, 1980) that determines h and $\frac{\partial h}{\partial t}$. To simulate the collapse of the mixed layer approximately one hour before sunset (Carson, 1973), the Steyn (1980) model values are replaced by a mechanically generated mixed layer height at 1900 PST. Benkley and Schulman (1979) propose, for a mechanical mixed layer depth (h_m),

$$h_m = c\frac{u_*}{f} \qquad (3.20)$$

where $c = 0.09$, and $u_* = 0.13\overline{u}$ at the Sunset site (Roth, 1993).

The Steyn model requires a number of important meteorological variables which were not measured during the June observational programme. Necessary inputs include: surface sensible heat flux, inversion intensity, initial temperature of the mixed layer, and a subsidence parameter. Initial temperatures of the mixed layer were taken from hourly surface observations, inversion intensities and subsidence parameters were determined

from upper air soundings, while hourly surface sensible heat fluxes were determined using a library of software for the calculation of surface fluxes (Beljaars and Holtslag, 1989), based on De Bruin and Holtslag (1982), Holtslag and van Ulden (1983), and van Ulden and Holtslag (1985), using routinely observed meteorological variables at Vancouver International Airport. The model calculates the net energy balance of the surface and partitions the net available energy using the modified Priestley-Taylor method. Calculated sensible heat fluxes were calibrated with this method on days for which heat flux data from Sunset Tower were available (6 days in August 1993, and 4 days in August 1992), by adjusting α, the modified Priestley-Taylor parameter given by Beljaars and Holtslag (1989) as,

$$\alpha = 1.85[1 - exp(-MA/100)] \qquad (3.21)$$

Best agreement between observed and calculated heat flux values were found for α=0.2. Moisture availability (MA) for α of that value is within the range of values of an urban surface (Stull, 1988). However, over urban surfaces in St. Louis and Indianapolis, Hanna and Chang (1992) use values for α of 0.5. In this study the anthropogenic heat flux was considered negligible, which is a reasonable assumption in summer (Grimmond, 1988). Similar to Hanna and Chang (1992), $\frac{Q_G}{Q^*}$=0.3, and β=20 W m^{-2}. The albedo of this suburban surface is 0.15 (Grimmond, 1988), and the roughness length is 0.52 m (Steyn, 1980). The generality of this heat flux model was, in this case, a good feature, as it was hoped that the model return was a spatially representative sensible heat flux that could be used to calculate the mixed layer depth across the whole model region.

Mixed layer depths were calculated at the centre-point of each box, with fetch distances from the land/sea discontinuity representative of that location. When available, acoustic soundings from Abbotsford were used to, in a sense, "anchor" the model output

to a known location at a known time. Mixed layer depths determined by Equation 3.20 for mechanically generated mixed layers are constant for each box.

3.6 Entrainment

Entrainment as described by Equation 3.5 is strictly volume entrainment, occurring only at times of mixed layer depth increases, so that,

$$(\overline{w'_j C'_j})_{z=h_j} = \frac{1}{h_j}(C_h - C_j)\frac{\partial h_j}{\partial t} \text{ for } \frac{\partial h_j}{\partial t} > 0 \tag{3.22}$$

$$(\overline{w'_j C'_j})_{z=h_j} = 0 \text{ for } \frac{\partial h_j}{\partial t} \leq 0 \tag{3.23}$$

Entrainment is neglected during the nocturnal regime.

Studies indicate slightly increasing CO$_2$ concentrations with altitude within the troposphere during summer months when the net surface CO$_2$ flux is downwards, due to the strength of photosynthesis by the land biota (Desjardins *et al.*, 1992; Tanaka *et al.*, 1983). Diurnal variation in net CO$_2$ exchange at the surface may cause the vertical profile of CO$_2$ concentration to be somewhat variable below the inversion base, especially under conditions of poor mixing or mesoscale flow oscillations like land/sea breeze circulations. However, the general case is for CO$_2$ concentrations just above the mixed layer to be approximately 3 to 7 ppmv greater than mean background values within it (R. Desjardins, Centre for Land and Biological Resources Research, Research Branch, Agriculture Canada). Similar temporal CO$_2$ traces to those in this study, observed at 30 metres (Tanaka *et al.*, 1985), indicate that the daily mean CO$_2$ concentration determined from hourly means is greater than that of tropospheric values measured between heights of 0.5 and 2.0 km. That is consistent with this study, where the daily mean CO$_2$

concentration observed at the Sunset Tower is 375 ppmv, and the concentration above the mixed layer is estimated to be 373 to 376 ppmv (based on above discussion). In the model, the concentration above the mixed layer is set at 373 ppmv, i.e. in the possible range, but below the daily mean measured at the Sunset Tower.

Figure 3.8 shows how the difference in mean CO$_2$ concentrations across the top of the mixed layer is modelled in an idealized set of summertime CO$_2$ profiles. Profile A is the well-mixed daytime profile (approximately 360 ppmv). Above the mixed layer the concentration, C_h, is constant, with a value representative of the mean concentration above the mixed layer (approximately 373 ppmv) to a height arbitrarily set as approximately 2 times the height of the mixed layer. Within the mixed layer, CO$_2$ profiles are governed by the net CO$_2$ exchange at the surface. CO$_2$ concentrations at night (profile B) are significantly higher (approximately 380 to 390 ppmv) than during the daytime. Throughout a diurnal period the CO$_2$ profile oscillates between day and night profiles, passing through the mean background concentration of 369 ppmv (profile C).

3.7 Model Implementation

For inclusion in the model, all source and sink strengths were discretized at six minute intervals, linearly interpolated from the hourly averages. Six minutes was used throughout as the model timestep. It is acknowledged that although a timestep of this length may be required for sufficient resolution of changes in mixed layer depth, it may be too short to fulfill the assumption of uniform mixing mentioned previously. Short term variance as seen in observations (Chapter 2) will not be adequately modelled here, and neither should it be, because the box model is sufficient only for longer term temporal variability. Short term variance of CO$_2$ is strongly local and unable to be modelled by
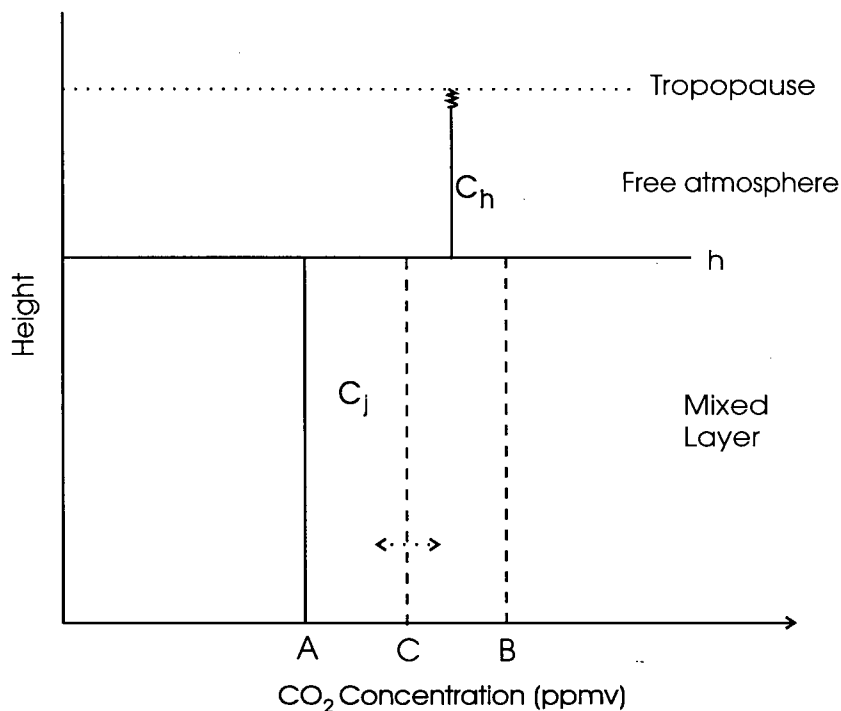
Figure 3.8: Model profiles of CO_2 concentrations within and above the mixed layer. Profile A is the daytime profile, B the nighttime profile, and C the mean background profile within the mixed layer, for a given box.

large boxes covering an area greater than that influencing the variance.

The model was run over the time period of interest, moving sequentially from box 1 to box 8, needing only the concentration of CO_2 in the previous box to solve the mass balance equation (Equation 3.5) at each time step. All other terms in Equation 3.5, including the background CO_2 concentration (C_0) and the CO_2 concentration above the mixed layer (C_h) are known for each box, either as constants or as quantities determined independently during simulation of the CO_2 concentration within the box of interest. It is difficult to make an estimate of possible errors associated with the model and inventory. However, in Chapter 4 the model is tested against the observations of Chapter 2.

Chapter 4

Model CO$_2$ Simulation

4.1 Introduction

The aim of the CO$_2$ model, as described in Chapter 3, was to simulate gross features of the observed summer daytime variation in CO$_2$ concentrations. Model design limited its use to days on which a convective boundary layer existed, with mean boundary layer winds near westerly, at 270° to 290°. These conditions were met typically on days when a sea breeze was established soon after sunrise. The sea breeze is indicative of strong land heating and the generation of a convective boundary layer, which is a necessary requirement for the use of the model of mixed layer depth (Steyn, 1980).

Typically the sea breeze duration is from 1100 PST to 1900 PST (Steyn and Faulkner, 1986). For the days chosen in this study, it was desirable to test the ability of the model to simulate the main diurnal variation, namely the reduction of CO$_2$ concentrations after about 0800 PST, and the subsequent rise between 1800 PST and 2100 PST (Figure 2.3). Necessary, then, were days for which the mean wind remained near 280° from 0800 PST until 2100 PST. Three days were chosen to adequately fulfill the aforementioned requirements, namely, June 4, 13 and 16, 1993. Many other days in the study period exhibited what appeared to be sea/land breeze circulations, but without the extended duration.

For each of the three days in June, the model was run from 0500 PST to 2100 PST,

83

the hours for which systematic variations in CO_2 concentration were observed. Nighttime concentrations were not modelled beyond the time of the drop in mixed depth due to:

a) inadequacies of the estimation of mixed layer depths during

the nocturnal regime, and

b) the very large variability in CO_2 concentration exhibited

during those hours.

Nocturnal mixed layer depths, as described by a mechanical mixed depth (Chapter 3), are not well defined at night, since there have been no attempts to calibrate the general equation (Equation 3.20) to nocturnal depths in this region. However, the nocturnal regime is generally characterized by a shallow mixed layer and light winds. CO_2 concentrations exhibit high variability due to the strong influence of very local sources and sinks under these conditions, which are not well resolved by the large boxes of the model.

Only summertime concentrations were modelled, as this was the only observational period to show a consistent diurnal signal, evidently due to the interactions of a diurnally developed convective boundary layer, associated diurnal wind patterns, and an extremely active biosphere. The winter period exhibited large aperiodic diurnal variability and much higher CO_2 concentrations (Chapter 2).

4.2 Model Results

4.2.1 Initialization

Initial CO_2 concentrations were determined for box 8 from the corresponding observations at 0500 PST at the Sunset tower for each day modelled. For boxes 1 to 7, initial concentrations within each box were prescribed based on an assumption of stationarity

Table 4.1: Initial model CO$_2$ concentrations (ppmv) prescribed for each box.

Box	June 4	June 13	June 16
1	387	386	383
2	387	386	383
3	387	386	383
4	387	385	383
5	386	384	382
6	386	383	382
7	385	381	381
8	383	380	381

applied to Equation 3.5, so that the sum of the source and sink terms for CO$_2$ at 0500 PST were in balance with the advective term, whereby

$$\frac{1}{h_j} \sum_{i=1}^{n} Q_{ij} = \frac{\overline{u}C_{j+1} - \overline{u}C_j}{\Delta x} \tag{4.1}$$

Prior to the modelled hours the net CO$_2$ flux was positive, albeit small, and assumed constant throughout the night (Chapter 3). Over this time mean winds are expected to be relatively constant, allowing the steady-state of Equation 4.1 to be established. As winds were predominantly light easterly before 0500 PST for all days, the upwind background concentration was designated to be C_{j+1} in Equation 4.1, the concentration from the adjacent upwind box. $\overline{u}$ is the mean wind speed averaged over 3 hours previous to 0500 PST. As shown in Table 4.1, the initial concentrations of CO$_2$ set up a pattern of spatial variability from box 1 to box 8 of 2-6 ppmv.

The daytime upwind background CO$_2$ concentration is prescribed to be 369 ppmv, and the CO$_2$ concentration above the mixed layer as 373 ppmv. The following sections will show model results for the three days chosen. Differences in model results among the days are due to differences in boundary layer variables, such as mixed layer depth and mean

wind, but not to source and sink strengths which are assumed to be identical during the course of each model run. Day-to-day variation in anthropogenic emissions are considered negligible. Mobile emissions patterns are virtually unchanged year round, while emissions from stationary sources have significant variability only on seasonal timescales (B.C. Gas). Day-to-day variation in photosynthesis rates may be significant, but difficult to quantify. Since photosynthesis is most affected by incident PAR, it is promising to note that attenuation of direct PAR by clouds can, in part, be offset by the greater absorption (by plants) of diffuse light under cloudy conditions (Russell *et al.*, 1989), and by less likelihood of mid-afternoon water stress (Neumann *et al.*, 1994). Model biospheric flux rates are similar for each day.

Initial values for model variables, model constants, and hourly averaged model variables are shown in Appendix C for each day of CO$_2$ simulation. It can be seen for June 4 and June 13 that, except for the first 3 hours, wind directions are virtually steady at 280° for most of the modelled hours. It is expected that this will not significantly affect model results as mean winds are very light at this time, thus raising the importance of CO$_2$ source and sink strengths, and entrainment, on modelled CO$_2$.

On June 16, afternoon winds differ by approximately 20° from the model grid. It is likely that model CO$_2$ will not be greatly affected, since the suburban surface's source and sink characteristics don't change drastically at small angles away from the model grid. Also, morning winds are light easterly. Later (Sections 4.2.3 and 4.2.4) it is suggested that winds are not important to the model CO$_2$ concentration during the early hours (especially when winds are light), and that the rate of increase of mixed layer depth is perhaps the most important model variable at that time. Additionally, with the tower located in the centre of box 8, local CO$_2$ emissions (when winds are light) are incorporated into the model by winds from any direction.

4.2.2 Mixed Layer Depths

Modelled mixed layer depths for June 4, June 13, and June 16 are shown in Figures 4.1, 4.2, and 4.3 respectively. All show similar structure during both daytime and nocturnal regimes. Mixed layer depths increase eastwards, from box 1 to box 8, consistent with the generation of a convective boundary layer downwind of the land/sea discontinuity in box 1. An exception to this is the morning of June 16, which shows that under inital light easterly winds before the sea breeze sets up, the mixed layer rises in a spatially uniform manner, until approximately 1000 PST. The marked increase in strength of the sea breeze after that time decreased mixed layer depths, and produced spatial variability in mixed heights across the model area, from box 1 to 8.

Mixed layer heights on June 16 were validated with available estimates of mixed layer depths from an acoustic sounder at Abbotsford, approximately 70 km east of the Sunset tower. No other days had available acoustic soundings. The diurnal shape of the mixed layer depth, as determined by the convective model at the Sunset site, was retained on this day. However, the model's inversion parameter was adjusted so as to constrain the maximum midday depths estimated over the study region to the form,

$$h = 100 + ax^{\frac{1}{2}} \qquad (4.2)$$

where a is determined from known heights (h) measured by acoustic sounder at Abbotsford, with a known fetch distance ($x = 70$ km) from the sea. Equation 4.2 was then applied (with known a) to the study area, with fetch distances as appropriate. Changes were made to the inversion parameter until mixing depths determined from the model equalled those from Equation 4.2. In this manner, maximum midday heights were reduced by about 15% of that produced by the mixed depth model (Steyn, 1980). Confidence in
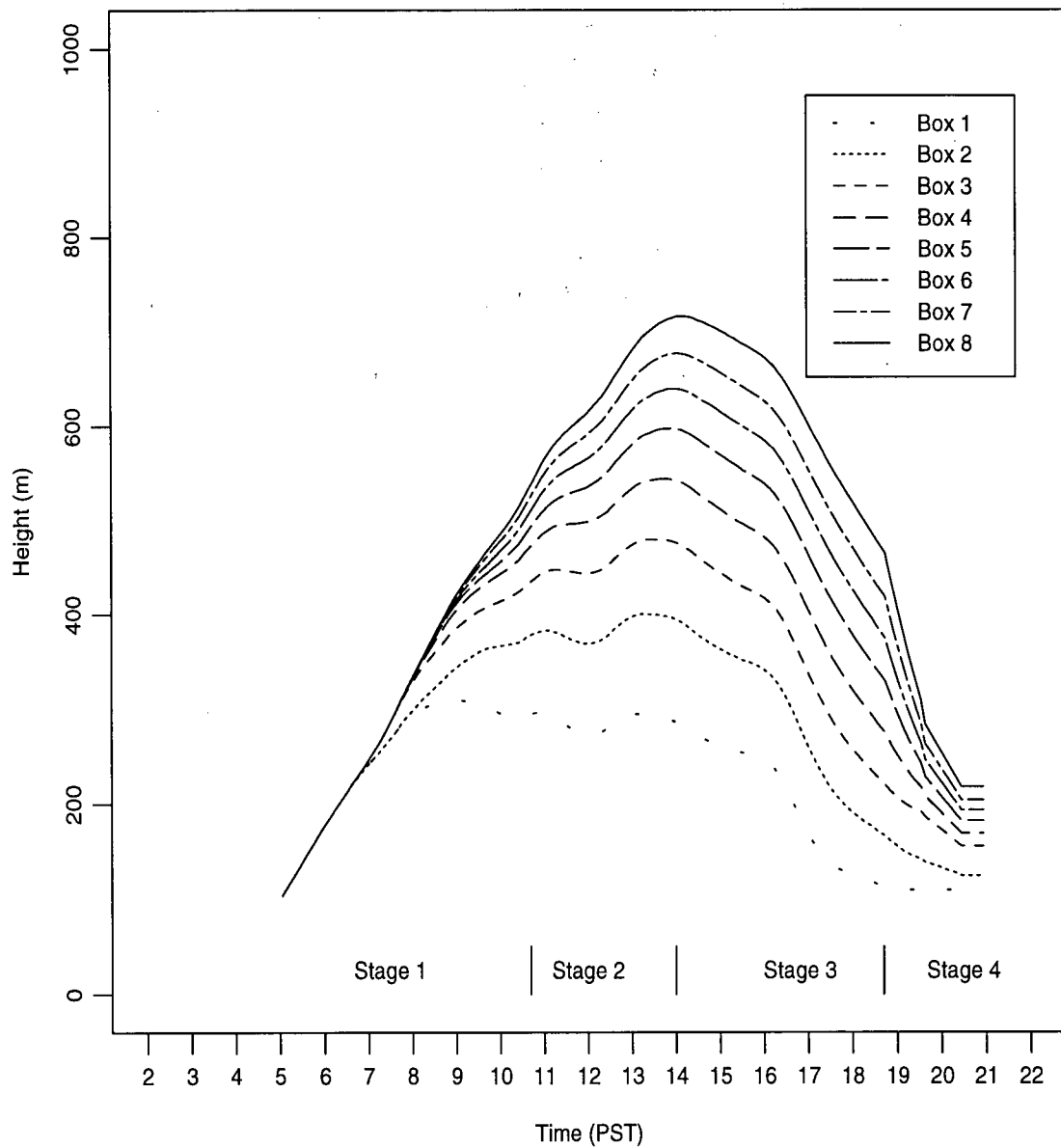
Figure 4.1: Modelled mixed layer depths for June 4, 1993, determined at the centre point of each box in the study region. Stages are described in Section 4.2.3.
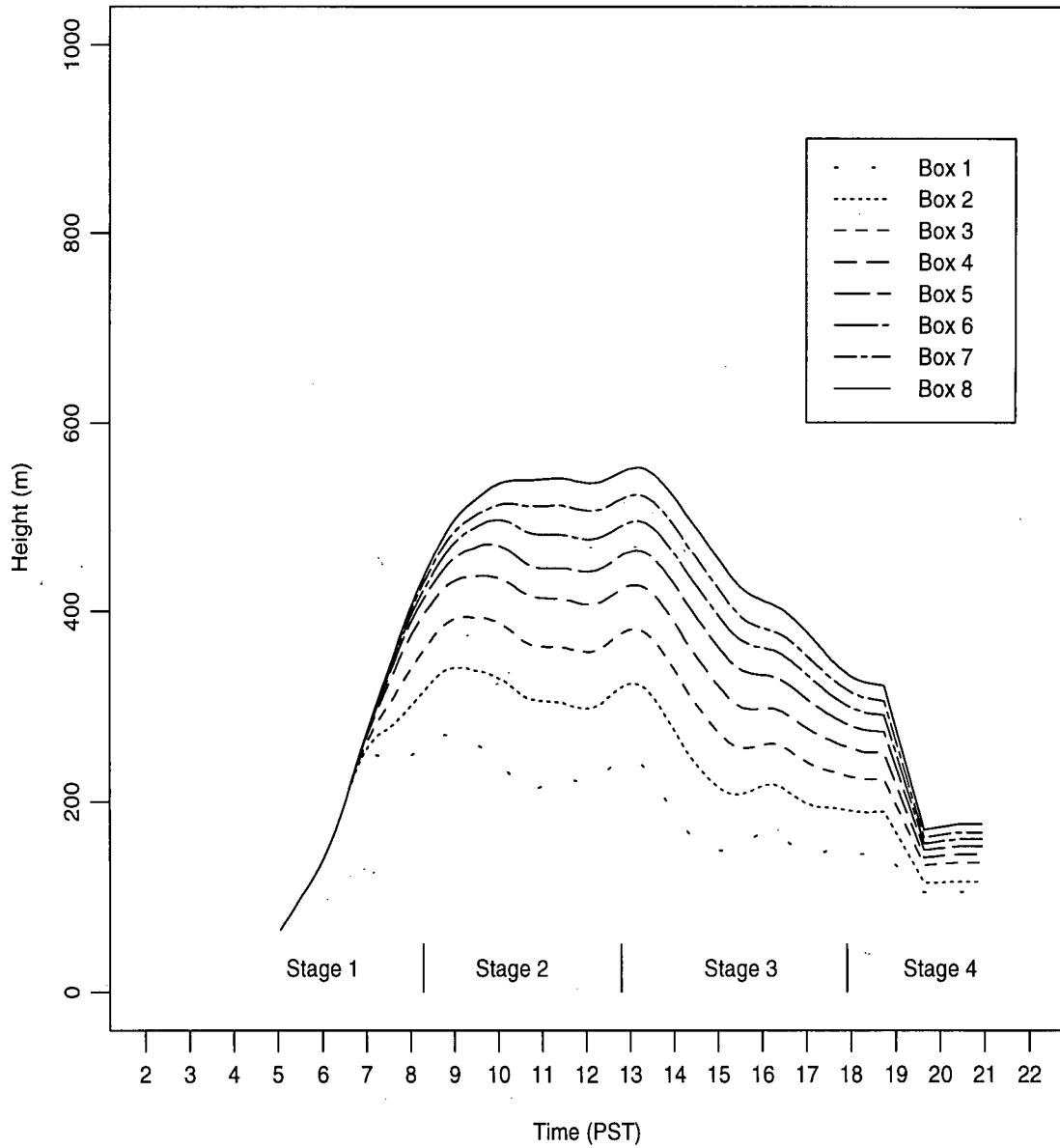
Figure 4.2: Modelled mixed layer depths for June 13, 1993, determined at the centre point of each box in the study region. Stages are described in Section 4.2.3.
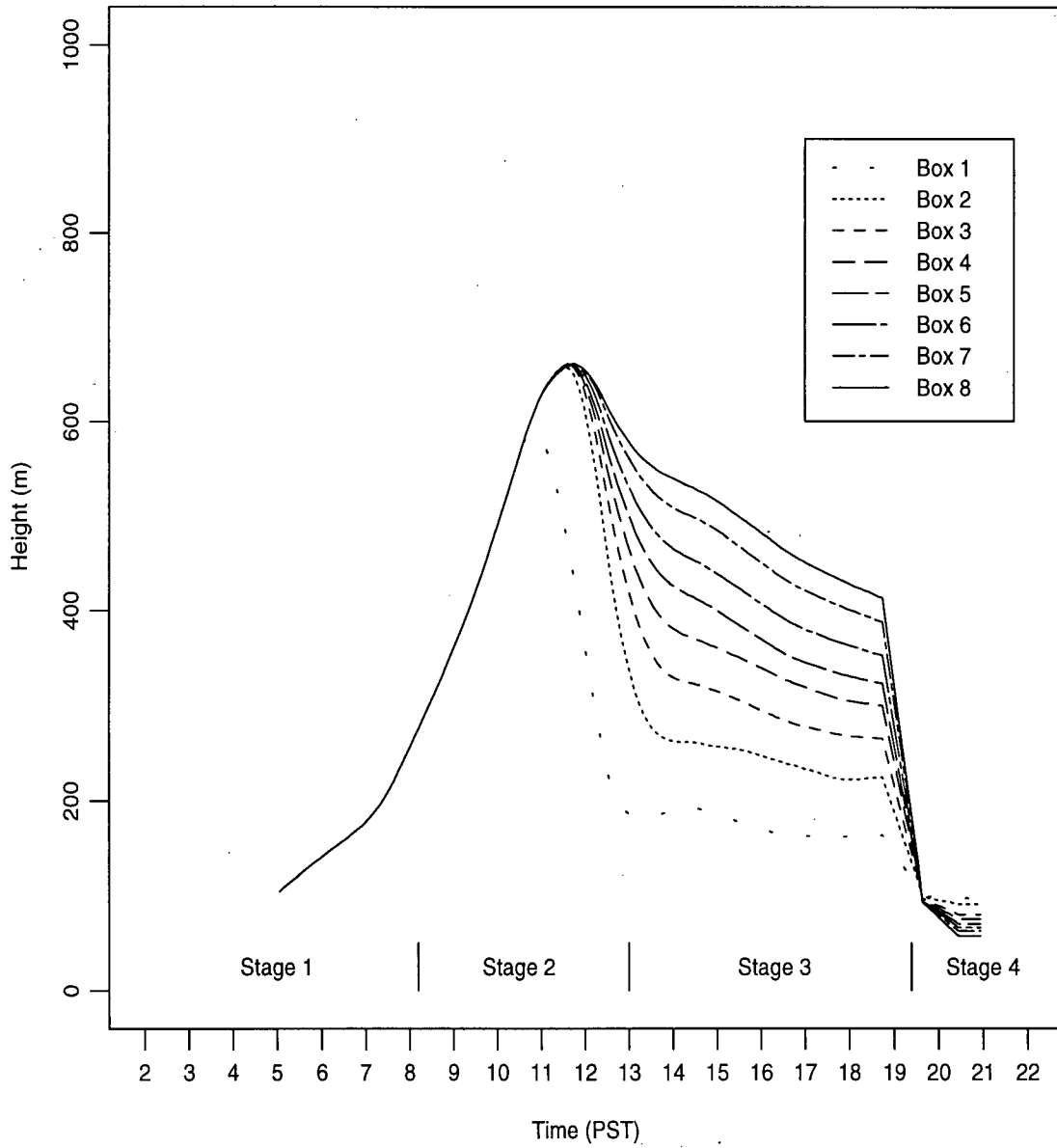
Figure 4.3: Modelled mixed layer depths for June 16, 1993, determined at the centre point of each box in the study region. Stages are described in Section 4.2.3.

the estimated mixed layer depths for this day is especially high.

Rapid decreases in height are noticeable at the onset of the nocturnal regime for all days. Modelled mixed layer depths during both day and night regimes are very different for the three days considered. Absolute mixed layer depths and rates of change are considered more fully in relation to modelled CO$_2$ concentrations in the next section.

4.2.3 Model CO$_2$ Results

June 16$^{\text{th}}$ was the only day for which mixed layer depths were calibrated by acoustic sounder data, and there appears to be particularly good agreement between modelled and observed CO$_2$ concentrations for that day (Figures 4.4 and 4.5). This day will be discussed in depth, followed by mention of June 3 and 4 to more fully illustrate important arguments and processes. All initialization data and subsequent hourly averaged model variables are tabulated in Appendix C.

Figure 4.5 shows clearly the relationship between modelled and observed CO$_2$ for June 16, 1993, as modelled for box 8, the location of the observations. Observed CO$_2$ concentrations have been smoothed to remove short term variance, although an estimate of the variability is retained by the thin solid lines ($\pm$ one standard deviation). Over the diurnal cycle, the plot can be broken into four distinct stages: 1) early morning peak, 2) drawdown from morning peak to afternoon minima, 3) afternoon minima, and 4) the rise from lower afternoon concentrations to high nocturnal CO$_2$ concentrations.

The first stage (approximately 0500-0800 PST) is characterized by a peak in observed concentrations and by large variance. Modelled concentrations in this stage are close to observed, with concentrations overlapping the observed, and within one standard deviation at all times. Major controls on the modelled concentration during this period are the large positive flux of CO$_2$, predominantly from anthropogenic emissions, but also
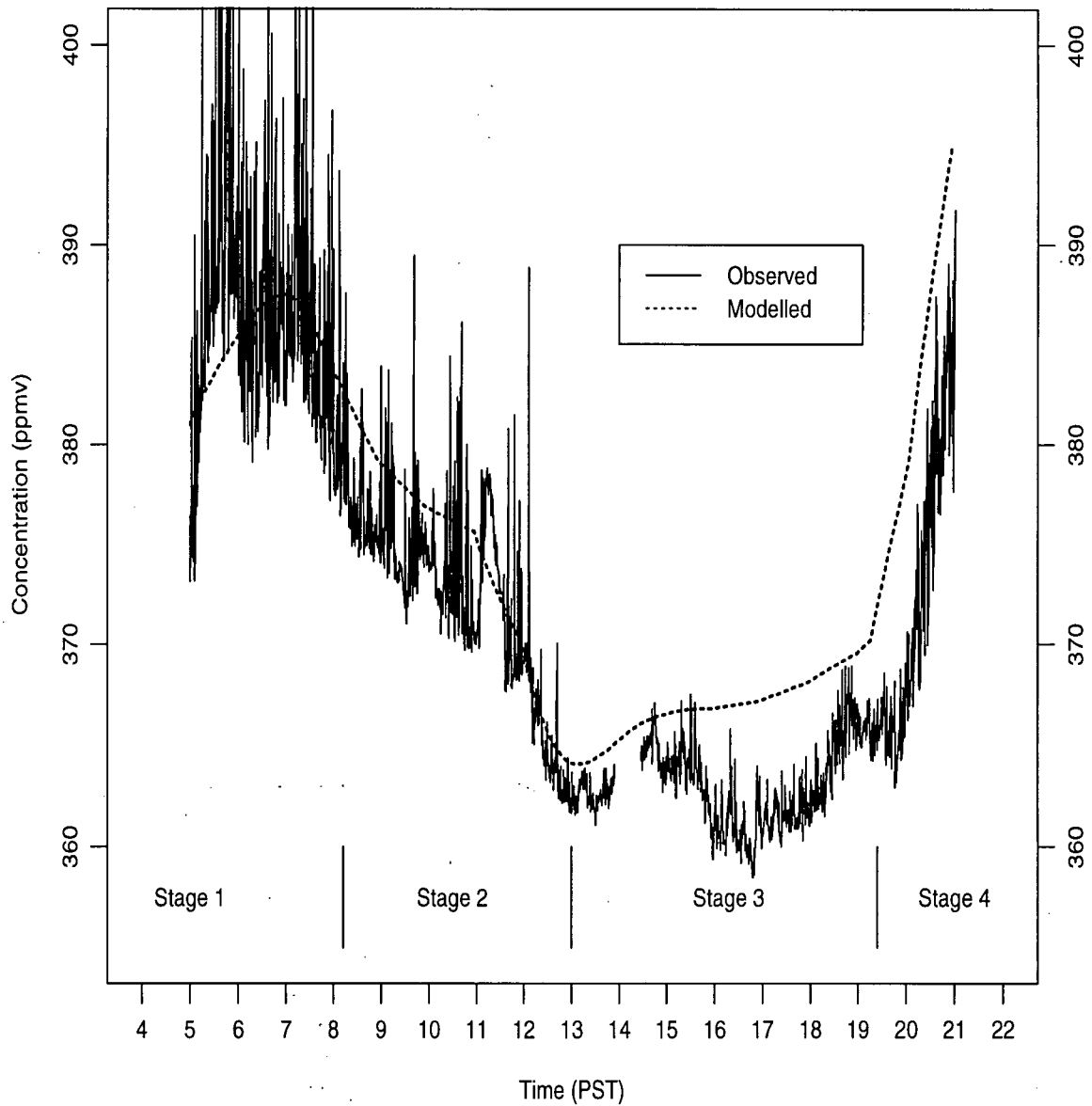
Figure 4.4: Modelled and observed diurnal CO_2 concentrations for June 16, 1993 at the Sunset site.
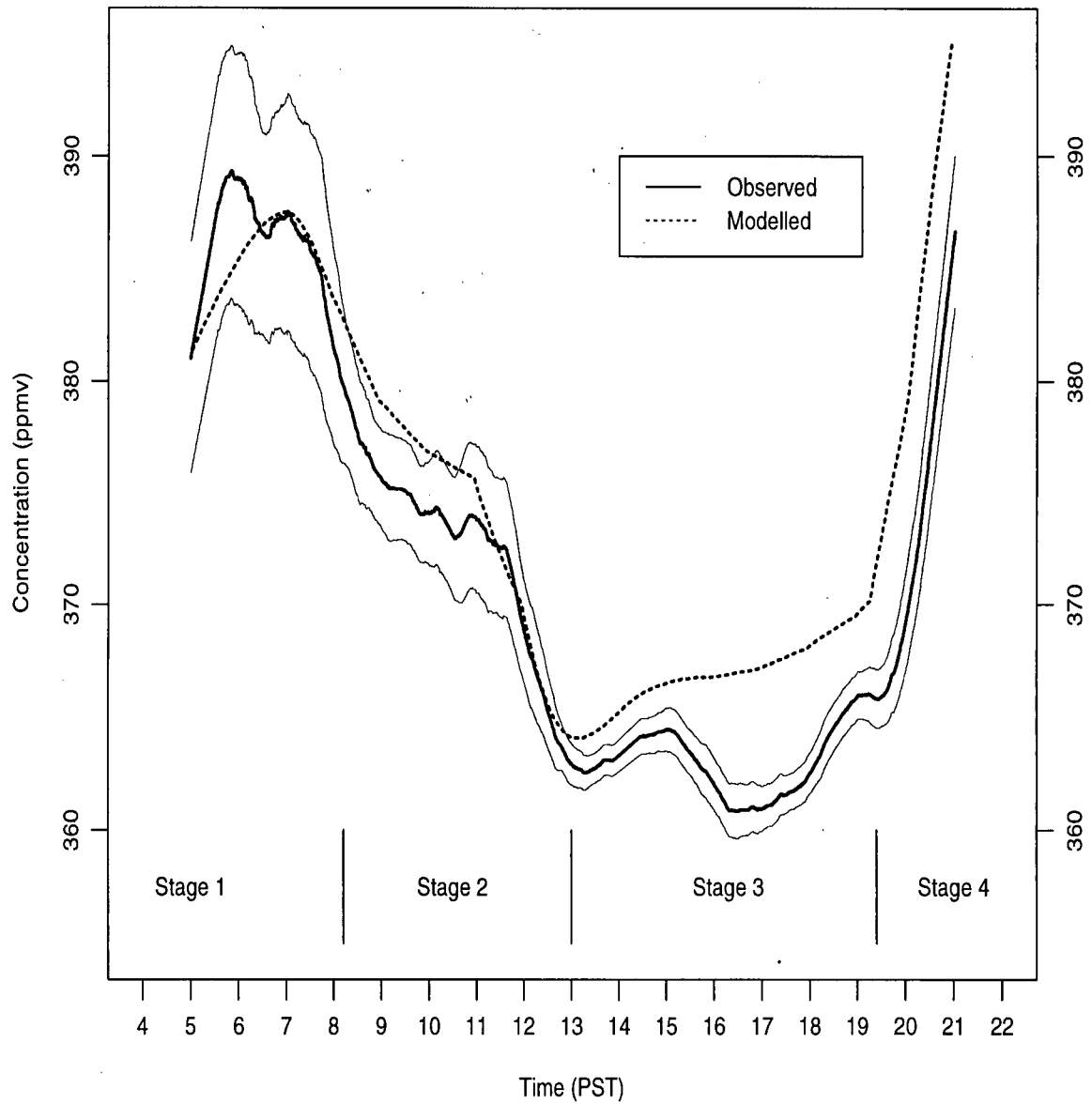
Figure 4.5: Modelled and observed diurnal CO$_2$ concentrations for June 16, 1993 at the Sunset site. Observed concentrations have been smoothed. Thin solid lines indicate one standard deviation on either side of the mean observed concentrations, for a sample length of ten minutes.

due in part to biospheric soil and dark respiration, the rate at which the mixed layer volume is increasing, and the role of entrainment of CO$_2$ from above the mixed layer. The role of advection is relatively minor at this time because wind speeds are generally light. The importance of CO$_2$ source and sink strengths, and entrainment, increases when the mixed height is low.

Convective mixed layer growth (Appendix C) nearly doubles (from 119 to 210 m) within two hours (0500 to 0700 PST). This rate of increase controls the modelled rise of CO$_2$ to the peak at 0730 PST, coincident with the peak in net CO$_2$ flux over the study region. Initial increases in the mixed layer depth in this stage reduce the potential concentration increase due to early net emissions into a shallow boundary layer (100 m at start of model integration).

Although the spatially averaged net flux of CO$_2$ remains positive over the model area until 0900 PST, and until after 1100 PST for boxes near the tower (Figure 3.6), peak model concentrations are reached earlier because the mixed layer growth causes net source strengths to become less significant. Also at this time, entrainment due to mixed layer growth is at its greatest. Approximately half of the volume of the mixed layer is from entrained air after the first two hours. Thus CO$_2$ concentrations begin to decline at a time when increasing emissions strength is balanced by entrainment of lower concentration air (373 ppmv) from above. Air advected from upwind boxes is still characterized by the initially high nocturnal concentrations (Table 4.1).

The second stage (approximately 0800-1300 PST) is a dynamic interaction of many processes bringing about a rapid decrease in CO$_2$ concentrations. Generally, contributions of lower CO$_2$ air by entrainment, and advection of air near background concentrations, control the rate of decrease. Entrainment is important when the mixed layer is still relatively shallow, and heights are increasing at their greatest rate (Appendix C). Wind speeds also increase with the onset of the sea breeze. Both processes act to remove

nocturnal and early morning CO_2 buildup, and mix CO_2 vertically into the deepening mixed layer (Berry and Colls, 1990a) . Net surface CO_2 fluxes are not significant in this stage (Figure 3.6).

Diurnal variation of CO_2 on June 16 is notably different from that of June 4 and June 13, as there is an inflection in the modelled decrease near 1100 PST. Before then the sea breeze has not been established, creating a period in which concentrations are being drawn down at a decreasing rate primarily due to entrainment. As a result CO_2 concentrations in the mixed layer become similar to those above. This is evidenced by a near-asymptotic decline to 373 ppmv, the free atmosphere concentration. Since winds are light, the advective contribution from upwind boxes is small. Near 1100 PST the effect of entrainment diminishes as $\frac{\partial h}{\partial t}$ decreases to only 1×10^{-2} m s^{-1}, allowing an increased rate of CO_2 drawdown below 373 ppmv, mostly due to an increase in wind speed, and the arrival of background air (369 ppmv) from upwind of the study area.

With maximum sequestration of CO_2 by photosynthesis near 1230 PST, the modelled CO_2 concentrations decrease below 369 ppmv, to a minimum of 364 ppmv. Stage 2 is generally well modelled, although the initial departure from observed concentrations alludes, on this day, to the possibility of entrained air being less than the 373 ppmv prescribed by the model. Nevertheless the shape is similar, and shows remarkable agreement in the latter part of the drawdown.

The third stage of the diurnal CO_2 cycle (approximately 1300-1900 PST)is characterized by the lowest variance observed for the whole day, and observed concentrations as much as 8 ppmv lower than background concentrations. This stage is poorly modelled. At no time do the modelled concentrations fall within one standard deviation of the observed values. They are higher at virtually all times. A peak in CO_2 concentrations near 1500 PST is only partly resolved by the model. Model concentrations show a levelling off at 1600 PST, as mixed layer heights and net photosynthesis decrease. CO_2 is being

removed, albeit at a slower rate, from a smaller volume. Concentrations remain relatively unchanged as advection, photosynthesis, and mixed layer decay reach a balance. Entrainment of CO$_2$ can be neglected because mixed layer heights fall slowly. Modelled concentrations during this period are as much as 5 ppmv higher than observed. Possible explanations for this discrepancy are discussed in the next section.

Finally, the fourth stage of the diurnal cycle (approximately 1900-2100 PST) is seen to conform well to the observed CO$_2$ rate of increase of CO$_2$ concentrations and its timing. Rapid CO$_2$ increases occur after 1900 PST as the mixed layer collapses quickly to only 78 m during the final simulation hour. CO$_2$ increases are attributed to moderate anthropogenic emissions and soil respiration into a very shallow nocturnal boundary layer. However, the absolute magnitudes of modelled and observed concentrations differ during this period of rapid increase. It is likely that accuracy in this stage suffers from the poor modelling encountered in stage 3. Differences would be very small if the modelled concentrations were forced artificially to observed concentrations at the beginning of this stage.

The capabilities of the model, and a measure of robustness, can be tested by looking at model results for June 4, 1993 and June 13, 1993, shown in Figures 4.6 and 4.7 respectively. Both days experience the four stages mentioned for June 16, although at different times. Likewise, there is reasonable agreement with the observations, with similar conclusions. The first and final stages, both with shallow mixed depths, fall within one standard deviation of the observations. The shape, or rate, of the morning CO$_2$ drawdown is modelled well, but its timing is seen to lead the observations by as much as an hour on June 4, and to lag them by about 30 minutes on June 13. Hourly mean wind observations may not be of sufficient temporal or spatial resolution to accurately integrate the advection of background CO$_2$ concentrations from upwind of the study area.

Sensitivity to CO$_2$ concentrations above the mixed layer are not sufficient to change
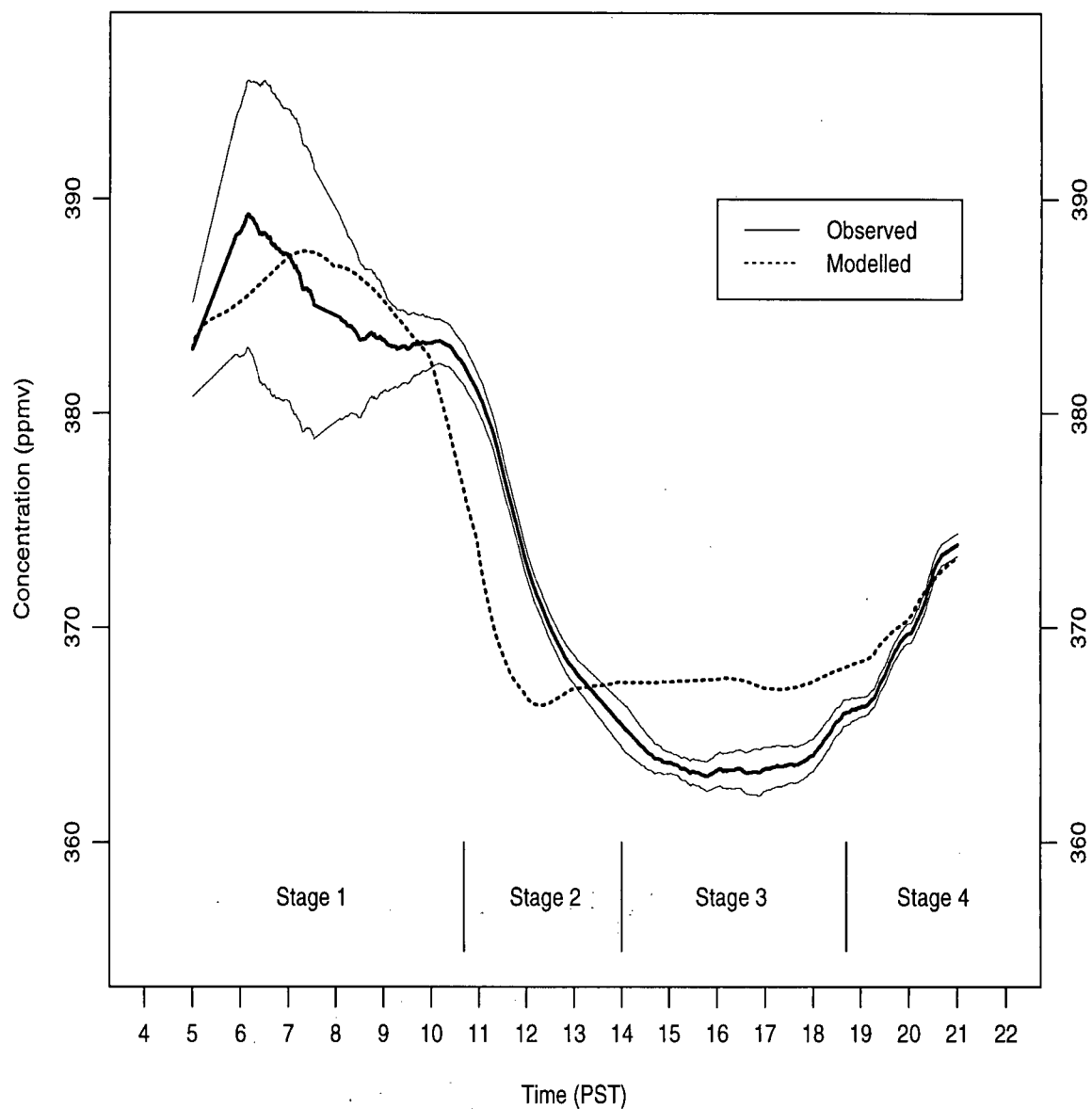
Figure 4.6: Modelled and observed diurnal CO$_2$ concentrations for June 4, 1993 at the Sunset site. Observed concentrations have been smoothed. Thin solid lines indicate one standard deviation on either side of the mean observed concentrations, for a sample length of ten minutes.
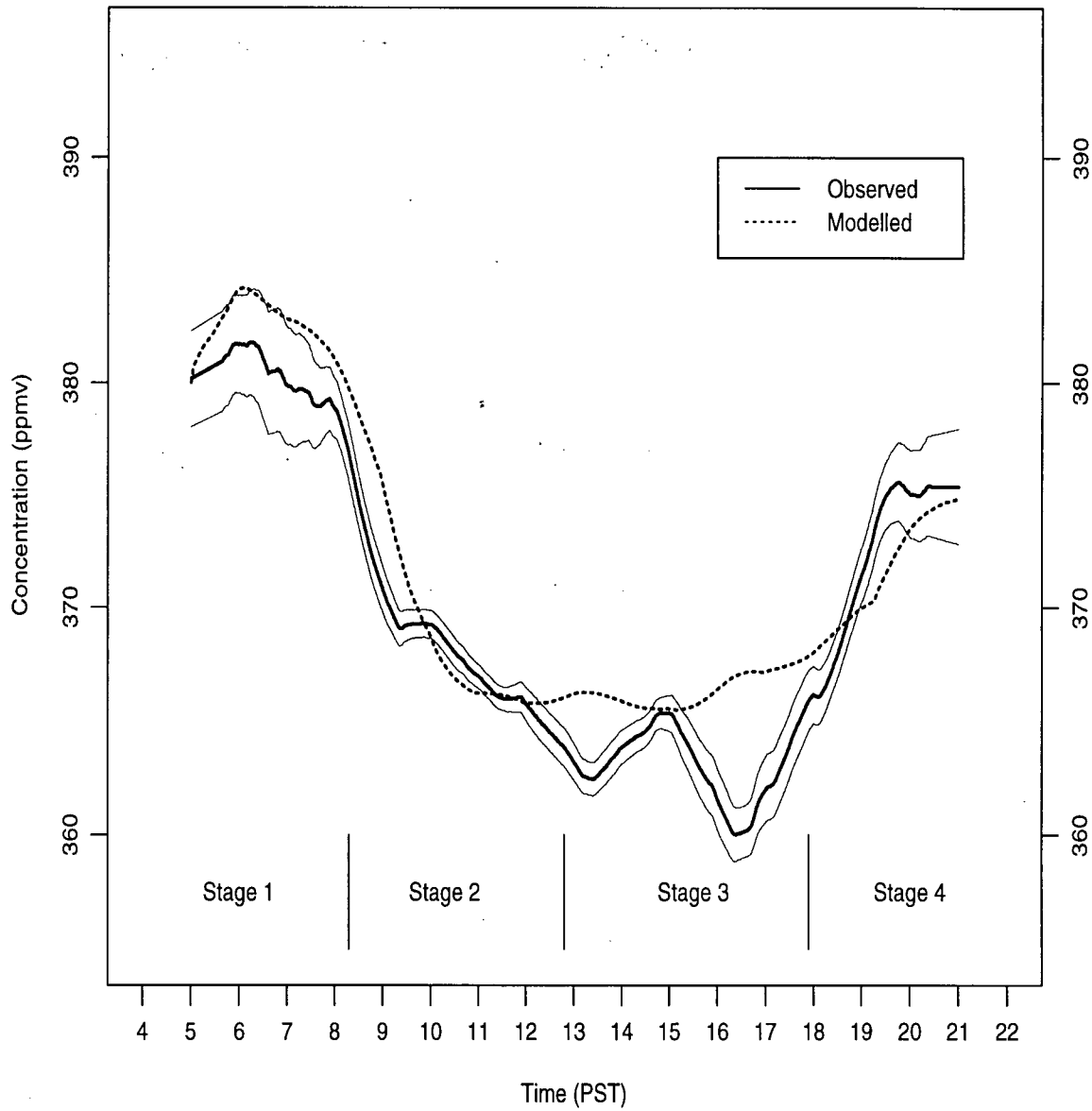
Figure 4.7: Modelled and observed diurnal CO_2 concentrations for June 13, 1993 at the Sunset site. Observed concentrations have been smoothed. Thin solid lines indicate one standard deviation on either side of the mean observed concentrations, for a sample length of ten minutes.

the time at which maximal drawdown occurs. Concentrations above the mixed layer were incremented by 1 ppmv across the possible range mentioned in Chapter 3 (372-376 ppmv) but produced virtually no difference in the timing of the onset of morning CO$_2$ reduction. Net photosynthetic rates were not adjusted since confidence in the CO$_2$ inventory was high.

Similar to the results for June 16, afternoon concentrations for June 4 and June 13 are poorly modelled in magnitude and shape. Modelled minimum concentrations are about 3 to 6 ppmv greater than observed. The observed local CO$_2$ maxima on June 13 at 1500 PST, like that on June 16, is mostly unresolved by the model. Explanation of this feature, in terms of model parameters, is difficult. Wind directions are consistent at 280°, mean wind speeds moderate and unchanging (Appendix C), and mixed layer profiles show no structure that could create a rapid rise in CO$_2$ concentrations. It is possible that the influence of very local vehicle emissions at a sub-grid scale, peak near 1500 to 1600 PST. Such a local scale effect could not be resolved by the model. However, a significant increase in variance at 1500 PST, expected with very local vehicle emissions, is not observed. Interestingly, though, a similar feature is not observed on the trace of June 4, when winds greater than 6 m s^{-1} were observed.

The difference between modelled and observed CO$_2$ concentrations for each day is shown in Figures 4.8, 4.9, and 4.10. Observed CO$_2$ concentrations are generally higher than those modelled. Large differences during stage 2 on June 4 and stage 4 on June 16 occur at times when concentrations are changing most rapidly. The average differences for the three days are shown in Figure 4.11. Afternoon concentrations are overestimated by the model. This is generally a period when standard deviations of observed concentrations are low. This overestimation is a failing of the model, and is discussed in the next section.
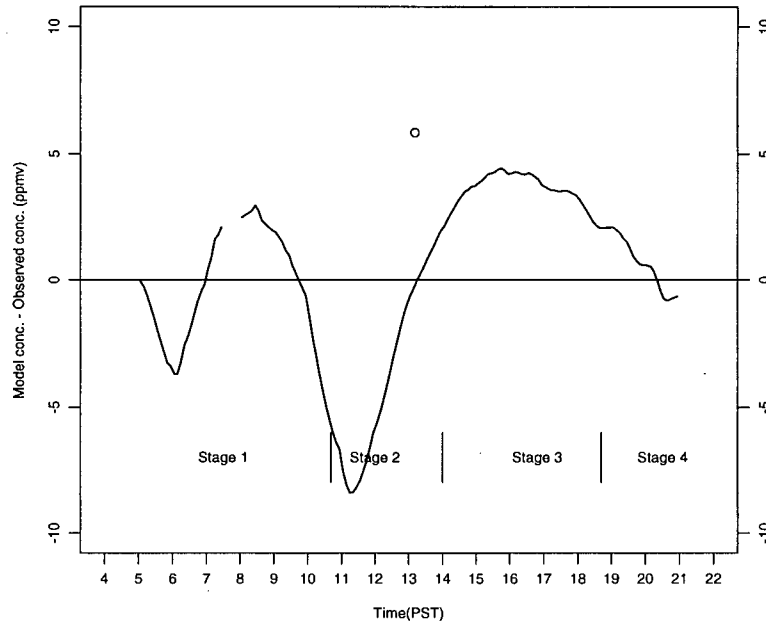
Figure 4.8: Model CO$_2$ - Observed CO$_2$ for June 4, 1993.
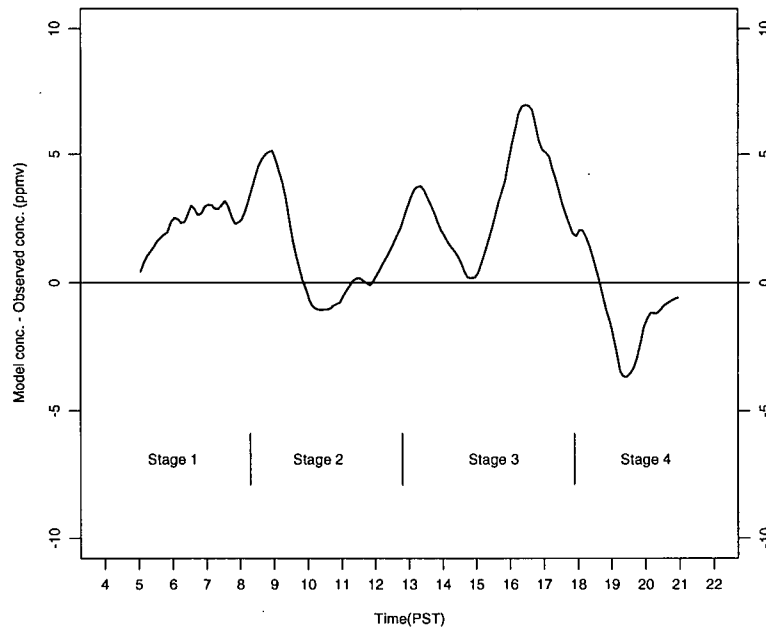
Figure 4.9: Model CO$_2$ - Observed CO$_2$ for June 13, 1993.
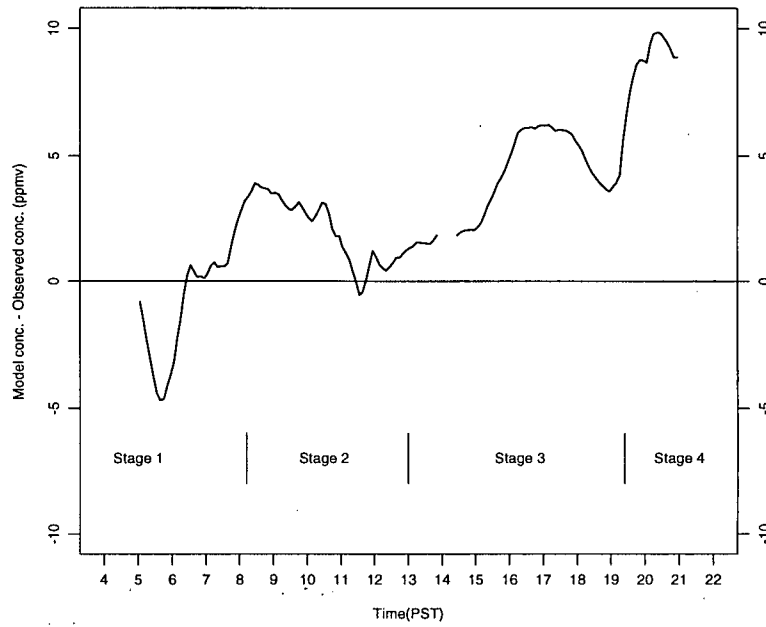
Figure 4.10: Model CO_2 - Observed CO_2 for June 16, 1993.
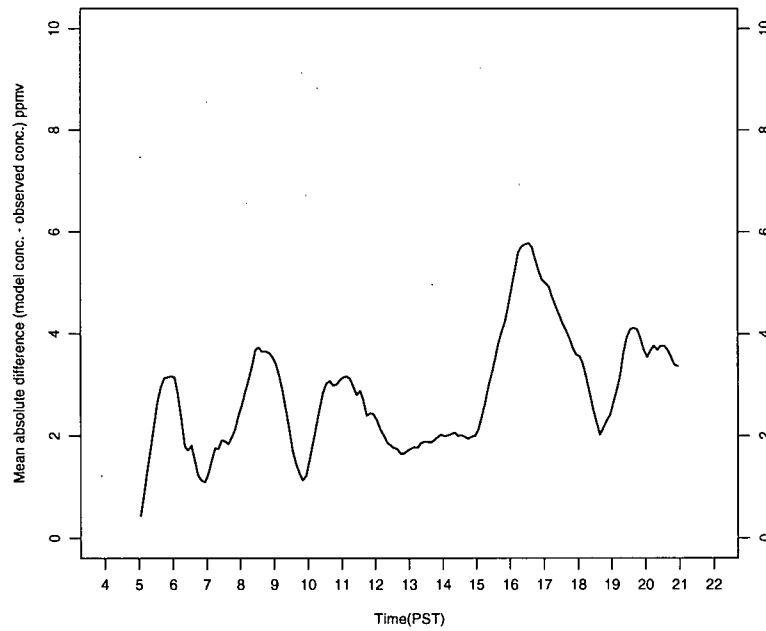
Figure 4.11: Mean $|$Model CO_2 - Observed $CO_2|$ for three days in June, 1993.

4.2.4 Model Evaluation

An insightful way to evaluate the model's performance for the three days is to look separately at the modelled diurnal concentrations (Figure 4.12) and the observed concentrations (Figure 4.13). It is promising to note that the observed concentrations are quite different for the three days. Since all diurnal stages, excepting the third, are well modelled (shown in Figures 4.5, 4.6, and 4.7), and the variability between the days is resolved by the model, this gives confidence in the model's overall ability.

Figure 4.14 shows absolute differences of observed CO$_2$ concentrations determined from averages of three pairs of days (June 4-June 16, June 4-June 13, and June 13-June 16). The largest differences occur in stages 1 and 2, due to the magnitude of the early morning peak, and the timing of the CO$_2$ drawdown. Notably afternoon observed concentrations are similar.

Figure 4.15 plots the data of Figure 4.14 (average absolute differences in observed concentrations) against average absolute differences between modelled and observed CO$_2$ at a given time. Most of the data fall above the 1:1 line, indicating that absolute differences in observed-observed diurnal CO$_2$ concentrations are greater than absolute differences in modelled-observed concentrations between the three days. Points below the 1:1 line are entirely from the afternoon during stage 3. This shows that the variability in observed CO$_2$ between days is greater than that between modelled and observed. Major influences on CO$_2$ are being adequately incorporated into the model to resolve CO$_2$ variations between days during all periods except the time of the mean afternoon minimum.

Similarities in the three days are evident in the existence of the four diurnal stages as previously discussed. Major differences arise in the timing, magnitude and duration of the morning peak in CO$_2$ concentration, and the rate of increase of concentration in
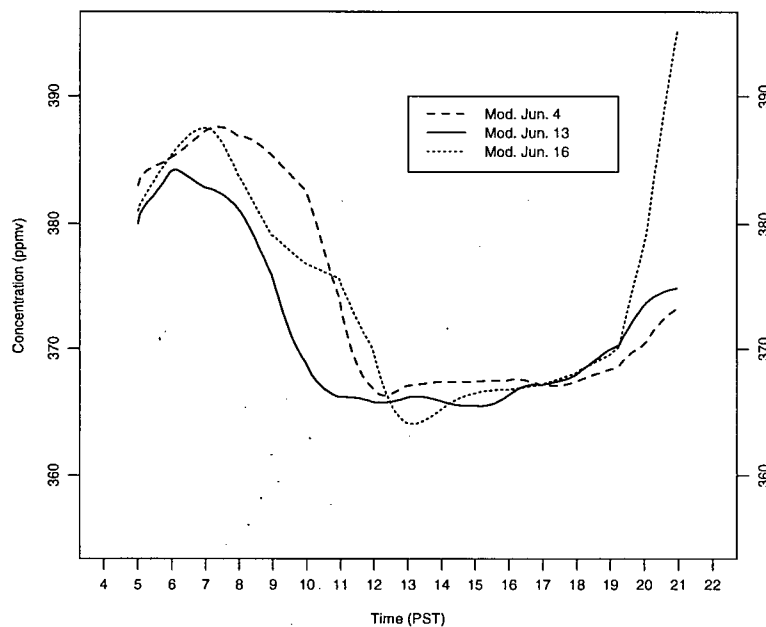
Figure 4.12: Modelled diurnal CO$_2$ concentrations for June 4, 13, and 16, 1993 at the Sunset site (box 8).
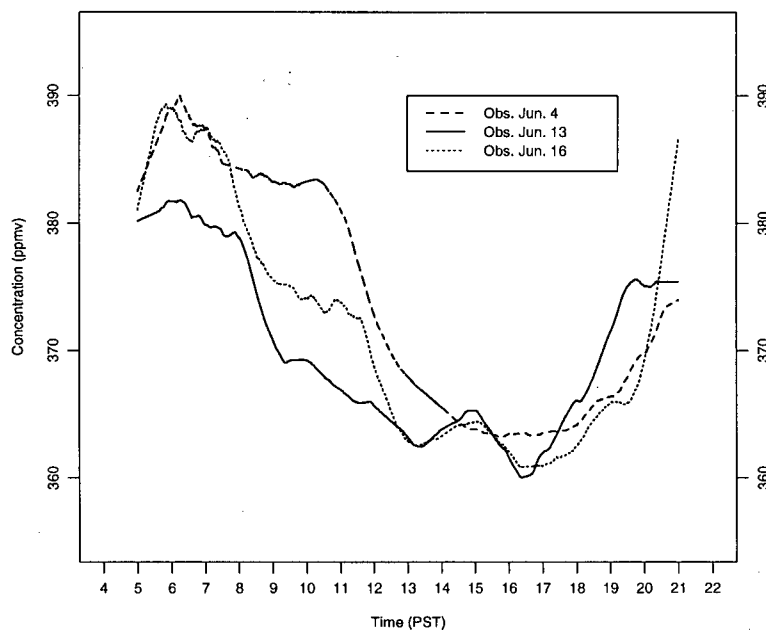
Figure 4.13: Observed diurnal CO$_2$ concentrations for June 4, 13, and 16, 1993 at the Sunset site. CO$_2$ concentrations have been smoothed.
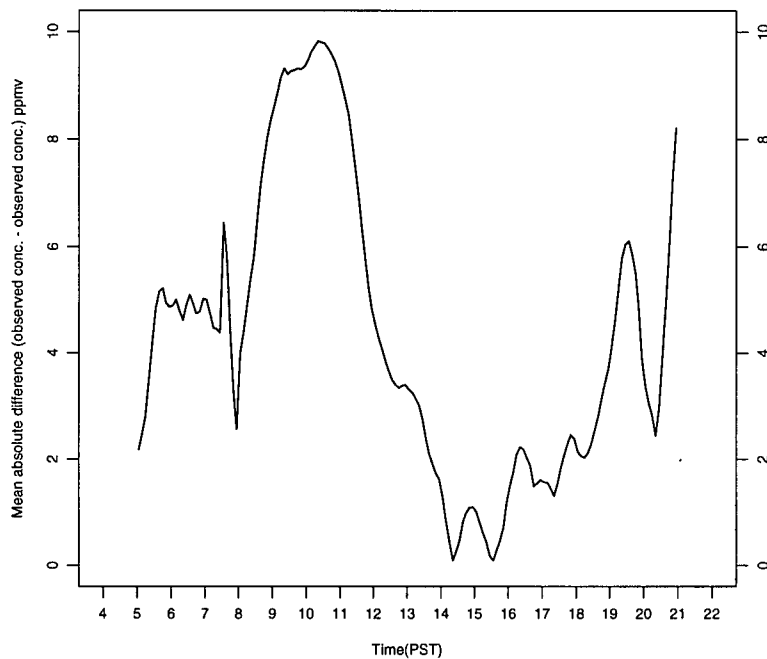
Figure 4.14: Mean |Observed CO$_2$ - Observed CO$_2$| for three pairs of days in June, 1993.
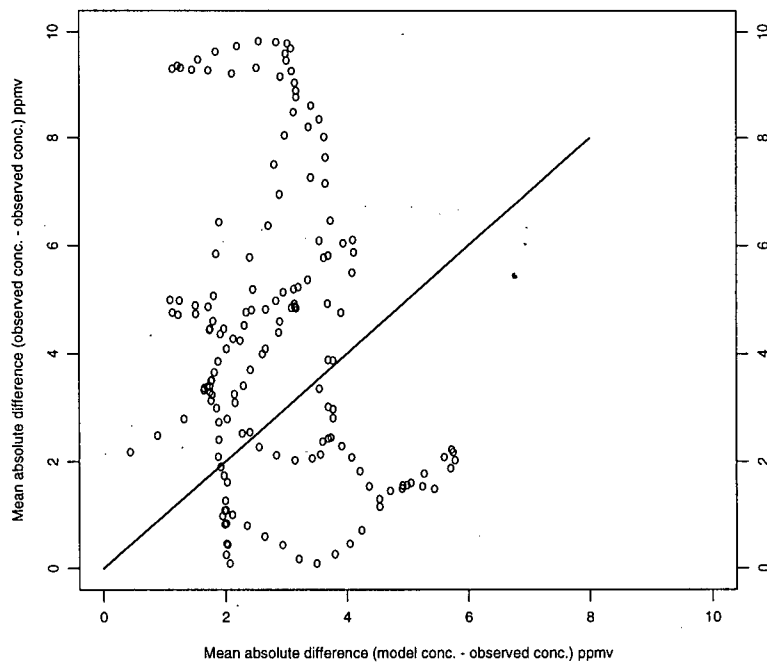
Figure 4.15: Scatterplot of mean |Observed CO$_2$ - Observed CO$_2$| against mean |Model CO$_2$ - Observed CO$_2$| for three pairs of days in June, 1993.

the nocturnal regime, due to control by boundary layer structures on the CO_2 signature imprinted by similar source and sinks strength each day. All are modelled well, and thus explainable by model parameters.

Early morning peaks of CO_2 vary significantly, reinforcing the thought that mixed layer depth is perhaps the strongest influence at this time of day. Modelled peak morning CO_2 concentrations are reached at 0600 PST on June 13, approximately 1 and 1.5 hours earlier than June 16 and June 4 respectively. Mixed layer depths on June 13 increase at a greater rate than on June 4 and June 16, over the initial model hours during stage 1 (Appendix C). This increase in the box volumes decreases the importance of surface sources at this time, thus increasing the importance (as mean winds are low) of entrained CO_2. Entrained air of lower concentrations cause early decreases in mixed layer CO_2 concentrations, as mixed layer depths increase rapidly at a time when the emissions strength can no longer be effective into a large mixed layer. Consequently the magnitude of the CO_2 peak is about 3 to 4 ppmv lower than June 16 and June 4, when the mixed layer is not seen to initially rise as quickly.

Mixed layer heights for June 4 are modelled to rise slowly, reaching maximum heights over two hours later than the other days. This leads to high concentrations from early emissions that are not diluted by entrainment until at least two hours later, giving a broad peak of CO_2. Mixed heights for June 16 are modelled to increase slowly at first (near 1×10^{-2} m s^{-1}), creating a high peak in CO_2 concentration with a duration slightly greater than that of June 13. After this a very rapid rise in mixed heights (rates greater than 3.5×10^{-2} m s^{-1}) appears to quickly reduce CO_2 concentrations by entraining air which is about 14 ppmv lower than current CO_2 concentrations within box 8.

Clearly, then, the timing of the CO_2 drawdown is very different for the three modelled days because of different balances between entrainment, advection, and emissions. Initially on June 16 concentrations decrease quickly by entrainment, then later more

quickly from advection of background CO$_2$ as concentrations decrease below 369 ppmv. Advection also plays an important role on June 13 as the sea breeze strengthens earlier, bringing in background air that is less modified by net emissions early in the day. For June 4 the drawdown doesn't proceed rapidly until after 1000 PST when the sea breeze increases in strength.

For the final stage, all modelled concentrations are seen to rise at the same time that the mixed layer collapses to the nocturnal regime. Simulations were also conducted with the nocturnal regime omitted. In this case, mixed depths were allowed to remain high and modelled concentrations rose only two or three ppmv due to anthropogenic and soil emissions into a large volume. Clearly the mixed layer collapse is important to CO$_2$ concentrations. The magnitude of the modelled rise in concentration conforms well to observations with the full nocturnal regime applied. Overall the model performs well, because modelled concentrations are close to those observed. This is not the case for stage 3.

As shown (Figure 4.9), modelled concentrations in stage 3 are consistently too high. Possible explanations for this may lie in the behaviour of model variables, such as entrainment, mean wind, net photosynthesis, and mixed layer depths. Volume entrainment defined by the model is negligible in stage 3, as $\frac{\partial h}{\partial t}$ is close to zero if not negative. However, turbulent entrainment, which is not parameterized in the model, would only act to increase concentrations, because CO$_2$ concentrations above the mixed layer are higher than mean concentrations within at this time. Entrainment, then, cannot be the answer.

A simple analysis shows that the modelled CO$_2$ concentration in stage 3 is sensitive to both mean wind speed and to the strength of net photosynthesis. Table 4.2 shows observed and modelled mean minimum CO$_2$ concentrations in stage 3. Modelled CO$_2$ concentrations are subject to scenarios of halved wind speeds and doubled net photosynthetic rates, with all other inputs unchanged. Decreases in mean wind speeds are

Table 4.2: Mean model CO$_2$ concentrations in stage 3 under scenarios of a) halved wind speeds, and b) doubled net photosynthesis.

	Mean afternoon CO$_2$ concentrations (ppmv) - Stage 3			
	Model			Observed
Date	Unchanged	2× Photosynthesis	Half $\overline{u}$	
June 4	367	362	366	363
June 13	366	361	364	360
June 16	364	360	363	361

seen to lower the afternoon concentrations by 1-2 ppmv, as air remains longer over the predominantly photosynthetically active surface of the study region during stage 3, allowing more uptake of CO$_2$ by net photosynthesis. Table 4.2 shows that halved mean wind speeds could account for only part of the differences between modelled and observed CO$_2$ concentrations during the afternoon.

On the other hand, doubling the net photosynthetic strength is sufficient to reduce modelled concentrations to the magnitude of the observed mean afternoon concentrations (Table 4.2). However, CO$_2$ flux rates of the necessary magnitude are not within the range quoted in the literature. Confidence in the accuracy of the surface biospheric inventory sheds doubt on the likelihood that it is in error by as much as a factor of two. It is unlikely that model values for the two variables identified above, or combinations of the two, are so poorly determined for the study region.

If mixing is limited by vertical diffusion or vertical transport when mixed layer heights are high in stage 3, then the mixed layer height may not give an accurate representation of the depth through which mixing is assumed to be uniform. This does not necessarily put doubt on the assumption that a relative measure of vertical mixing can be made through the changing depth of the mixed layer, because changes in mixed layer height could be correlated with changes in turbulent mixing related to the largest eddy sizes, which

are scaled by the top of the mixed layer. However, it does infer that the characteristic timescale for full vertical mixing of 5 to 6 minutes (Chapter 3) may be too long a time for uniform mixing of surface CO$_2$ sources and sinks to the top of the mixed layer to occur before CO$_2$ is carried out of the box by advection (Tennekes, 1976). This may explain the similarity of the modelled afternoon stages for each of the three days. It is possible that the large modelled mixed layer depths damp the CO$_2$ concentration variability compared to that if mixing was limited to a height much less than the inversion base. Consistent with the doubling of photosynthesis noted previously, it would take an approximate halving of the afternoon mixed layer depth to account for the needed CO$_2$ sequestration by photosynthesis, i.e. limiting vertical mixing to less than 350 m for box 8 on all days.

It is difficult to isolate single influences on CO$_2$ concentrations for both observed and modelled CO$_2$ traces. It is likely that the lack of CO$_2$ uptake has contributions from many processes. Vertical mixing may be limited when mixed heights are high. Mean boundary layer wind speeds over the study area may be different than those recorded at the Airport. Variability in background CO$_2$ concentrations could also contribute to the 3 to 6 ppmv higher afternoon observed CO$_2$ concentrations. Prolonged westerly winds may also advect "cleaner" air as the afternoon progresses, with lower concentrations closer to that expected by the global CO$_2$ monitoring stations nearby (Chapter 2), thus reducing observed concentrations.

4.3 Model Conclusions

To summarize, it has been shown that major changes in diurnal CO$_2$ are well modelled, and explained by the boundary layer processes explicit in equation 3.5. Model

architecture limits the use of the model to days defined by certain meteorological parameters (Chapter 3), which were observed for at least 3 days in June 1993. There is uncertainty in several of the model inputs. Mean wind speeds are not well resolved spatially or temporally, and may account, in part, for errors in the timing of features, and the magnitude of the afternoon drawdown. Observed background concentrations exhibit some diurnal variability that could not be applied to the model. CO$_2$ concentrations of entrained air, during mixed layer growth, were not measured.

However, given these limitations and uncertainties, the large variability in boundary layer CO$_2$ concentrations can be modelled well in stages 1 and 2. Stage 4 is also well-modelled, but appears to suffer in accuracy because of poor modelling in stage 3. This performance gives confidence that the variables of the model are all important, and that diurnal CO$_2$ variations at this site are not only the product of very local sources and sinks. Increased precision in the magnitude and timing of diurnal CO$_2$ features may be possible with a more realistic parameterization of vertical mixing, and with higher resolution meteorological observations.

Chapter 5

Conclusions

5.1 Introduction

The measurement programme shows there are large diurnal variations in boundary layer CO_2 concentrations at a suburban site. Summertime diurnal variability is observed to be relatively periodic, with mean hourly concentrations ranging from about 360 ppmv to nearly 390 ppmv. Winter periods show little diurnal periodicity, much higher concentrations, and greater short term variability.

Since the observing site was located in a busy suburban region, it is expected that CO_2 concentrations would be closely correlated with anthropogenic emissions, especially those from mobile sources. However, observed CO_2 patterns strongly suggest that other important factors act upon boundary layer CO_2 concentrations, because the diurnal CO_2 pattern closely resembles that of rural CO_2 concentrations in summertime. Consistent with this is the fact that the CO_2 inventory shows that the biosphere covers over 50% of the surface area of this suburban region. In winter the CO_2 traces from this site are more representative of urban locations (Berry and Colls, 1990a).

A model developed to simulate mixed layer CO_2 concentrations, and to determine important temporal processes acting upon them, showed accurate simulations for three days in June 1993. The most important variables are the varying depth of the mixed layer, surface CO_2 source and sink strengths, and interactions between the two. At times

of low mixed layer depths, the significance of surface source and sink strengths increases. Results indicate that summertime diurnal CO_2 periodicity is due to an active biosphere (the only mechanism by which CO_2 concentrations are reduced below background levels) and a diurnal pattern of mixing dependent primarily on mixed layer depths, and varying wind speed.

5.2 Insights

It is thought that a more complete knowledge of global biogeochemical cycling of carbon, and a better realization of the increasing quantity of CO_2 in the atmosphere can come about through smaller scale studies such as this one that isolates a suburban "ecosystem" (Peterjohn *et al.*, 1993). The present study shows that temporal variability of CO_2 at a specific urbanized site is high. Therefore reference to mean global background concentrations are meaningless when considering local CO_2 concentrations. Undisturbed background concentrations are atypical of populated areas, and, more importantly, are atypical of areas where crops are grown. Models of increased plant growth under conditions of greater CO_2 (Bazzaz and Williams, 1991) need to consider the full range of CO_2 concentrations exhibited at a given site. A better descriptor, albeit one that does not resolve diurnal changes, may be the mean afternoon CO_2 concentration. However, large nighttime buildups of CO_2 must be considered when estimating the amount of CO_2 in the global atmosphere.

Local CO_2 concentrations have not been modelled previously in a manner similar to that described in this thesis. Results indicate that boundary layer structure, defined by a well mixed layer below the inversion base, is an extremely important variable that can both lower concentrations by enhancing vertical mixing, and raise concentrations by

bounding significant surface sources of CO_2 in a shallow layer. Conversely CO_2 traces can, under some conditions, be used to infer boundary layer height. Very local sources and sinks of CO_2 (within 100 m) may be important, but it is clear that CO_2 concentrations can, and should be, modelled to include meteorological variables at larger scales.

5.3 Future work

The application of a multiple-box model of the type described in this thesis to CO_2 concentrations appears to be successful. This raised the possibility of practically applying it to validate local or regional CO_2 emissions inventories. Concerns about local CO_2 responsibilities with regard to increasing atmospheric CO_2 are leading the construction of local inventories, such as that in Vancouver (B.C. Carbon Project, 1992). Validation of emissions estimates for the region could be accomplished with continuous CO_2 monitoring, both upwind and downwind of the region, together with a multiple-box model applied to solve the inverse problem; namely that of estimating the diurnally varying surface CO_2 source and sink rates. A daily budget could be determined by averaging over many days. With extensive measurements at varying times of the year, a budget of greater timescale is possible.

The model described here is limited to periods of westerly winds in a convective boundary layer. However, a model designed to operate over a full day would need to be adaptable to more varied meteorological parameters. Further, the routinely observed wind speeds used in this model may not fully represent mean air motion over the region. Consequently, more *in situ* measurements of wind speed and direction might be set needed. Also necessary are actual measurements of CO_2 concentrations in entrained air, which has only been estimated in this study. Analysis in Chapter 4 indicates that more

accurate results during the afternoon may be achieved with greater vertical resolution of mixing between the surface and the base of the inversion layer.

References

[1] Bacastow, R. B., C. D. Keeling, and T. P. Whorf, 1985: Seasonal amplitude increase in atmospheric CO_2 concentration at Mauna Loa, Hawaii. *Journal of Geophysical Research* 90(D6), 10529-10540.

[2] Baldocchi, D. D., and T. P. Meyers, 1991: Trace gas exchange above the floor of a deciduous forest. *Journal of Geophysical Research* 96, 7271-7285.

[3] Bazzaz, F. A., and W. E. Williams, 1991: Atmospheric CO_2 concentrations within a mixed forest: Implications for seedling growth. *Ecology* 72, 12-16.

[4] Begon, M., J. L. Harper, and C. R. Townsend, 1986: *Ecology: Individuals, Populations, and Communities.* Sinauer Associates, Sunderland, MA.

[5] Beljaars, A. C. M., and A. A. M. Holtslag, 1989: *A Software Library for the Calculation of Surface Fluxes Over Land and Sea,* Royal Netherlands Meteorological Institute, The Netherlands.

[6] Benkley, C. W., and L. L. Schulman, 1979: Estimating hourly mixing depths from historical meteorological data. *Journal of Applied Meteorology* 18, 772-780.

[7] Berry, R. D., and J. J. Colls, 1990a: Atmospheric carbon dioxide and sulphur dioxide on an urban/rural transect - I. Continuous measurements at the transect ends. *Atmospheric Environment* 24A, 2681-2688.

[8] Berry, R. D., and J. J. Colls, 1990b: Atmospheric carbon dioxide and sulphur dioxide on an urban/rural transect - II. Measurements along the transect. *Atmospheric Environment* 24A, 2689-2694.

[9] B. H. Levelton and Associates Ltd., 1990: *Carbon Dioxide Inventory for British Columbia,* British Columbia Ministry of Energy, Mines and Petroleum Resources.

[10] Boden, Thomas A., Robert J. Sepanski, and Frederick W. Stoss (eds.), 1991: *Trends '91: A Compendium of Data on Global Change.* Carbon Dioxide Information Analysis Center, ORNL/CDIAC-46.

[11] Bolin, B., 1983: The carbon cycle, in *The Major Biogeochemical Cycles and their Interactions,* B. Bolin and R. B. Cook (eds.), SCOPE Report.

[12] Bolin, B., 1986: How much CO_2 will remain in the atmosphere?, in *The Greenhouse Effect, Climatic Change and Ecosystems,* B. Bolin et al. (eds.), SCOPE Report 29.

[13] B.C. Carbon Project, 1992: *Urban carbon cycle model/budget*, Science Council of B.C. Special Initiatives Fund, #21-90/91.

[14] B.C. Carbon Project, 1993: *Application of the Powertech Waterbodies carbon cycle model to the Province*, Science Council of B.C. Special Initiatives Fund, #21-90/91.

[15] Campbell, B. A., and C. Paull, 1991: *1990 Residential End Use Survey*, prepared for B. C. Hydro, Campbell Goodell Consultants Ltd., Vancouver, British Columbia.

[16] Carson, D. J., 1973: The development of a dry inversion-capped convectively unstable boundary layer. *Quarterly Journal of the Royal Meteorological Society* 99, 450-467.

[17] City of Toronto, 1991: *The changing atmosphere: Strategies for reducing CO_2 emissions, Technical Volume*, Special Advisory Committee on the Environment, Report #2, Volume 2.

[18] City of Vancouver, 1990: *Clouds of Change*, Final report of the City of Vancouver Task Force on Atmospheric Change.

[19] Clarke, J. F., and R. B. Faoro, 1966: An evaluation of CO_2 measurements as an indicator of air pollution. *Journal of the Air Pollution Control Association* 16, 212-218.

[20] Clarke, J. F., 1969: A meteorological analysis of carbon dioxide concentrations measured at a rural location. *Atmospheric Environment* 3, 375-383.

[21] Conway, Thomas J., Pieter P. Tans, and Lee S. Waterman, 1991: Atmospheric CO_2 - modern record: Mauna Loa, in *Trends '91: A Compendium of Data on Global Change*, Thomas A. Boden, Robert J. Sepanski, and Frederick W. Stoss (eds.), Carbon Dioxide Information Analysis Center.

[22] De Bruin, H. A. R., and A. A. M. Holtslag, 1982: A simple parameterization of the surface fluxes of sensible and latent heat during daytime compared with the Penman-Monteith concept. *Journal of Applied Meteorology* 21, 1610-1621.

[23] Demerjian, K. L., and K. L. Schere, 1979: Applications of a photochemical box model for O_3 air quality in Houston, Texas, in Proceedings of Specialty

Conference on Ozone/Oxidants: Interactions with the Total Environment, Environmental Protection Agency, Research Triangle Park, N. C.

[24] Desjardins, R. L., R. L. Hart, J. I. MacPherson, P. H. Schuepp, and S. B. Verma, 1992: Aircraft- and tower-based fluxes of carbon dioxide, latent, and sensible heat. *Journal of Geophysical Research* 97, 18477-18485.

[25] Dörr, H., and K. O. Münnich, 1987: Annual variation in soil respiration in selected areas of the temperate zone. *Tellus* 39B, 114-121.

[26] Enoch, H. Z., 1977: Diurnal and seasonal variations in the carbon dioxide concentration of the lower atmosphere in the coastal plain of Israel. *Agricultural Meteorology* 18, 373-385.

[27] Falkowski, Paul G. and Cara Wilson, 1992: Phytoplankton productivity in the North Pacific ocean since 1900 and implications for absorption of anthropogenic CO_2. *Nature* 358, 741-743.

[28] Foute, S., and S. Andrews, 1991: Denver, Colorado's CO_2 transportation strategies, in *Cities and global change*, J. McCulloch (ed.), Climate Institute, Washington.

[29] Gifford, F. A., and S. R. Hanna, 1973: Technical note: Modelling urban air pollution. *Atmospheric Environment* 7, 131-136.

[30] Gilbert, R., 1991: Cities and global warming, in *Cities and global change*, J. McCulloch (ed.), Climate Institute, Washington.

[31] Giovannoni, J-M, and M. Swan, 1988: A case study of air pollution in a swiss valley with a multi box model, in *17th International Technical Meeting of NATO-CCMS on Air Pollution Modelling and its Applications*, VII, Downing College, Cambridge.

[32] Griffin, R. C., 1987: CO_2 release from cement production 1950-1985, in *Estimates of CO_2 emissions from fossil fuel burning and cement manufacturing*, G. Marland, T.A. Boden, R.C. Griffin, S.F. Huang, P. Kanciruk and T.R. Nelson, Oak Ridge National Laboratory.

[33] Grimmond, C. S., 1988: *An Evaporation-Interception Model for Urban Areas*, Ph.D. Thesis, The University of British Columbia, Vancouver, British Columbia.

[34] Halter, B. C., and J. T. Peterson, 1981: On the variability of atmospheric carbon dioxide concentration at Barrow, Alaska, 1973-1979. *Tellus* 34, 166-175.

[35] Hanna, S. R., G. A. Briggs, R. P. Hosker, Jr, 1982: *Handbook on Atmospheric Diffusion*, Office of Energy Research, U. S. Department of Energy.

[36] Hanna, S. R., and J. C. Chang, 1992: Boundary-layer parameterizations for applied dispersion modeling over urban areas. *Boundary-Layer Meteorology* 58, 229-259.

[37] Harvey, D., 1991: The role of municipalities in combatting global warming. *Ecodecision* 2, 74-76.

[38] Holtslag, A. A. M., and A. P. van Ulden, 1983: A simple scheme for daytime estimates of the surface fluxes from routine weather data. *Journal of Climate and Applied Meteorology* 22, 517-529.

[39] Hosler, Charles R., 1966: Natural radioactivity (Radon-222) and air pollution measurements in Washington, D. C. *Journal of Applied Meteorology* 5, 653-661.

[40] Houghton, J.T., G.J. Jenkins and J.J. Ephraums, (eds.), 1990: *Climate Change*, IPCC Scientific Assessment, Cambridge.

[41] Houghton, J.T., B. A. Callander, and S. K. Varney, (eds.), 1992: *Climate Change 1992*, IPCC Scientific Assessment (update), Cambridge.

[42] Jaques, A. P., 1992: *Canada's Greenhouse Gas Emissions: Estimates for 1990*, Environment Canada, Report EPS 5/AP/4.

[43] Jarvis, P. G., G. B. James, and J. J. Landsberg, 1975: Coniferous Forest, in *Vegetation and the Atmosphere*, J. L. Monteith (ed.), Academic Press, New York.

[44] Jarvis, P. G., R. S. Miranda, and R. I. Meutzelfeldt, 1985: Modelling canopy exchanges of water vapor and carbon dioxide in coniferous forest plantations, in *Forest-Atmosphere Interactions*, Proceedings of the Forest Environmental Measurements Conference, B. A. Hutchison and B. B. Hicks (eds.), Oakridge, Tennessee.

[45] Jensen, N. O., and E. L. Petersen, 1979: The box model and the acoustic sounder, a case study. *Atmospheric Environment* 13, 717-720.

[46] Kauppi, P. E., K. Mielikainen and K. Kuusela, 1992: Biomass and carbon budget of european forests, 1971 to 1990. *Science* 256, 70-74.

[47] Keeling, C. D., 1973: Industrial production of CO_2 from fossil fuels and limestone. *Tellus* 28, 174-198.

[48] Keeling, C. D., R. B. Bacastow, A. E. Bainbridge, C. A. Ekdahl, P. R. Guenther, L. S. Waterman, and J. F. S. Chin, 1976: Atmospheric carbon dioxide variation at Mauna Loa observatory, Hawaii. *Tellus* 28, 538-551.

[49] Kim, J., and S. B. Verma, 1990: Carbon dioxide exchange in a temperate grassland ecosystem. *Boundary-Layer Meteorology* 52, 135-149.

[50] Kim, J., S. B. Verma, and R. J. Clement, 1992: Carbon dioxide budget in a temperate grassland ecosystem. *Journal of Geophysical Research* 97, 6057-6063.

[51] Komhyr, W. D., R. H. Gammon, T. B. Harris, L. S. Waterman, T. J. Conway, W. R. Taylor, and K. W. Thoning, 1985: Global atmospheric CO_2 distribution and variations from 1968-1982 NOAA/GMCC CO_2 flask sample data. *Journal of Geophysical Research* 90(D3), 5567-5596.

[52] Lee, X., T. A. Black and M. D. Novak, 1994: Comparison of flux measurements with open- and closed-path gas analyzers above an agricultural field and a forest floor. *Boundary-Layer Meteorology* 67, 195-202.

[53] Lettau, Heinz H., 1970: Physical and meteorological basis for mathematical models of urban diffusion processes, in *Proceedings of Symposium on Multiple Source Urban Diffusion Models*, Air Pollution Control Official Publication No. AP 86, Environmental Protection Agency.

[54] Leverenz, J. W., 1981: Photosynthesis and transpiration in large Douglas-fir: diurnal variation. *Canadian Journal of Botany* 59, 349-356.

[55] Lottermoser, J., 1991: Experiences with the concept of CO_2 reduction in the city of Saarbrücken, in *Cities and global change*, J. McCulloch (ed.), Climate Institute, Washington.

[56] Mahrt, L., J. I. MacPherson, and R. Desjardins, 1994: Observations of fluxes over heterogeneous surfaces. *Boundary Layer Meteorology* 67, 345-367.

[57] Marceau, R. L., and K. K. Lau, 1992: Carbon Dioxide implications of building materials. *Journal of Forest Engineering* 3, 37-43.

[58] Marland, Gregg and Ralph M. Rotty, 1984: Carbon dioxide emissions from fossil fuels: a procedure for estimation and results for 1950-1982. *Tellus* 36B, 232-261.

[59] Marland, G., T. A. Boden, R. C. Griffin, S. F. Huang, P. Kanciruk, T. R. Nelson, 1989: *Estimates of CO_2 Emissions from Fossil Fuel Burning and Cement Manufacturing*, based on the United Nations Energy Statistics and the U. S. Bureau of Mines Cement Manufacturing Data, ORNL/CDIAC-25, NDP-030, Oak Ridge National Laboratory.

[60] Maskell, J., 1991: Leading the way to sustainability: A role for first world cities. *Ecodecision* 2, 64-66.

[61] McConnell, J. C., and M. B. McElroy, 1971: Natural sources of atmospheric CO. *Nature* 233, 187-188.

[62] Michaels, Patrick J., and David E. Stooksbury, 1992: Global Warming: A Reduced Threat? *Bulletin of the AMS* 73, 1563-1577.

[63] Neumann, H. H., G. den Hartog, K. M. King, and A. C. Chipanshi, 1994: Carbon dioxide fluxes over a raised open bog at the Kinosheo Lake tower site during the Northern Wetlands Study (NOWES). *Journal of Geophysical Research* 99, 1529-1538.

[64] Oke, T. R., 1976: The distinction between canopy and boundary-layer urban heat islands. *Atmosphere* 14, 268-277.

[65] Oke, T. R., 1995: The heat island of the urban boundary layer: characteristics, causes and effects. *Wind Climate in Cities*, 81-107.

[66] Oke, Tim, and John Hay, 1994: *The Climate of Vancouver.* B.C. Geographical Series, Number 50, University of British Columbia, Department of Geography.

[67] Pales, J. C., and C. D. Keeling, 1965: The concentration of atmospheric carbon dioxide in Hawaii. *Journal of Geophysical Research* 70, 6053-6076.

[68] Perry, D. A., J. G. Borchers, D. P. Turner, S. V. Gregory, C. R. Perry, R. K. Dixon, S. C. Hart, B. Kauffman, R. P. Neilson, and P. Sollins, 1991: Biological feedbacks to climate change: Terrestrial ecosystems as sinks and sources of carbon and nitrogen. *The Northwest Environmental Journal* 7, 203-232.

[69] Peterjohn, William T., Jerry M. Melillo, Paul A. Steudler,Kathleen M. Newkirk, Francis P. Bowles, and John D. Aber, 1994: The response of trace gas fluxes and N availability to experimentally elevated soil temperatures. *Ecological Applications* 4(3), 617-625.

[70] Peterjohn, William T., Jerry M. Melillo, Francis P. Bowles, and Paul A. Steudler, 1993: Soil Warming and trace gas fluxes: Experimental design and preliminary flux results. *Oecologia* 93, 18-24.

[71] Press, W. H., S. A. Teukolsky, W. T. Vetterling, and B. P. Flannery, 1992: *Numerical Recipes in FORTRAN: The Art of Scientific Computing*, Cambridge University Press.

[72] Price, D. T., and T. A. Black, 1989: Estimation of forest transpiration and CO_2 uptake using the Penman-Monteith equation and a physiological photosynthesis model, in *Estimation of Areal Evapotranspiration*, T. A. Black, D. L. Spittlehouse, M. D. Novak, and D. T. Price (eds.), Int. Assoc. Hydrol. Sci., Publication. No. 177.

[73] Price, D. T., and T. A. Black, 1990: Effects of short-term variation in weather on diurnal canopy CO_2 flux and evapotranspiration of a juvenile Douglas-fir stand. *Agricultural and Forest Meteorology* 50, 139-158.

[74] Price, D. T., and T. A. Black, 1991: Effects of summertime changes in weather and root-zone soil water storage on canopy CO_2 flux and evapotranspiration of two juvenile Douglas-fir stands. *Agricultural and Forest Meteorology* 53, 303-323.

[75] Quay, P. D., B. Tilbrook, and C. S. Wong, 1992: Oceanic uptake of fossil fuel CO_2: Carbon-13 evidence. *Science* 256, 74-79.

[76] Ragland, K. W., 1973: Multiple box model for dispersion of air pollutants from area sources. *Atmospheric Environment* 7, 1017-1032.

[77] Raich, J. W. and W. H. Schlesinger, 1992: The global carbon dioxide flux in soil respiration and its relationship to vegetation and climate. *Tellus* 44B, 81-99.

[78] Randerson, D., 1970: A numerical experiment in simulating the transport of sulfur dioxide through the atmosphere. *Atmospheric Environment* 4, 615-632.

[79] Reiquam, H., 1970: An atmospheric transport and accumulation model for airsheds. *Atmospheric Environment* 4, 233-247.

[80] Ripley, E. A., and B. Saugier, 1974: Energy and mass exchange of a native grassland in Saskatchewan, in *Proceedings of the 1974 International Seminar on Heat and Mass Transfer in the Environment of Vegetation*, Dubrovnik.

[81] Ripley, E. A., and R. E. Redman, 1975: Grassland, in *Vegetation and the Atmosphere, Volume II: Case Studies*, J. L. Monteith (ed.), Academic Press, New York.

[82] Robertson, J. E., and A. J. Watson, 1992: Thermal skin effect of the surface ocean and its implications for CO_2 uptake. *Nature* 358, 738-740.

[83] Roth, M., 1991: *Turbulent Transfer over a Suburban Surface*, Ph.D. Thesis, The University of British Columbia, Vancouver, British Columbia.

[84] Roth, M., 1993: Turbulent transfer relationships over an urban surface. II: Integral statistics. *Quarterly Journal of the Royal Meteorological Society* 119, 1105-1120.

[85] Russell, G., B. Marshall, and P. G. Jarvis (eds.), 1989: *Plant Canopies: Their growth, form and function*, Cambridge University Press, Cambridge.

[86] Sarmiento, Jorge L., Ulrich Siegenthaler, and James C. Orr, 1992: A perturbation simulation of CO_2 uptake in an ocean general circulation model. *Journal of Geophysical Research* 97, 3621-3645.

[87] Sarmiento, Jorge L. and E. T. Sundquist, 1992: Revised budget for the oceanic uptake of anthropogenic carbon dioxide. *Nature* 356, 589-593.

[88] Schmid, HP. E., 1988: *Spatial scales of sensible heat flux variability: Representativeness of flux measurements and surface layer structure over suburban terrain*, Ph.D. Thesis, The University of British Columbia, Vancouver, British Columbia.

[89] Siegenthaler, Ulrich, 1986: Carbon Dioxide: Its natural cycle and anthropogenic perturbation, in *The Role of Air-Sea Exchange in Geochemical Cycling*, P. Buat-Menard (ed.), NATO ASI series, Holland.

[90] Smith, S. V. and F. T. Mackenzie, 1991: Comments on the role of oceanic biota as a sink for anthropogenic CO_2 emissions. *Global Biogeochemical Cycles* 5, 189-190.

[91] Spittlehouse, D. L., and E. A. Ripley, 1977: Carbon dioxide concentrations over a native grassland in Saskatchewan. *Tellus* 29, 54-65.

[92] Statistics Canada, 1988: *Census Tracts, Vancouver: Part 2, Profiles, Canada, 1986*, Minister of Supply and Services Canada.

[93] Statistics Canada, 1994: *Gas Utilities: Feb. 1994*, Catalogue 55-002 Monthly, Statistics Canada.

[94] Steyn, D. G., 1980: *Turbulence, Diffusion and the Daytime Mixed Layer Depth Over a Coastal City*, Ph.D. Thesis, The University of British Columbia, Vancouver, British Columbia.

[95] Steyn, D. G., and T. R. Oke, 1982: The depth of the daytime mixed layer of two coastal sites: A model and its validation. *Boundary-Layer Meteorology*, 24, 161-180.

[96] Steyn, D. G., and D. A. Faulkner, 1986: The climatology of sea breezes in the Lower Fraser Valley, British Columbia. *Climatological Bulletin*, 20, 21-39.

[97] Stull, R. B., 1988: *An Introduction to Boundary Layer Meteorology*, Kluwer Academic Publishers.

[98] Tanaka, M., T. Nakazawa, and S. Aoki, 1983: Concentration of atmospheric carbon dioxide over Japan. *Journal of Geophysical Research* 88, 1339-1344.

[99] Tanaka, M., T. Nakazawa, and S. Aoki, 1985: Atmospheric carbon dioxide variations in the suburbs of Sendai, Japan. *Tellus* 37B, 28-34.

[100] Tans, Pieter P., Inez Y. Fung, and Taro Takahashi, 1990: Observational constraints on the global atmospheric CO_2 budget. *Science* 247, 1431-1438.

[101] Tans, Pieter P., and Thomas J. Conway, 1993: *Atmospheric Carbon Dioxide Mixing Ratios - Cooperative Flask Sampling Network, 1968-1992*, NOAA Climate Monitoring and Diagnostics Laboratory.

[102] Taylor, N. K., 1992: The role of the ocean in the global carbon cycle. *Weather* 47, 146-151.

[103] Tennekes, H., 1976: Observations on the dynamics and statistics of simple box models with a variable inversion lid, in *Third Symposium on Atmospheric Turbulence, Diffusion and Air Quality*, AMS, Raleigh, N. C.

[104] Thompson, G. A., 1985: *Vegetation Classification of the endowment land*, Technical Paper #4, University Endowment Lands - Forest Park Research, U.B.C. Technical Committee on the Endowment Lands, GVRD Parks Dept.

[105] Trivett, N. B. A., and K. Higuchi, 1989: Trends and seasonal cycles of atmospheric CO_2 over Alert, Sable Island, and Cape St. James, as analyzed by forward stepwise regression technique, in *The Statistical Treatment of CO_2 Data Records*, W. P. Elliot (ed.), Air Resources Laboratory, Silver Spring, Maryland.

[106] Tsunogai, Shizuo, Tsuneo Ono, and Shuichi Watanabe, 1993: Increase in total carbonate in the Western North Pacific water and a hypothesis on the missing sink of anthropogenic carbon. *Journal of Oceanography* 49, No. 3 (in press).

[107] van Ulden, A. P., and A. A. M. Holtslag, 1985: Estimation of atmospheric boundary layer parameters for diffusion applications. *Journal of Climate and Applied Meteorology* 24, 1196-1207.

[108] Verma, S. B., D. D. Baldocchi, D. E. Anderson, D. R. Matt, and R. J. Clement, 1986: Eddy fluxes of CO_2, water vapor, and sensible heat over a deciduous forest. *Boundary-Layer Meteorology* 36, 71-91.

[109] Verma, S. B., J. Kim, and R. J. Clement, 1989: Carbon dioxide, water vapor and sensible heat fluxes over a tallgrass prairie. *Boundary-Layer Meteorology* 46, 53-67.

[110] Verma, S. B., J. Kim, and R. J. Clement, 1992: Momentum, water vapor, and carbon dioxide exchange at a centrally located prairie site during FIFE. *Journal of Geophysical Research* 97, 18629- 18639.

[111] Volkov, Y. A., L. G. Yelagina, V. V. Kudryavtsev, A. I. Lazarev, and S. O. Lomadze, 1988: Measurement of moisture and carbon dioxide transfer in the atmospheric ground layer. *Izvestiya, Atmospheric and Oceanic Physics* 24, 589-593.

[112] Walsh, John J., 1991: Importance of continental margins in the marine biogeochemical cycling of carbon and nitrogen. *Nature* 350, 53-55.

[113] Wellisch, Maria, 1992: MB Carbon Budget for the Alberni Region, *MB Research*.

[114] Wofsy, S. C., M. L. Goulden, J. W. Munger, S.-M. Fan, P. S. Bakwin, B. C. Daube, S. L. Bassow and F. A. Bazzaz, 1993: Net exchange of CO_2 in a mid-latitude forest. *Science* 260, 1314-1317.

[115] Woodwell, G. M., and W. R. Dykeman, 1966: Respiration of a forest measured by carbon dioxide accumulation during temperature inversions. *Science* 154, 1031-1034.

Appendix A

Scientific Background and Literature Review: CO_2 Global context

A.1 Introduction

This appendix summarizes the nature of the global carbon cycle, with reference to reservoirs of carbon storage, and to the processes involved in transferring carbon, primarily as fluxes of CO_2 from or to each reservoir. Although the processes involved in, and the constraints put upon, the cycling of carbon operate at the micro-scale, it is important to examine the significance of each ecosystem with regards to the global carbon cycle, and to realize that each ecosystem is inextricably linked to others through CO_2 exchange processes. Figure A.1 shows the magnitude (in Gt C) of the major carbon reservoirs, indicating that the atmospheric reservoir is comparable in magnitude to that of the land biota and the surface mixed layer of the ocean. Also indicated by arrows are the exchanges of carbon (in Gt C/year), as CO_2. Mechanisms by which these fluxes occur will be covered in the discussion of three main topics: a) the terrestrial biosphere, including the land biota, soil, and detritus, b) the ocean, including the surface waters, intermediate and deep waters, and the oceanic biota, and c) the atmosphere. However, it is necessary to first understand concepts that govern the system as a whole.
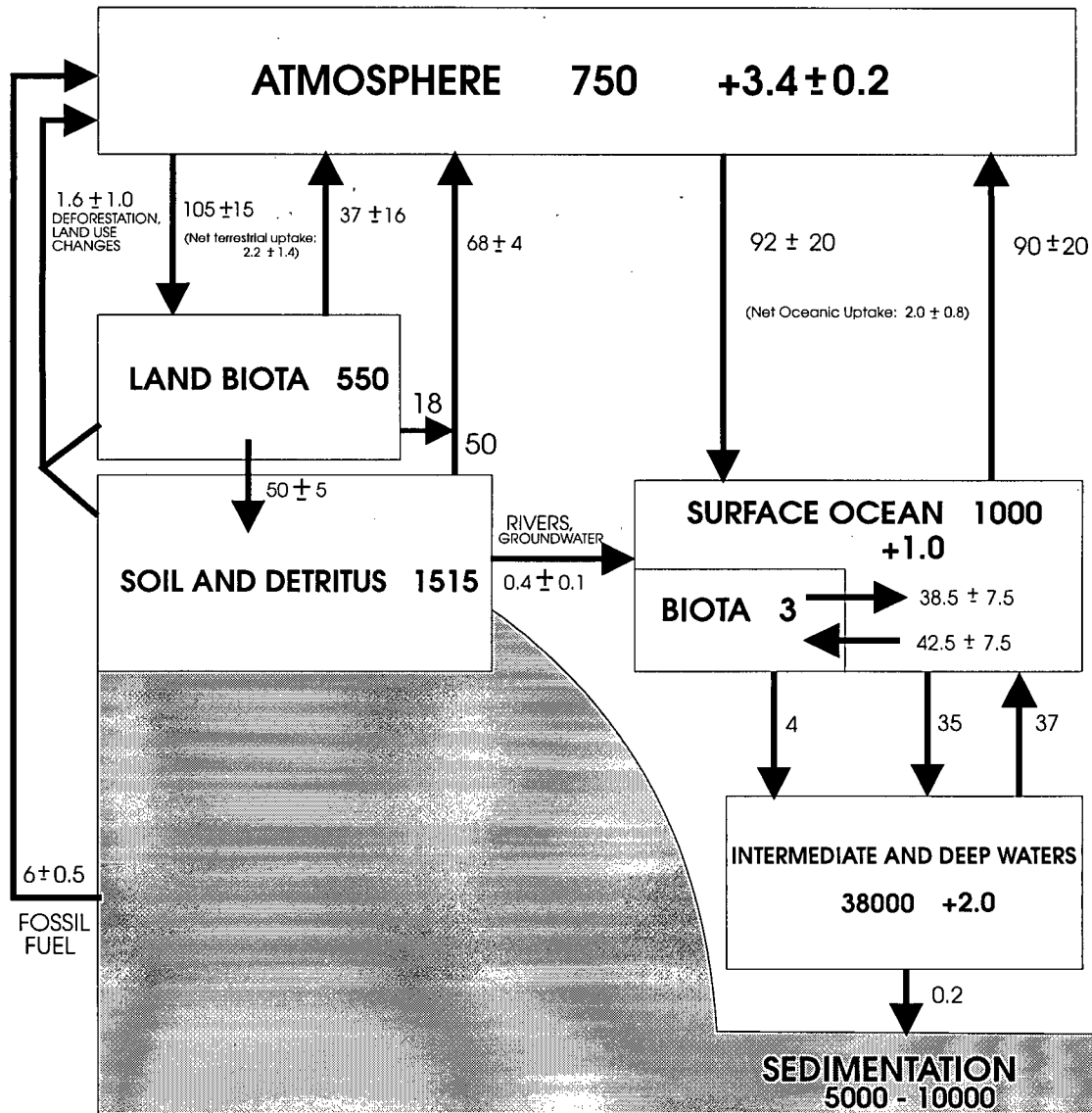
Figure A.1: Major carbon reservoirs and annual fluxes. Units are Gt C for the reservoir values, and Gt C/year for the fluxes (denoted by arrows) and for the changes in storage. Source: Adapted from Houghton *et al.* (1990) with updated estimates from Bolin (1983), Falkowski *et al.* (1992), Houghton *et al.* (1992), and Raich and Schlesinger (1992). See text.

A.2 The Global Carbon Cycle

The estimated gross fluxes in the global carbon cycle are shown in Figure A.1. This model of the carbon cycle is dependent upon the assumption of pre-industrial steady state equilibrium. It is an integral part of the model, as it allows the assumption to be made that the natural cycling of carbon has been operating for a sufficiently long period of time to have developed a steady state. Thus, in the pre-industrial era (approximately before 1850) the major carbon reservoirs were neither accumulating nor degrading in carbon and carbon fluxes into a reservoir, such as the ocean, were exactly balanced by fluxes out over an annual period. Interannual, or seasonal, imbalances, such as the seasonal dependence on carbon uptake of the terrestrial biota by photosynthesis, are important and therefore annual carbon budgets (or budgets of greater timescale) are the only significant indicator of long term changes in carbon storage. Annual imbalances, perhaps caused by phenomena such as El Niño, have not been well quantified in carbon budgets due to the large errors (as much as 22% for the ocean-atmosphere) in gross exchange fluxes. Seasonal changes, however, are much more pronounced and clearly evident from the atmospheric CO$_2$ concentration measurements made at Mauna Loa, Hawaii (Keeling *et al.*, 1976). Since approximately 1850 anthropogenic emissions have disrupted this equilibrium by initiating changes in carbon storage as the system seeks to attain another equilibrium.

The steady-state assumption allows the current carbon budget to be balanced by only accounting for the anthropogenic perturbation CO$_2$. It is assumed that increasing atmospheric CO$_2$ concentration is due to anthropogenic perturbation of the natural carbon cycle, by fossil fuel combustion, deforestation, and other land use changes. Figure A.1 indicates that the carbon cycle is not in equilibrium, and there is a redistribution of C

storage from one reservoir to another. The extraction of 6 ± 0.5 Gt C/year (Houghton *et al.*, 1992) from deep sediments, and emitted to the atmosphere by fossil fuel combustion, in addition to the 1.6 ± 1.0 Gt C/year (Houghton et al., 1992) emitted to the atmosphere through deforestation, give an anthropogenic perturbation to the natural cycling of carbon of 7.6 ± 1.1 Gt C/year.

Based upon measurements of atmospheric CO_2 storage of 3.4 ± 0.2 Gt C/year (Houghton *et al.*, 1992) it is recognized that not all of the perturbation CO_2 remains in the atmosphere. The remainder, approximately 4.2 Gt C/year, is deposited elsewhere. Studies by Quay *et al.* (1992) and Tans *et al.* (1990) indicate that the oceans and terrestrial biosphere are both capable of taking up some of the anthropogenic perturbation. Ocean modelling studies give consistent estimates of oceanic uptake of 2.0 ± 0.8 Gt C/year (Houghton *et al.*, 1992), thus leaving 2.2 ± 1.4 Gt C/year (calculated as a residual) to be taken up by the terrestrial biosphere, perhaps due to the fertilization effect, whereby CO_2 is sequestered more abundantly by photosynthesis under conditions of increased atmospheric CO_2 concentration. Few estimates of net terrestrial uptake determined independently are this high. Actual estimates of the uptake of anthropogenic carbon by the terrestrial biosphere are difficult to make, due to the complexity of the many diverse ecosystems, and the poor spatial coverage of CO_2 flux studies over these ecosystems. However a recent study proposes that the terrestrial uptake may be as high as 3.4 Gt C/year (Tans *et al.*, 1990) based upon reduced estimates of oceanic uptake. This paper has been criticized and adjusted to conform more closely to the values shown in Figure A.1 (Houghton *et al.*, 1990 and Sarmiento and Sundquist, 1992).

A.3   Terrestrial Biosphere Carbon Flux Processes

This section will summarize the terrestrial biospheric carbon cycle and the significant processes involved in this integrated ecosystem. Immediately two main spheres of interest can be identified. They are: the above-ground vegetation (land biota), including all woody and green organic matter with associated root structure, and soils. The general term "soils" will in this case refer to not only the soil itself, but also all dead organic matter contained within, including surface litter. The terrestrial biosphere is mainly linked to the rest of the carbon cycle through the processes of photosynthesis and respiration, but a minor link to the Oceans, independent of the atmosphere, is the removal of C from the terrestrial biosphere by groundwater and by rivers. Estimates of the magnitude of this component are poorly known, but are thought to be relatively small. Sarmiento and Sundquist (1992) indicate that this sink from the terrestrial biosphere is 0.4 ± 0.1 Gt C/year.

A.3.1   Photosynthesis

Photosynthesis is the process by which carbon is sequestered from atmospheric CO_2 to create living systems of carbohydrates. Net photosynthesis is composed of two reactions, namely a) the light reaction - the capture of light energy by chlorophyl, and b) the dark reaction - the use of the products of the light reaction to make carbohydrates for plant growth from CO_2 entering leaves through the stoma. CO_2 is also given off during the dark reaction, albeit in smaller quantities than that sequestered. The overall photosynthetic reaction is,

$$CO_2(g) + H_2O(l) + light \rightarrow CH_2O(aq) + O_2(g) \qquad \text{(A.1)}$$
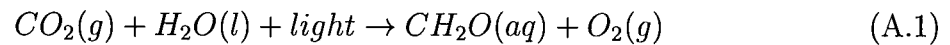
The photosynthetic reaction rate is dependent on moisture, PAR (photosynthetically active radiation), temperature, and growth stage (Kim and Verma, 1990). The reaction is dependent on available moisture, as water is the medium in which metabolic chemical activity takes place. A greater supply of water, up to a saturation point, will increase the reaction rate. PAR, which is absorbed by the plant chlorophyl, predominantly near 700 nm, is used as an energy source in the reaction. At certain photon flux densities, photo-saturation is reached, above which there is no additional response.

As shown in Figure A.2, there are two classes, based upon their photosynthetic response to an increase in the photon flux density. C_3 plants reach a plateau in their response to photon flux density, beyond which the photosynthetic rate ceases to increase with increased photon flux density as the photosynthesizing leaves are saturated with light. C_4 plants differ by having an increasing photosynthetic rate over the photon flux density range exhibited in the terrestrial biosphere, typical of warm weather plants. The C_4 plants are also shown to have a higher water use efficiency, thereby increasing the amount of carbon fixed per unit of water (Begon *et al.*, 1986). For these reasons C_4 plants are more abundant in arid and tropical areas. The response of C_4 plants to increased CO_2 concentrations is not clear, but C_3 plants have shown reduced total respiration at higher CO_2 concentrations, thus increasing their biomass. C_3 plants are approximately 95% of the global vegetation.

A study over temperate grassland (Kim and Verma, 1990) clearly shows the diurnal and seasonal variation of photosynthesis. During daytime there is a downward flux of CO_2 which is closely correlated to PAR in magnitude, thus indicating that photosynthesis increases with increasing PAR. Night-time upward fluxes are representative of respiration
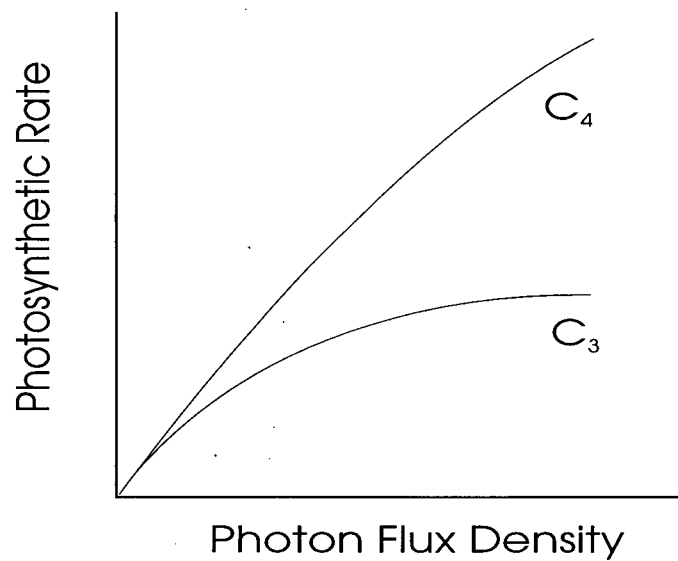
Figure A.2: Photosynthetic response of C_3 and C_4 plants as a function of photon flux density. Source: Begon *et al.* (1986).

rates when photosynthesis is inactive. Seasonally it can be seen that the downward CO_2 flux (photosynthesis) decreases during dry spells, and also decreases during vegetation dormancy in the winter months. The same study also shows that as the ecosystem comes into its dry season, the diurnal peak in the downward flux of CO_2 peaks before that of PAR, perhaps due to the drying out of the soil towards solar noon, thus limiting photosynthetic activity. The dependence on growth stage is evidenced by seasonal changes in the net daytime CO_2 flux. Already into senescence by October, the net flux of CO_2 from the atmosphere is rarely positive as biospheric respiration dominates the exchange flux. This seasonal role of photosynthesis is evident in the CO_2 concentration measurements taken at Mauna Loa, Hawaii (Keeling *et al.*, 1976) which clearly indicate lower CO_2 concentrations during the photosynthetically active Northern Hemisphere summer.

A.3.2 Respiration and Soils

Carbon is returned to the atmosphere from the terrestrial biosphere by respiration. The two main components of respiration are a) respiration of CO_2 from living vegetation (autotrophic respiration) and b) respiration from dead organic matter (heterotrophic respiration), primarily contained in soils, but also in surface litter. The first process is a result of the dark photosynthetic reaction, whereby chemical metabolic activity converts organic carbon back into CO_2 and emits it to the atmosphere via stomata in leaves and to the soil by roots. This is an ongoing process, independent of light, and therefore, unlike photosynthesis, occurs at all times. CO_2 emitted into the soil by roots can remain stored in its inorganic form in the soils while maintaining equilibrium with the atmosphere. This equilibrium is dependent on partial pressures of CO_2 at the atmosphere/soil interface. It is thought (Raich and Schlesinger, 1992) that live root respiration could account for as much as 30%-70% of total soil respiration. However, Raich and Schlesinger (1992) estimate that globally live root respiration accounts for approximately 18 Gt C/year (26%) of the total 68 ± 4 Gt C/year emitted to the atmosphere from soil respiration.

The balance of soil respiration is from decomposition of dead organic matter within the soil and surface litter. This is accomplished by the consumption of dead organic matter by soil organisms which replace high carbon organic matter (C:N ratio = 40) with low carbon biomass (C:N ratio = 10), thus allowing oxidation of the available carbon, and emission as CO_2 (Perry *et al.*, 1991). The rate at which this CO_2 leaves the soil to enter the atmosphere is a function of a) CO_2 production by decomposition within soils and surface litter, b) CO_2 concentration gradient between soil and atmosphere, c) temperature, d) soil pore size, e) soil moisture and f) wind speed.

A.3.3 Terrestrial Biosphere Carbon Fluxes

Global terrestrial biospheric carbon fluxes are shown diagrammatically in Figure A.3. It is estimated that the flux of carbon from the atmosphere to the land biota is 90 - 120 Gt C/year (Houghton *et al.*, 1990). The flux is determined by the ability of the land biota to sequester carbon from CO_2 through the process of photosynthesis. This amount is the gross primary productivity (GPP) of the terrestrial biosphere. At the same time, the same aboveground living organic matter that is able to photosynthesize is respiring CO_2 through pathways such as the stomata of leaves. This is the aboveground autotrophic respiration and is calculated as the residual from:

$$\text{aboveground autotrophic resp.} = GPP - \text{Total soil resp.} - \text{Fire} - \text{Herbivores} \qquad (A.2)$$

$$= (105 \pm 15) - (68 \pm 4) - (3.5 \pm 1.5) - (3) = 31 \pm 16 \text{ Gt C/year} \qquad (A.3)$$

Best estimates for a GPP of 105 ± 15 Gt C/year (Houghton *et al.*, 1990), emissions due to fire of 3.5 ± 1.5 Gt C/year (Raich and Schlesinger, 1992), emissions due to herbivores of approximately 3 Gt C/year with no error estimate (Raich and Schlesinger, 1992), and a total soil respiration of 68 ± 4 Gt C/year (Raich and Schlesinger, 1992), were used. The minor sink of leaching to the Oceans has been ignored in this calculation.

It is important to note here that the value for total soil respiration includes the belowground autotrophic respiration of live roots. This convention is adopted due to the difficulty of separating respiration of CO_2 by decomposition in soils from autotrophic root respiration when measuring CO_2 fluxes above a given soil type.
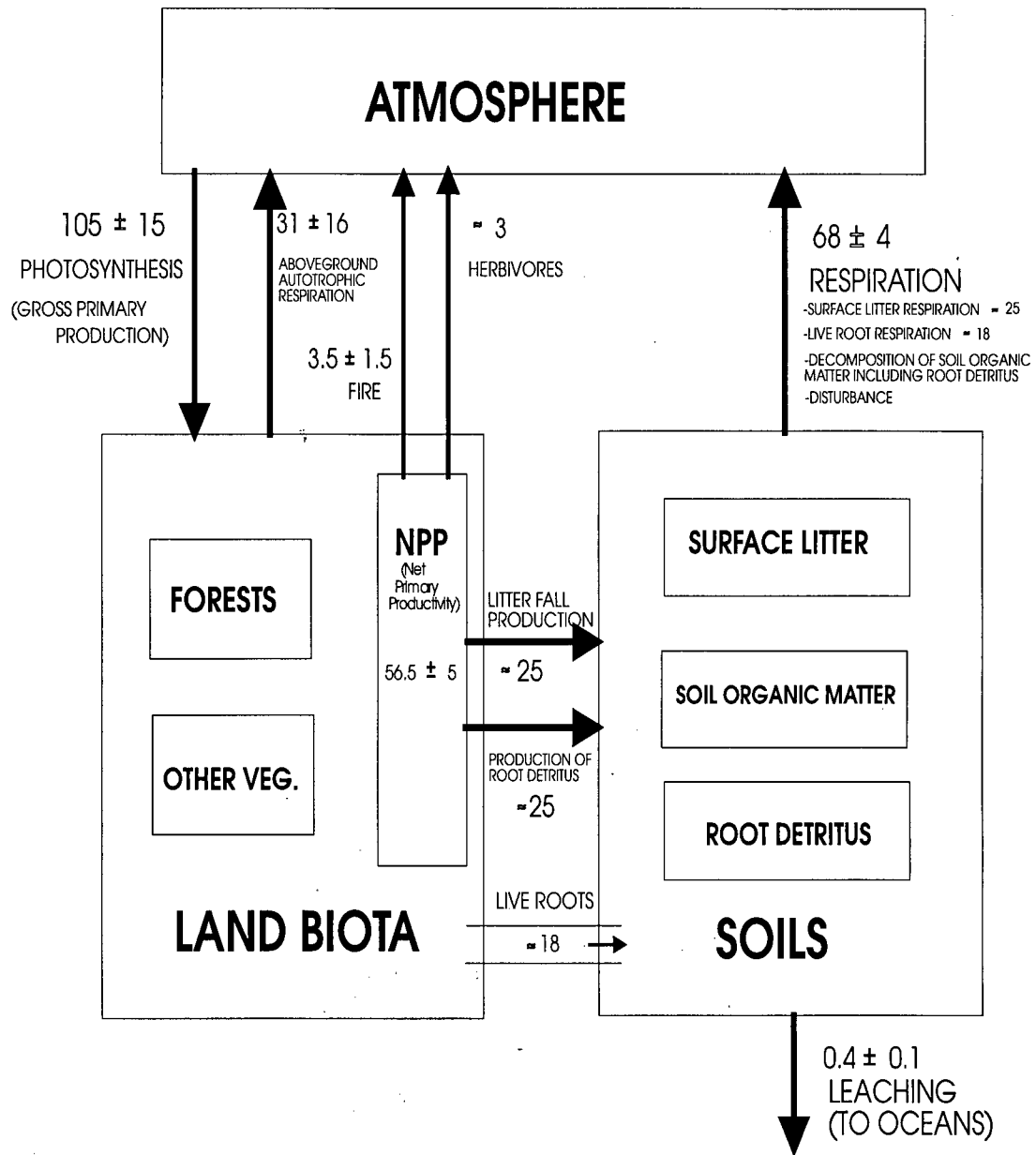
Figure A.3: Global terrestrial biospheric carbon fluxes. Fluxes are in Gt C/year and are indicated by arrows. Boxes indicate carbon storage in Gt C. Sources: Houghton *et al.* (1990), and Raich and Schlesinger (1992). See text.

If a steady state equilibrium exists, with no change in storage, then there must be a transfer of C from the land biota to the soils which will allow the total soil respiration to be 68 ± 4 Gt C/year. Raich and Schlesinger (1992) estimate the contribution from live roots to be approximately 18 Gt C/year. The error on this estimate may be large, as they acknowledge the importance of species type on root respiration, and the thought that root respiration may be as high as 30% to 70% of total soil respiration. Be this as it may, the land biota are left to transfer approximately 50 Gt C/year to the soils by way of litter fall production and the production of root detritus, which are thought to contribute nearly equally on a global scale.

This amount, plus emissions by fire and herbivores, is the net primary productivity (NPP) and is calculated to be 56.5 ± 5 Gt C/year from Figure A.3, as:

$$(68 \pm 4) - (18) + (3.5 \pm 1.5) + (3) = 56.5 \pm 5 \text{ Gt C/year.}$$

This estimate of NPP falls within common published estimates for NPP of 50-60 Gt C/year (Houghton *et al.*, 1990).

The greatest storage of carbon in the terrestrial biosphere is in dead soil organic matter (1515 Gt C), which includes surface litter and root detritus, and is nearly three times that of the land biota (550 Gt C). The land biota is defined as all living organic matter of forests and vegetation. The magnitude of carbon storage in forest trees is thought to be of the same order as all other vegetation combined. The highest forest C storage is in old growth forests where each tree is approximately 45% carbon. Surface litter storage is also higher in this ecosystem than most others (Bolin, 1986 and Wellisch, 1992).

Studies have been initiated (Peterjohn *et al.*, 1994) to determine the response of soil respiration to changing climatic variables. The difficulty of isolating the numerous processes involved is a main reason why soils are not well understood or quantified, especially outside the mid-latitudes where most studies have been conducted. Peterjohn

et al. (1993) have set up a program to measure CO_2 fluxes over a mid-latitude soil in a mixed deciduous forest, and to determine the soil ecosystem response to a constant annual 5°C soil temperature increase over normal. Consensus of many studies indicates significant increases in global soil respiration with increased soil temperature, and increased precipitation (and thus soil moisture) for a global aggregate of soils (Raich and Schlesinger, 1992). Peterjohn *et al.* (1994) find the same relation for their soils with respect to soil temperature, but the opposite correlation for precipitation. They obtain a slight decrease in CO_2 efflux as soil moisture increases. However, most of the variability in global soil respiration (SR) can be explained by the equation (Raich and Schlesinger, 1992),

$$SR = 9.88T + 0.344P + 0.112TP + 2.68 \qquad \text{(A.4)}$$

where,

SR = soil respiration $(gC/m^2/yr)$, T = temperature (°C), and P = precipitation (mm).

It is likely that more variability could be explained by this equation if a soil moisture variable, rather than precipitation was used. Precipitation as a surrogate for soil moisture has the obvious advantage of being much more readily available, but the soil moisture/precipitation relationship is a complex one. The study also showed lower soil moisture, likely due to greater evaporation, in soils with elevated soil temperatures.

The increase in soil CO_2 emissions with temperature is due to increased microbial decomposition and root respiration. These are short term results and may not be indicative of long term processes. To give a clear prediction of soil responses to future climate change it is necessary to determine the effect that temperature has on evapotranspiration, and thus soil moisture.

A.3.4   Terrestrial Biosphere Conclusions

Research on a large scale (Michaels and Stooksbury, 1992 and Kauppi et al., 1992) indicate that there has already been a response by the ecosystem to the fertilization effect. It has been determined that since pre-industrial atmospheric CO_2 concentrations, plants have adapted their stomata to become more water efficient, and that the C storage in European forests has increased within the last 30 years. Both are possible effects of the CO_2 fertilization effect. However, these estimates rely on historical data and limited sampling. The results are interesting, but not conclusive.

The necessity for continued study over varying ecosystem types is unquestionable, as photosynthetic and respiration rates vary widely among and within vegetation biomes. This may reduce the large errors in the estimates of flux magnitudes, but the thought that continued research may at some point allow the absolute magnitude of the net terrestrial uptake to be calculated seem unrealistic. It will, however, allow greater understanding of the processes involved, and of the possible feedbacks.

A.4 The Oceanic Carbon Cycle

The role of the Oceans in the global carbon cycle is thought to be the most important component in terms of long term climate change. This assumption is justified by the fact that the Oceans are the largest reservoirs of carbon (Figure A.1), and thus may have a large capacity for taking up anthropogenic carbon (in the form of CO_2) over long periods of time. Figure A.4 shows the important reservoirs and exchange fluxes in the oceanic carbon cycle.

Clearly the flow of carbon in this ecosystem is driven by the exchange of CO_2 between the atmosphere and the surface waters of the oceans (approximately the upper 75 metres), as these are the largest exchange fluxes. This is itself partly dependent on the magnitude of the anthropogenic perturbation to the atmosphere.

CO_2 that invades surface waters in gaseous form is then dissolved into dissolved inorganic carbon (DIC) or taken up by biological organisms to create living organic matter which later, upon decay, forms dissolved organic carbon (DOC). A small, but not insignificant flux, of 0.4 ± 0.1 Gt C/year (Sarmiento and Sundquist, 1992) enters the surface ocean as both DIC and DOC from rivers and groundwater (As discussed later, this is also an important flux of nutrients). If these were the only mechanisms in the ocean carbon cycle, the surface waters would eventually become saturated with dissolved inorganic carbon, thus slowing and then stopping the dissolution of gaseous CO_2. However, physical processes such as ocean currents, diffusion and thermocline ventilation, and biological processes are continually drawing carbon out of the surface mixed layer above the thermocline and depositing it into the intermediate and deep ocean reservoirs, allowing more carbon to invade as CO_2 into the surface waters. Figure A.5 shows clearly the decreased concentration of total dissolved inorganic carbon closest to
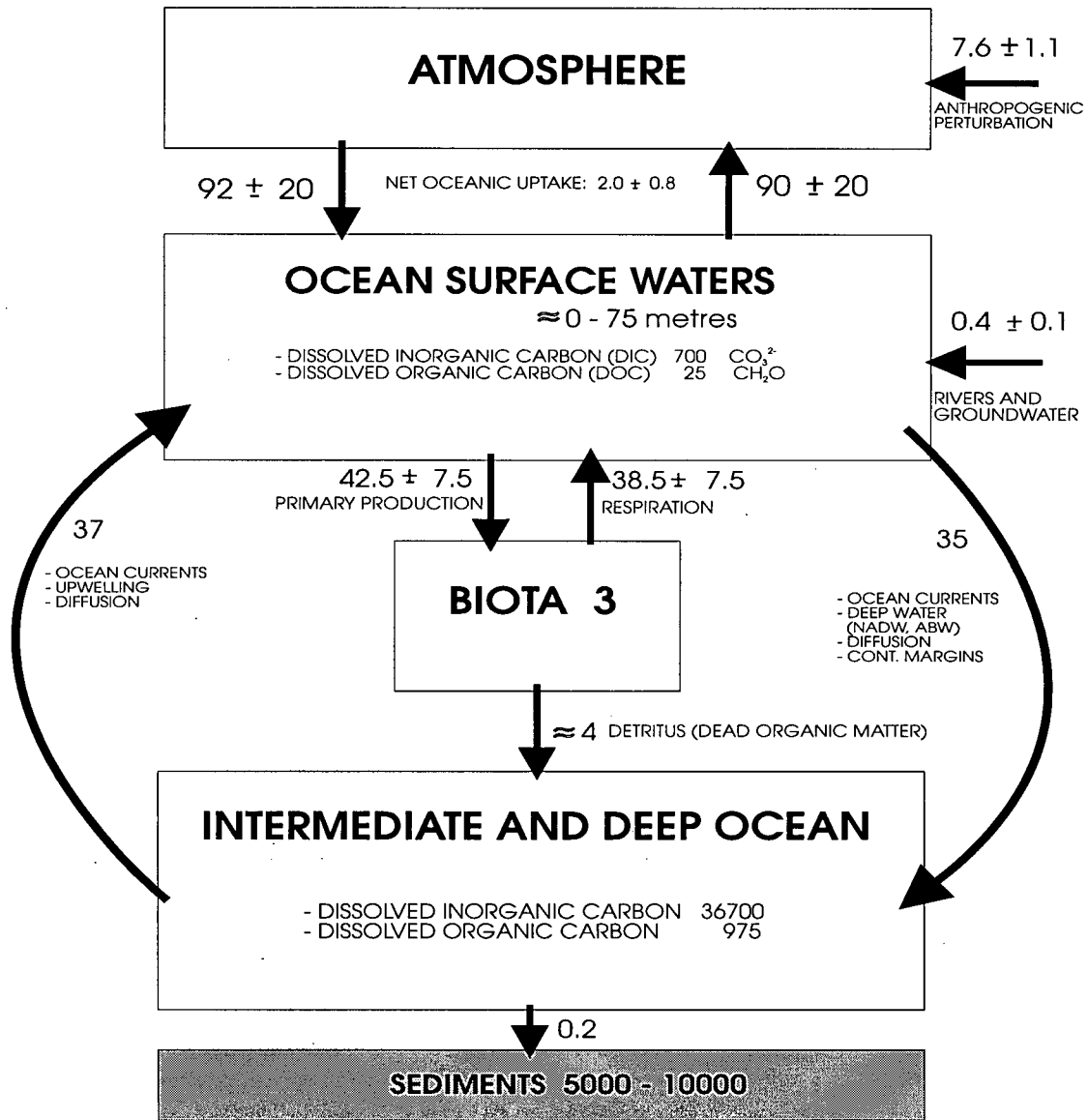
Figure A.4: Global oceanic carbon fluxes. Fluxes are in Gt C/year and are indicated by arrows. Values in boxes indicate carbon storage. Sources: Bolin (1983), Bolin (1986), Falkowski *et al.* (1992) and Houghton *et al.* (1990). See text.
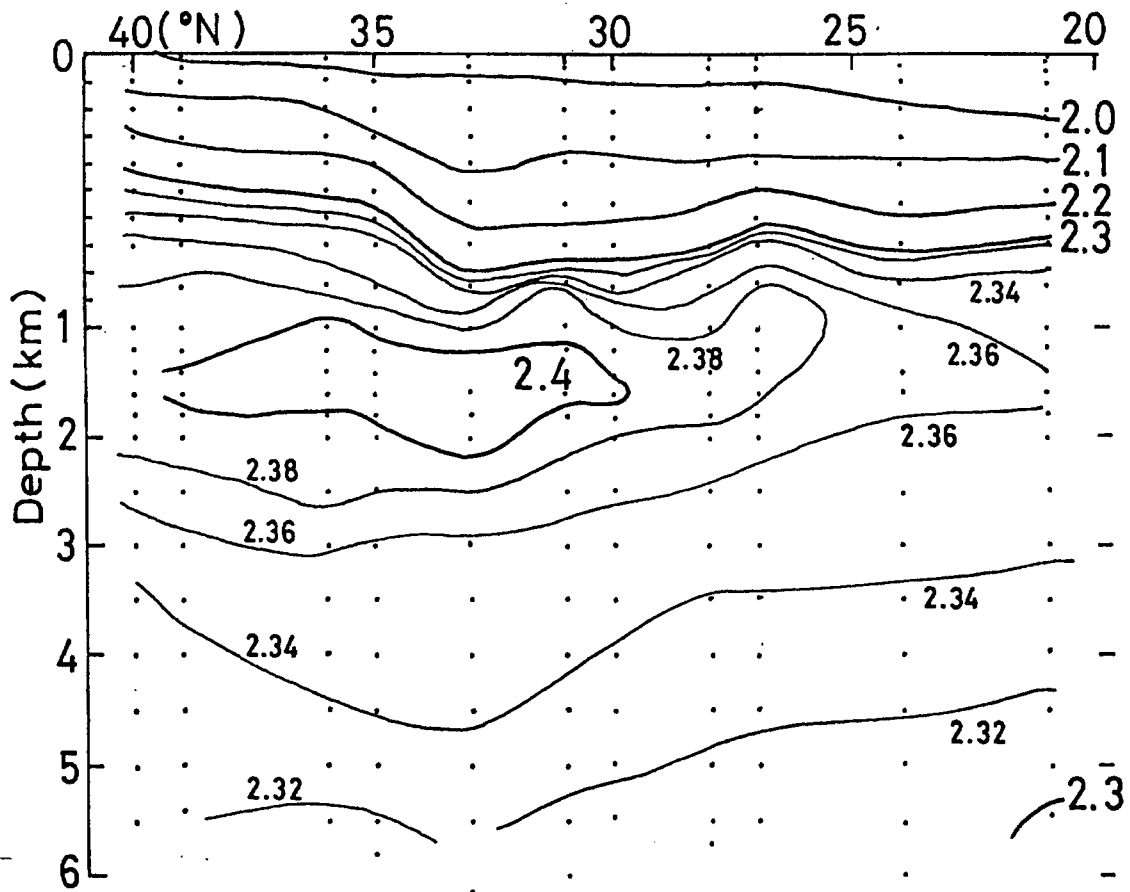
Figure A.5: North-south section of normalized total dissolved inorganic carbon (in mmol/kg) in the North Pacific along 165°E observed in 1991. Source: Tsunogai *et al.* (1993).

the surface, and down to approximately 1000 metres in depth (Tsunogai *et al.*, 1993).

A total of 2.4 ± 0.8 Gt C/year is entering the oceans via the surface waters, with approximately 0.2 Gt C/year leaving the ocean system as a flux to sediments. The result is a storage of about 2.2 ± 0.8 Gt C annually in the Oceans. Using a slightly larger estimate of the influx from rivers and groundwater, Houghton *et al.* (1990) suggest that the rate of increase is 1.0 Gt C/year for the surface waters, and 2.0 Gt C/year for the intermediate and deep ocean. In effect the oceans are attempting to equilibrate with the atmosphere by increasing the total dissolved inorganic and organic carbon, thereby decreasing the rate at which CO_2 is taken up. For now the oceans appear to be acting effectively as a sink for anthropogenic perturbation CO_2, although there is question as to how they might act in the future.

A consequence of the assumption of steady-state equilibrium on the model of Figure A.4 is that in the pre-industrial era there must have been a net outgassing of CO_2 from the oceans equal to the river and groundwater flux, less that which is deposited in ocean sediments. The processes shown in figure A.4 and their significance to the uptake of anthropogenic perturbation CO_2 will be discussed in turn.

A.4.1 CO_2 Gas Exchange

The exchange of CO_2 in gaseous form across the atmosphere-ocean interface is, excepting the input from rivers and groundwater, and removal by sedimentation, the only mechanism by which the oceans can accept or give up CO_2. The process is governed primarily by the physical factor of diffusion or molecular transfer across a CO_2 gradient. However the magnitude of the exchange is inextricably linked to the chemistry of sea water and is especially important when considering future oceanic uptake under conditions of increasing atmospheric CO_2. But first, the net exchange flux can be expressed as,

$$F_{CO_2} = F_{CO_{2_{in}}} - F_{CO_{2_{out}}}$$ (A.5)

The net exchange is an equilibrium difference between an invasion flux and an evasion flux and (Robertson and Watson, 1992):

$$F_{CO_2} = k([CO_{2_s}] - [CO_{2_{dds}}])$$ (A.6)

where F_{CO_2} is the flux of CO_2 into the ocean in $\frac{moles\ of\ CO_2}{m^2}$,

k is the gas transfer coefficient in $\frac{moles\ of\ CO_2}{m^2\ yr\ ppm}$,

$[CO_{2_s}]$ is the concentration of dissolved gaseous CO_2 at the surface and,

$[CO_{2_{dds}}]$ is the concentration of dissolved gaseous CO_2 at the base of the

oceanic diffusion-dominated sublayer, which is approximately 50μm thick (Robertson and Watson, 1992).

In practice the CO_2 concentrations are approximated by much more readily measured quantities.

Thus,

$$[CO_{2_s}] = S(pCO_2)_{atmos}$$ (A.7)

$$[CO_{2_{dds}}] = S(pCO_2)_{ocean}$$ (A.8)

where,

S is the solubility of gaseous CO_2 in seawater,

$(pCO_2)_{atmos}$ is the partial pressure of CO_2 in the atmosphere, and

$(pCO_2)_{ocean}$ is the partial pressure of CO_2 in the ocean surface layer.

Now, $(pCO_2)_{atmos}$ and $(pCO_2)_{ocean}$ are readily observable quantities, and S, the solubility, is a known function of temperature and salinity. Thus from observations, the CO_2 exchange flux can be simply calculated from

$$F_{CO_2} = kS[(pCO_2)_{atmos} - (pCO_2)_{ocean}] \tag{A.9}$$

From Figure A.4 it can be seen that the exchange fluxes are 92 ± 20 Gt C/year in, and 90 ± 20 Gt C/year out of the oceans. The large uncertainties are due to the fact that the oceans are poorly observed both temporally and spatially. The spatial variability is large due to the variability of k, and of S. The gas transfer coefficient is dependent on turbulent exchange at the ocean-atmosphere interface, and also partly on temperature. So,

$$k = f(\overline{u}, T) \tag{A.10}$$

is the parameterization most sought for k, where $\overline{u}$, the wind speed (in m/s) is used as a surrogate for turbulence. T is the temperature. It is recognized (Tans *et al.*, 1990) that k is more sensitive to wind speed, and increases linearly with wind speed if the temperature effect is taken out. The temperature effect on k is in the opposite direction, but to a lesser extent. The relation is that as interfacial temperature decreases, the exchange coefficient decreases.

Similarly for the solubility, the other coefficient in equation A.9:

$$S = f(T) \tag{A.11}$$

where T is the temperature of the ocean surface or mixed layer. It is known that the solubility of CO_2 in sea water increases with decreasing temperature.

From the above discussion of k and S one would expect larger exchange fluxes in regions of strong winds, such as in the mid to high latitudes. With respect to temperature the result is not so clear. Decreased temperatures, which occur primarily at high latitudes, increase the solubility of CO_2 in sea water. This would, independent of k, increase the net flux into the oceans. However, the temperature effect on k would work in the opposite direction at higher latitudes where it is colder. Siegenthaler (1986) is unable to distinguish a significant latitudinal trend in k, due to the opposing influences of wind speed and temperature.

Tans *et al.* (1990) give a similar derivation to equation A.9, and let

$$E = kS \tag{A.12}$$

and assume that the effects of temperature on kS nearly cancel each other so that the product is only a function of wind speed. This is an extremely useful derivation as it allows the global net flux of CO_2 to be calculated simply from charts of $(pCO_2)_{atmos}$, $(pCO_2)_{ocean}$ and wind speed. At present the ocean is not well observed spatially or temporally.

Attempts to determine k have been accomplished by using tracers to calibrate equation A.9. Common tracers used are radon and ^{14}C. The increase of ^{14}C in the atmosphere has been well observed (Siegenthaler, 1986) since nuclear testing. With observations of the change in ^{14}C in the oceans during this time, the net uptake can be calculated. It is assumed that CO_2 uptake would be similar to that of ^{14}C, but it is known that the buffer factor (as discussed later) affects CO_2, but not ^{14}C. Furthermore the source functions for ^{14}C and CO_2 differ spatially. Regardless, the analogue remains.

However, it is thought that the net CO_2 exchange flux is not very sensitive to k, but is governed by mechanisms which draw down CO_2 or bring up CO_2 to the surface

mixed layer (Houghton et al., 1992), such as vertical mixing and biological processes. The $(pCO_2)_{ocean}$ is highly variable and is responsible for the major part of the spatial and temporal variation in the flux of CO_2. Generally there is high $(pCO_2)_{ocean}$ near the equator (due to upwelling of CO_2 rich sub-surface waters), and low $(pCO_2)_{ocean}$ towards the poles where CO_2 is being drawn out of the surface layer by physical and biological processes.

Over time periods long enough to average out pCO_2 anomalies such as those caused by El Niño, and integrating over all oceans, it is expected that the average ΔpCO_2 will increase as the atmospheric pCO_2 rises, thereby increasing the net uptake of the oceans. The rate at which the atmosphere-ocean pCO_2 distribution tends to equilibrium is dependent on both gas transfer, as given by equation A.9, by solubility, and by vertical mixing processes that can remove or augment the CO_2 distribution in the surface layer. The point of equilibrium, where a given atmospheric CO_2 concentration is in equilibrium with the ocean pCO_2, is dependent on the carbonate chemistry of sea water which affects the CO_2 exchange between gas phase and solution.

A.4.2 Physical Processes

As the atmosphere is well-mixed, the variability in ΔpCO_2 is mainly due to the variability in $(pCO_2)_{ocean}$. This variability is caused partly by the temperature effect on solubility, physical processes in the ocean, and biological processes in the ocean. The role of continental margins is also thought to be of considerable importance (Walsh, 1991).

Figure A.4 indicates the importance of physical processes in the oceanic circulation of carbon. Approximately 35 Gt C/year is removed from the surface mixed layer, while at the same time 37 Gt C/year is brought into the surface mixed layer in different regions. This indicates the movement, or redistribution, of carbon in the ocean and storage in

areas where it is not entering the oceans. The net accumulation is approximately 2 Gt C/year in the surface mixed layer by physical processes which bring up CO$_2$ rich intermediate and deep waters.

The main physical process that draws down surface $(pCO_2)_{ocean}$ values in some regions is the continual ventilation of the thermocline by flow along isopycnal surfaces. These constant density surfaces outcrop at the surface of the ocean near the polar front in both hemispheres, and cover a wide area (Taylor, 1992). Surface water, fed by the subtropical gyres, are in these areas in each hemisphere able to sink freely along the sloping surfaces. Eventually they begin to slope upwards until they converge near the equator. The origin of these currents is the cold ocean, and thus the solubility is high. Clearly, then, this is an efficient method for drawing CO$_2$ out of the mixed layer, as the waters in these regions are plentiful in CO$_2$ (high pCO_2 due to the high solubility) and the transport by the sinking water is fast. $(pCO_2)_{ocean}$ values are seen to rise dramatically near the equator where convergence produces upwelling. The significance of this process is that it transfers CO$_2$ from high latitudes to the deep equatorial oceans. It is estimated (Taylor, 1992) that the timescale for ventilation in this manner is 7 - 20 years.

A much slower movement of CO$_2$ out of the surface layer is achieved by vertical eddy diffusion across the path of the isopycnal surfaces, and within subtropical gyres. This is not an efficient method of CO$_2$ transport out of the surface layer due to a stable density profile near the equator, thereby hindering downward mixing.

The formation of deep water (North Atlantic Deep Water and Antarctic Bottom Water) at high latitudes in winter is also important for advecting CO$_2$ out of the surface layer and depositing it in the deep ocean. Most remains in solution where it may upwell near the equator, but a small amount, approximately 0.2 Gt C/year (Houghton et al., 1990) is settled out into sediments on the ocean floor.

A.4.3 Biological Processes

Unlike the physical processes, the biological processes are a net sink for CO_2 out of the mixed layer (Figure A.4). In areas where the biological processes are active CO_2 is being removed, thereby increasing the pCO_2 gradient (ΔpCO_2) and allowing the flux of CO_2 into the ocean to increase. It is thought that in the future, if biological activity were to increase (new primary productivity) this might be an important sink for anthropogenic perturbation CO_2. Unlike the response of vegetation in the terrestrial biosphere, phytoplankton sequestering of CO_2 is not enhanced by CO_2 fertilization in the atmosphere (Smith and Mackenzie, 1991).

Figure A.4 shows the ocean phytoplankton to be photosynthesizing 42.5 ± 7.5 Gt C/year (Bolin, 1983), and respiring 38.5 ± 7.5 Gt C/year (Bolin, 1983) for a net primary production of approximately 4 Gt C/year. This same amount is lost as dead organic matter that settles out of the surface mixed layer to accumulate in the intermediate and deep waters.

A.4.4 Oceanic Uptake Studies

To date the bulk of oceanic uptake studies has been achieved by ocean modellers who have reached an agreement on the amount of anthropogenic perturbation CO_2 taken up. Houghton *et al.* (1990) state this amount to be 2.0 ± 0.8 Gt C/year. A recent study (Sarmiento *et al.*, 1992) using a three-dimensional global circulation model has concluded that their perturbation approach gives a lower bound of 1.9 Gt C/year on uptake for the decade 1980-1989. The modelling community has disputed the Tans *et al.* (1990) article which claims that the oceans could not take up more than 1.0 Gt C/year.

Tans *et al.* (1990) use atmospheric pCO_2 values combined with $(pCO_2)_{ocean}$ observations to come up with a net transfer of CO$_2$ to the oceans of 0.3 - 0.8 Gt C/year of anthropogenic perturbation CO$_2$. The conclusion is that the additional anthropogenic perturbation CO$_2$, the so called "missing sink" of CO$_2$, must be taken up by the Northern Hemisphere's terrestrial biosphere. It is assumed that it must be taken up in the Northern Hemisphere due to the constraints on atmospheric transport from the North, where most of the anthropogenic CO$_2$ is being emitted into the atmosphere, to the South.

A correction to the Tans *et al.* (1990) estimate of oceanic uptake is an additional 0.1-0.6 Gt C/year for an adjustment due to the effects of ocean surface temperature (Sarmiento and Sundquist, 1992). A further correction was proposed (Sarmiento and Sundquist, 1992) due to the neglect of interhemispheric transport of carbon monoxide to the southern hemisphere where it is oxidized to CO$_2$. This removes 0.25 - 0.29 Gt C/year from the Northern Hemisphere to the Southern, where it is assumed to be an additional uptake in the Southern oceans.

If the carbon cycle was in steady state in the pre-industrial era then there would be a net transfer of CO$_2$ from the oceans to the atmosphere by an amount equal to the river source (0.4 $\pm$ 0.1 Gt C/year) minus that which is deposited in sediments (approximately 0.2 Gt C/year). Thus an additional correction of 0.1-0.3 Gt C/year must be made to the Tans *et al.* (1990) calculation to account for this uptake of anthropogenic perturbation CO$_2$ above that of gas exchange.

The total of these three corrections is about 0.8 $\pm$ 0.3 Gt C/year which must be added to the oceanic uptake. The original estimate was 0.3-0.8 Gt C/year (Tans *et al.*, 1990). The revised estimate is 1.3 $\pm$ 0.5 Gt C/year, which is approximately within the range of perturbation ocean modelling studies (Houghton et al, 1990).

The most substantial work to date of actually observing the oceanic increase of DIC is that of Quay *et al.* (1992). Their approach examines the uptake of the natural tracer,

^{13}C. The amount, or concentration, of ^{13}C is usually expressed as δ^{13}C where δ^{13}C is a deviation from the ratio of concentrations of ^{13}C to ^{12}C from a standard.

It is known that the background δ^{13}C of CO$_2$ in the atmosphere is -8 per mil and that anthropogenic CO$_2$ emissions (from fossil fuels and deforestation) are -27 per mil. This difference is due to the isotopic fractionation during photosynthetic sequestering of CO$_2$. Anthropogenic emissions have decreased the average atmospheric δ^{13}C from -7.5 per mil in 1978 to -7.8 in 1988. Observations show that the δ^{13}C of inorganic carbon in the ocean is also decreasing, inferring that lower δ^{13}C anthropogenic perturbation CO$_2$ is being taken up.

Quay *et al.* (1992) look at profile data of δ^{13}C from various parts of the ocean in 1970 and compare that to data collected in 1990, and apply this to a time varying carbon budget equation of source and sink terms. Their results show a decrease in δ^{13}C since 1970, and calculate an oceanic sink for anthropogenic CO$_2$ of 2.1 Gt C/year.

An important concept revealed by changes in the observed latitudinal distribution of δ^{13}C (Figure A.6) is that the greatest changes are in the subtropical gyres. This is most likely due to the long residence times of water in these regions (as there is little vertical mixing) and therefore greater storage. It is surprising at first to note that in the higher latitudes where one expects most of the anthropogenic perturbation CO$_2$ to be entering the oceans, the change in δ^{13}C is small. This is attributable to the short time scale for ventilation of the mixed layer in these areas where density stratification does not suppress vertical mixing. The minimum at the equator is a consequence of divergence and some upwelling of water which has been long enough out of contact with the atmosphere to have little or no trace of anthropogenic δ^{13}C.
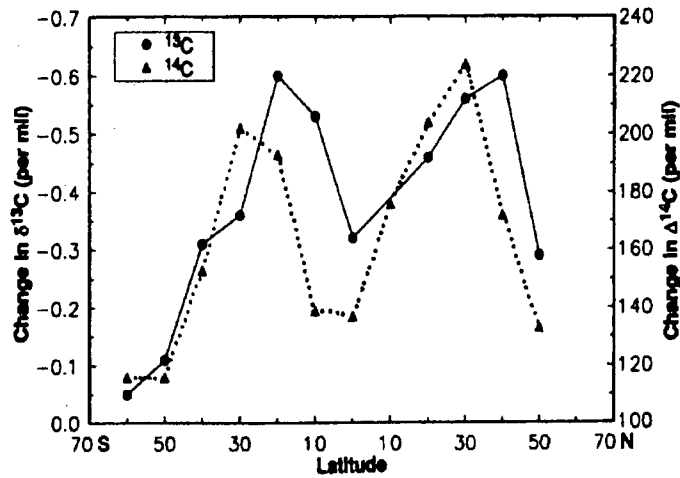
Figure A.6: The latitudinal trends of changes in δ^{13}C values (per mil) and nuclear weapons produced Δ^{14}C (per mil) in the mixed layer of the Pacific Ocean. Source: Quay *et al.*, 1992.

A.4.5 Ocean Conclusions

Although estimates of uptake approximately agree for Quay *et al.* (1992), Tans et al. (1990), and Sarmiento *et al.* (1992) there is still much uncertainty regarding the magnitude of perturbation CO$_2$ uptake. However, it seems most likely that the global carbon budget will be closed by continued study of the oceans, and not the terrestrial biosphere where ecosystem variability is high.

A.5 The Atmosphere

A.5.1 Anthropogenic Carbon Dioxide Emissions

This section will examine the processes involved in producing the anthropogenic perturbation of 7.6 ± 1.1 Gt C/year to the global carbon cycle. Of this, approximately 45% remains as the airborne fraction (α) in the atmosphere, where

$$\alpha = \text{net annual atmos. accumulation} / \text{net annual } CO_2 \text{ emitted to the atmosphere}$$

$$= \frac{3.4 GtC/year}{7.6 GtC/year} = .45 \text{ or } 45\%$$

Since CO_2 is virtually inert in the troposphere, and assuming that mixing with the stratosphere is small enough to neglect, this amount is well mixed throughout the troposphere, where it accumulates.

Most of the anthropogenic perturbation is due to the combustion of fossil fuels, and to the related activities of production and transportation, causing emissions to the atmosphere as CO_2. The most comprehensive tabulation of global CO_2 emissions is that of Marland and Rotty (1984) following on from Keeling (1973). Their results are available from the Carbon Dioxide Information Analysis Centre (Oak Ridge National Laboratory, Marland *et al.*, 1989). Results of emissions to 1990 are shown in Figure A.7, including cement production data for completeness.

It is difficult to tabulate consumption data due to the vast number of fossil fuel users around the globe, and the vast number of end products. Instead, the accounting problems of consumption data can be overcome by using production data. There are many fewer producers, and it is assumed that all fuel produced is combusted or diverted to other uses, such as manufacturing of secondary products where it is oxidized more slowly. Account must be taken for these secondary products that are not oxidized. For a global budget
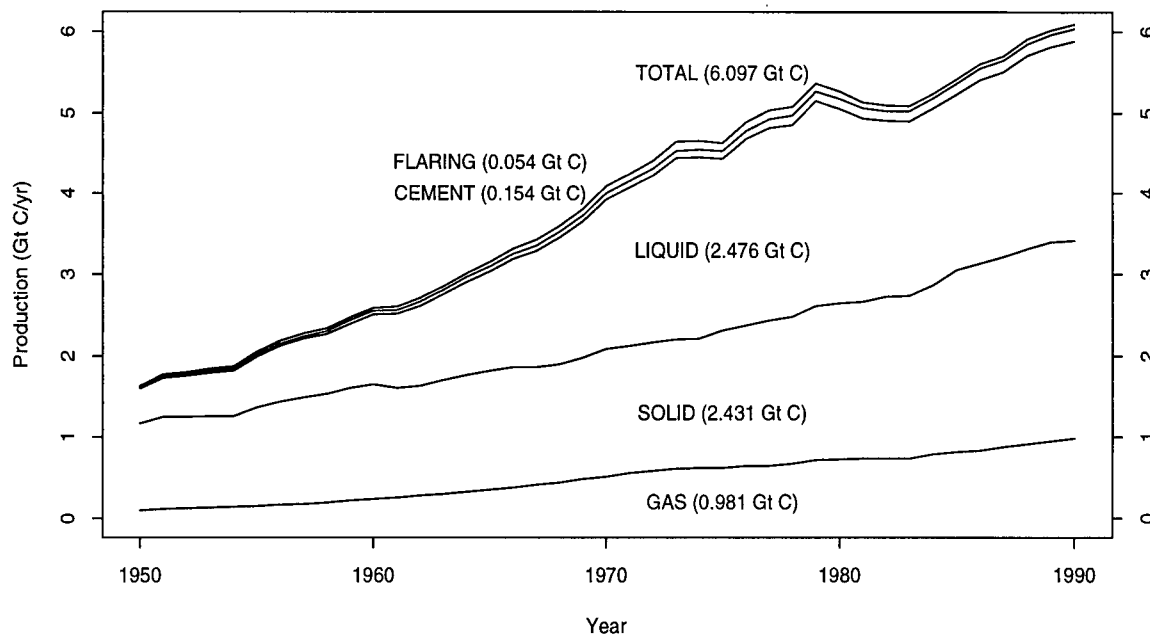
Figure A.7: Global annual carbon dioxide emissions from production, in Gt C per year. Quantities in brackets are estimated emissions for 1990.   Source: NDP030r4 (Carbon Dioxide Information Analysis Centre, Oak Ridge National Laboratory, 1990).

this should be adequate, although there may be small differences due to changes in fossil fuel stores which are either augmented or depleted on a year to year basis. It is likely that averaged over a number of years the change in storage term can be neglected. In any case, the errors from using production data over consumption data are likely to be small compared to other errors in the budget.

Most anthropogenic CO$_2$ emissions from the use of liquid, solid, and gaseous fossil fuels are from combustion. The complete combustion reaction (Marland and Rotty, 1984) is:

$$C_xH_y + (x + \frac{1}{4}y)O_2 \longrightarrow xCO_2 + \frac{1}{2}yH_2O(gas) + \Delta H_L \qquad (A.13)$$

or

$$C_xH_y + (x + \frac{1}{4}y)O_2 \longrightarrow xCO_2 + \frac{1}{2}yH_2O(liquid) + \Delta H_H \qquad (A.14)$$
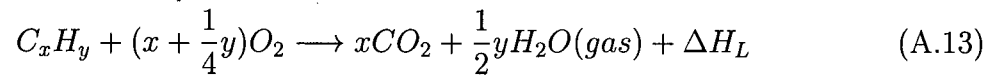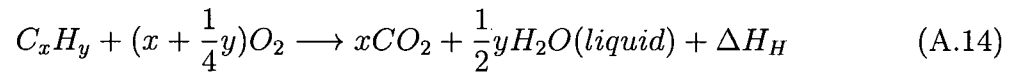
The fossil fuel, or hydrocarbon, is generalized as C_xH_y, and ΔH is the heat of reaction which is in this case negative as the process is exothermic. ΔH_H is the gross (or higher) heating value, ΔH_L is the net (or lower) heating value, and $\Delta H_H > \Delta H_L$ due to the energy of vapourization of liquid water. The generalized form of the fossil fuel, C_xH_y, is used since the variables x and y vary *among* fuel types (spatially and temporally) and *between* fuel types.

Equations A.13 and A.14 are for complete combustion. However in the consumption of most fossil fuels, the combustion process is not a complete one. It is therefore not such a simple process of just determining x in equations A.13 and A.14 for the total amount of fuel used to get xCO_2, the amount emitted to the atmosphere. Marland and Rotty (1984) take a straightforward approach for calculating CO_2 emissions to the atmosphere, CO_{2_i}, with simply:

$$CO_{2_i} = (P_i)(FO_i)(C_i) \qquad (A.15)$$

where the subscript i refers to the fossil fuel phase: solid, liquid, or gas, and,

P_i = amount of fuel produced

FO_i = fraction of fuel oxidized

C_i = carbon content of fuel,

for each fuel type.

The amount of each fuel type produced (P_i) is well documented by national statistics departments, and by the United Nations. However, for administrative purposes it is often documented in energy equivalent units (rather than mass), thereby recognizing the inherent differences among fuels of the same type. Often the energy equivalent is the caloric value, which is a measure of the heat liberated during complete combustion with oxygen, which can then be related to the carbon content of the fuel.

FO_i, the fraction oxidized, is a factor dependent on the effectiveness, or completeness, of combustion for annually consumed fuels and on an estimation of the fraction of the produced fuel that is diverted toward combustion. Some fuel produced but not combusted may accumulate in storage, and some may be diverted to other uses (non-combustible uses) where the time-scale of oxidation to CO_2 is much longer.

C_i is a factor relating the energy equivalent units (of P_i) to the amount of carbon available for combustion to CO_2. Generally the higher the C content of fuels, the greater the energy released during combustion. Global statistics relate the heating value, ΔH, of the fuel to the carbon content of that fuel.

It seems appropriate now to briefly summarize the composition of the main components of the anthropogenic emissions shown in Figure A.7. The largest emitter is the liquid fossil fuels category. Liquid fossil fuels are mainly crude petroleum, but also partly (3%) natural gas liquids (NGL). Most of this fuel is oxidized quickly when combusted as energy products in the form of motor gasoline, distillate fuel oil, kerosene, liquid petroleum gas (LPG), residual fuel oil, and jet fuel. However some, 10.2% of the total in 1979 (Marland and Rotty, 1984), is given over to non-energy uses such as asphalt, lubricants, and other sectors of the petro-chemical industry, where timescales of oxidation to CO_2 are variable. A portion of this (Marland and Rotty estimate 6.7 $\pm$ 2% of all liquids produced) will remain unoxidized, or oxidizing very slowly, each year as products such as plastics, tires, and asphalt.

An estimate was made of the amount of liquid fuels from the energy use sector that remain unoxidized due to incomplete combustion. Using U.S. EPA estimates from pollutant models and measurements of carbon monoxide (CO) and hydrocarbons (HC's), emissions inventories were obtained of these, products which are accounted for as carbon emissions from incomplete combustion, and thus carbon from liquid fuels that is no longer available as CO$_2$. Clearly this is not an ideal estimate due to the extrapolation of the U.S. data to represent the globe. The uncertainty of the CO and HC inventories will be carried on to the CO$_2$ inventory.

Solid fossil fuels contributed (from Figure A.7) 2.431 Gt C as CO$_2$ to the atmosphere in 1990. Primarily this was from combustion of coal in transportation, industrial use, electrical utilities, and coke plants. Coal types are numerous, differing markedly in carbon content (C_s) and thus heating value (ΔH). For standardization the amount of coal is expressed as tons of coal equivalent to allow for the discrepancies among coal types. Almost all coal produced (mined) is used in combustion, and with current technology, the combustion of coal is nearly complete.

The smallest of the main fossil fuel contributions is that of natural gas extracted from gas and oil wells at 0.981 Gt C/year. The error on production is estimated to be $\pm$ 10%. Gas is used primarily as fuel in the industrial, residential, commercial, and electrical utilities sectors. About 3% of natural gas production is for non-fuel use where the oxidation rate is slower. It is thought that approximately 2/3 of this is oxidized to CO$_2$ via ammonia production, thereby leaving 1% to remain unoxidized on the time scale of interest. Another loss is that of "extraction loss" due to the extraction of liquid fuels, mainly as ethane, during processing.

Like the other fossil fuels the carbon content of natural gas is closely related to the heating value and can be explained closely by the regression equation:

$$C_g = 13.708 + 0.0828 x 10^{-3}(\Delta H_H - 37234) \tag{A.16}$$

where the average ΔH_H is 37200 kJ/m^3.

The flaring, or combustion, of natural gas at the oil well site is a minor component of the anthropogenic emissions, at 0.054 Gt C/year. This source is associated with oil production where there are no facilities to recover the natural gas. The combustion is virtually complete, and FO_f is 1.0 ± 1%.

The approach taken by Marland and Rotty (1984) is similar to that of Keeling (1973) but with a much better error analysis. With the errors from each fuel group weighted by the 1980 emissions estimates, Marland and Rotty (1984) indicate the error range to be 6-10%, depending on whether or not the uncertainties for the individual fuels are mutually independent. If they are then the error is 6%. Likely the error is somewhere in between these estimates. Error is attributable mostly to the lack of data on the carbon content of the fuels and the related problem of extrapolating the carbon content data from well documented countries, such as the U.S., to other parts of the world. Production data also contain much uncertainty.

The only other significant source of CO_2 identified by Marland and Rotty (1984) is that emitted during the production of cement, or lime. Figure A.7 indicates this source to be small compared to the fossil fuels, but still larger than emissions from flaring of natural gas.

A.5.2   Atmospheric CO_2 Concentrations

Atmospheric CO_2 is both well-mixed and well-observed, allowing the CO_2 concentration, which is closely monitored to a high degree of accuracy at many sites, including

Mauna Loa, Hawaii (Keeling *et al.*, 1976) to be indicative of increased atmospheric storage. There is clearly an upward trend, which currently corresponds to an increase of 3.4 ± 0.2 Gt C/year in the atmosphere, an average increase of 1.5 ppmv/year over the decade 1980-1990 at Mauna Loa (Conway *et al.*, 1991). Similar time series for other sites on the globe have been obtained (Boden *et al.*, 1991). The global average atmospheric concentration of CO_2 was 355 ppm in 1992 (Houghton *et al.*, 1992), indicating a total of approximately 750 Gt C in the atmosphere.

The global CO_2 concentrations show considerable temporal and spatial variability (Boden *et al.*, 1991). Primarily this is due to the distribution of major CO_2 source and sink regions. Atmospheric CO_2 concentrations are drawn down in the Northern Hemisphere during the Northern Hemispheric summer when sequestering of atmospheric CO_2 by the terrestrial biota by photosynthesis is strongest. In winter the biota are less active photosynthetically, while soil respiration continues. At this time atmospheric CO_2 concentrations are highest.

Also noticeable from CO_2 records is the higher concentration in the Northern Hemisphere, due to greater anthropogenic sources in this Hemisphere. Although the atmosphere is well-mixed within hemispheres, there is little intra-hemispheric mixing. Therefore the only major sources or sinks of atmospheric CO_2 are the oceans and the terrestrial biosphere. A minor tropospheric source is the oxidation of CO to CO_2. Virtually all CO will oxidize to CO_2 in 0.1 - 0.4 years (Jaques, 1992).

Appendix B

Observations for June Sampling Period

B.1   Observations: June 3 - June 24, 1993
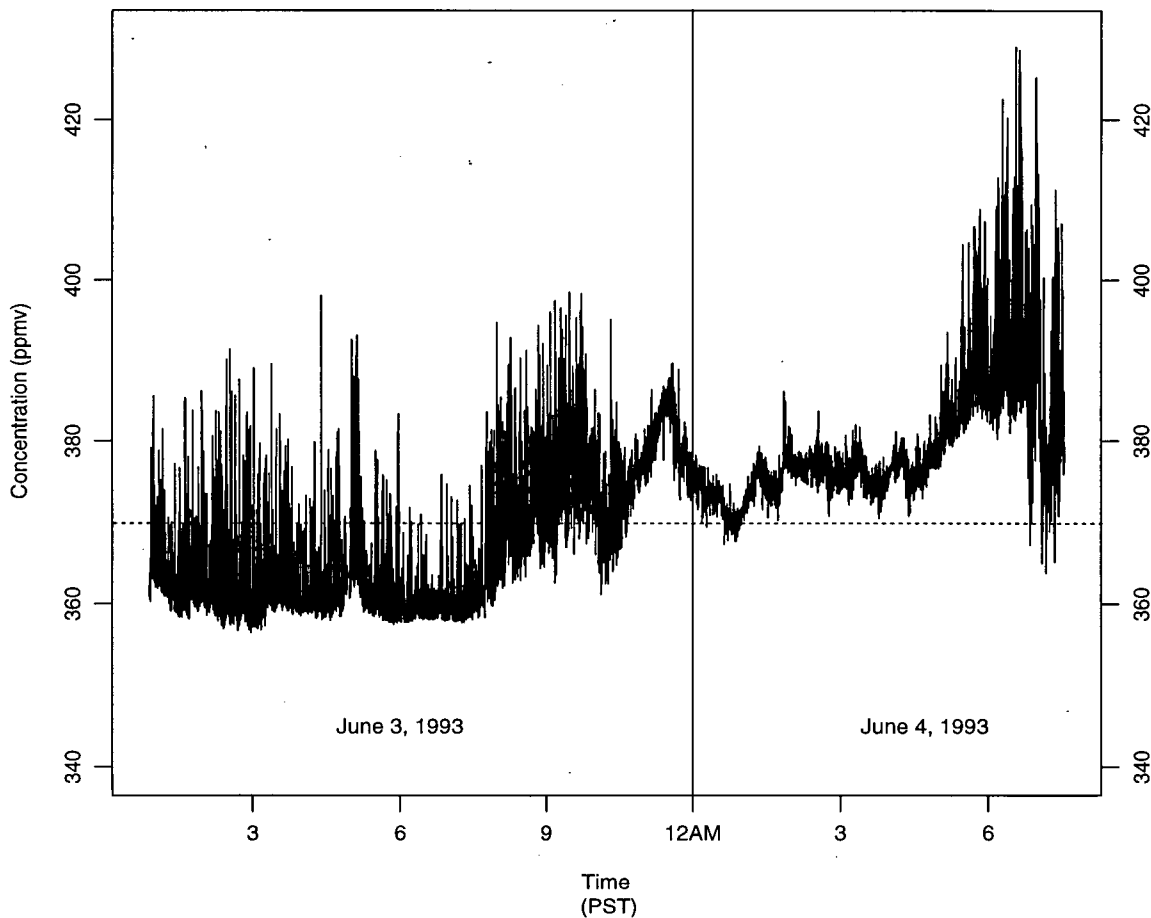
Figure B.1: Atmospheric CO_2 Concentration trace for June 3 - 4, 1993, with continuous sampling every 20 seconds. The background concentration (369.4 ppmv) is shown as a dotted line.
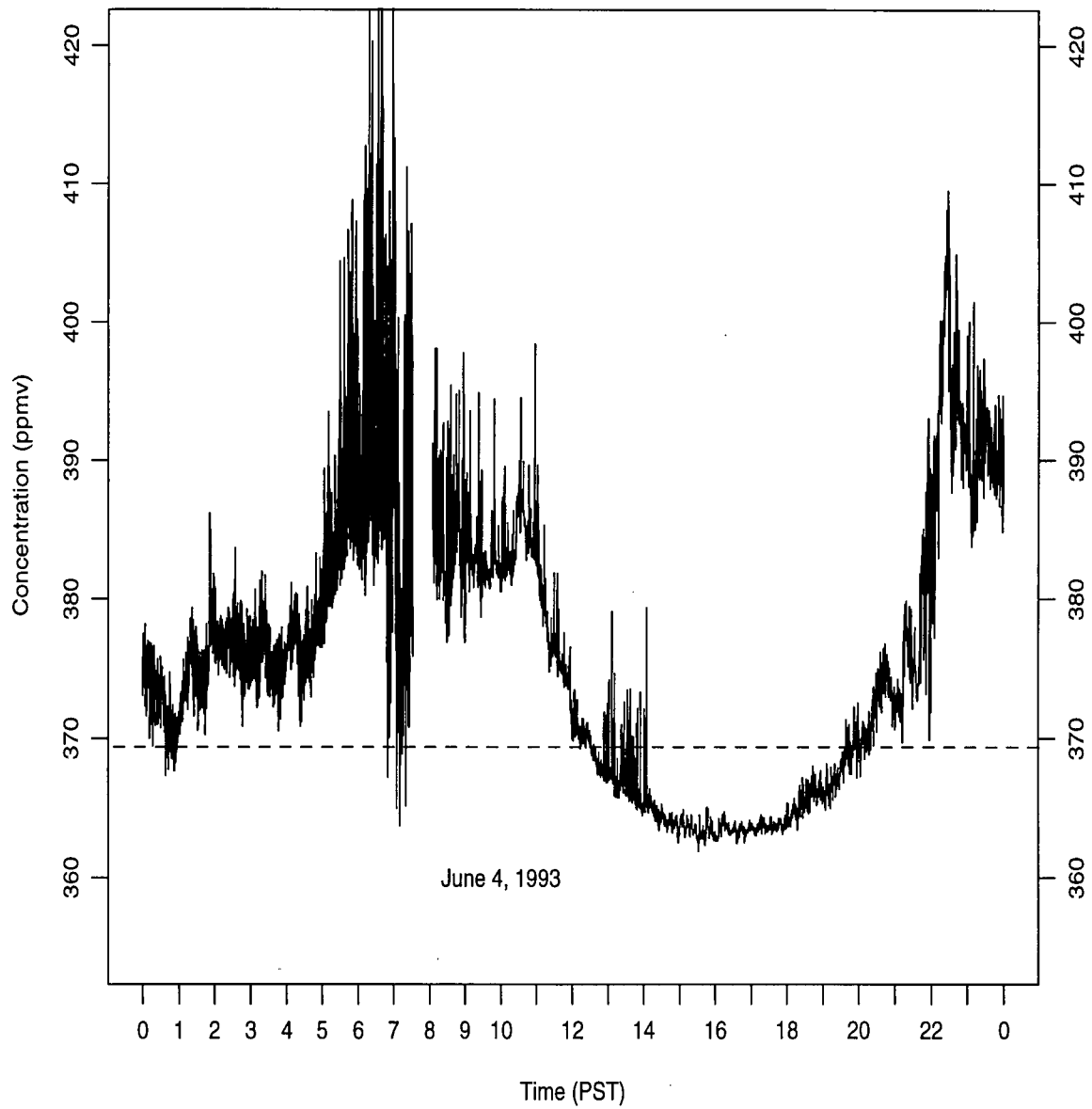
Figure B.2: Atmospheric CO_2 Concentration trace for June 4, 1993, with continuous sampling every 20 seconds. The background concentration (369.4 ppmv) is shown as a dotted line.
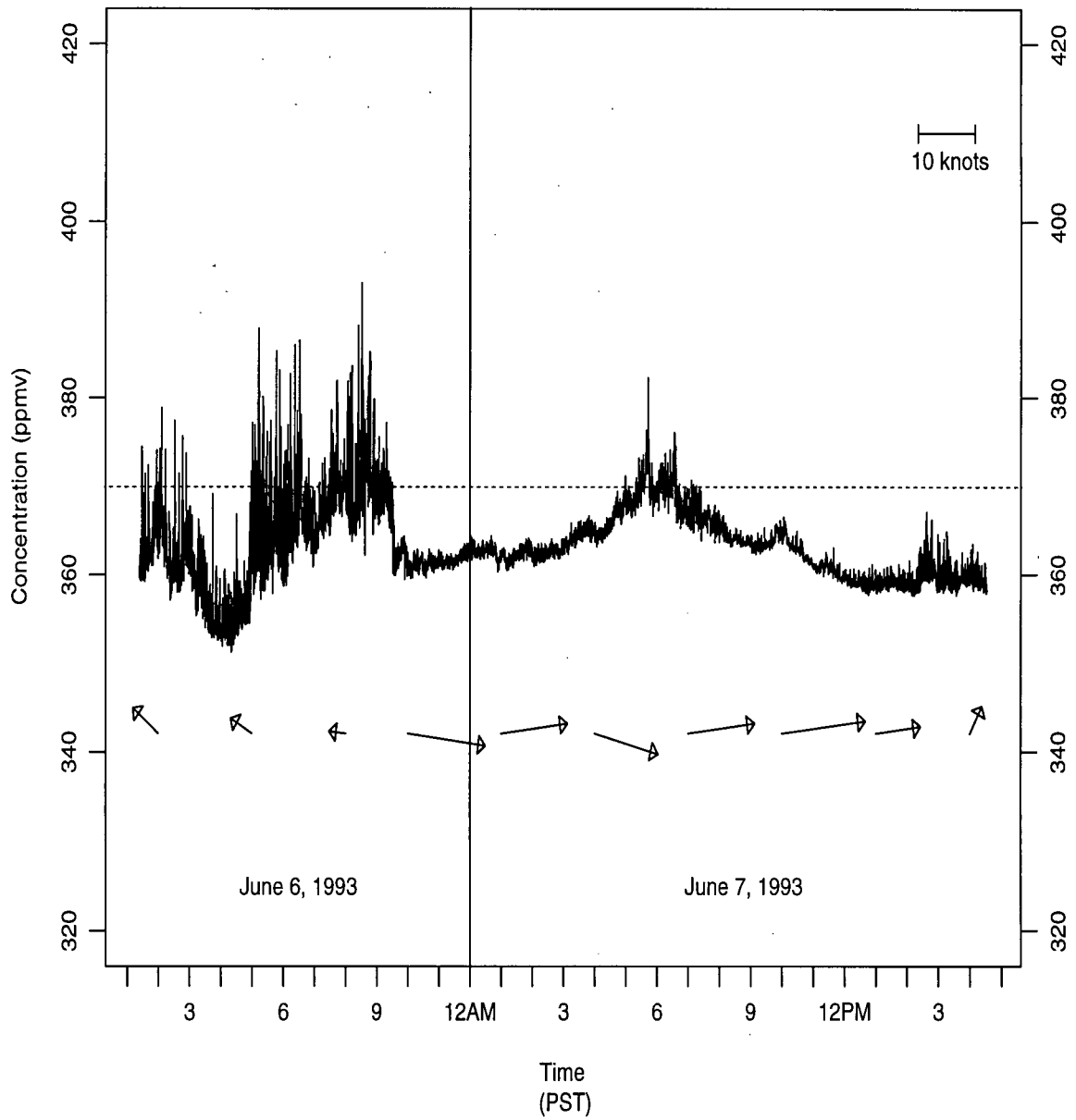
Figure B.3: Atmospheric CO_2 Concentration trace for June 6 - 7, 1993, with continuous sampling every 20 seconds. The background concentration (369.4 ppmv) is shown as a dotted line.
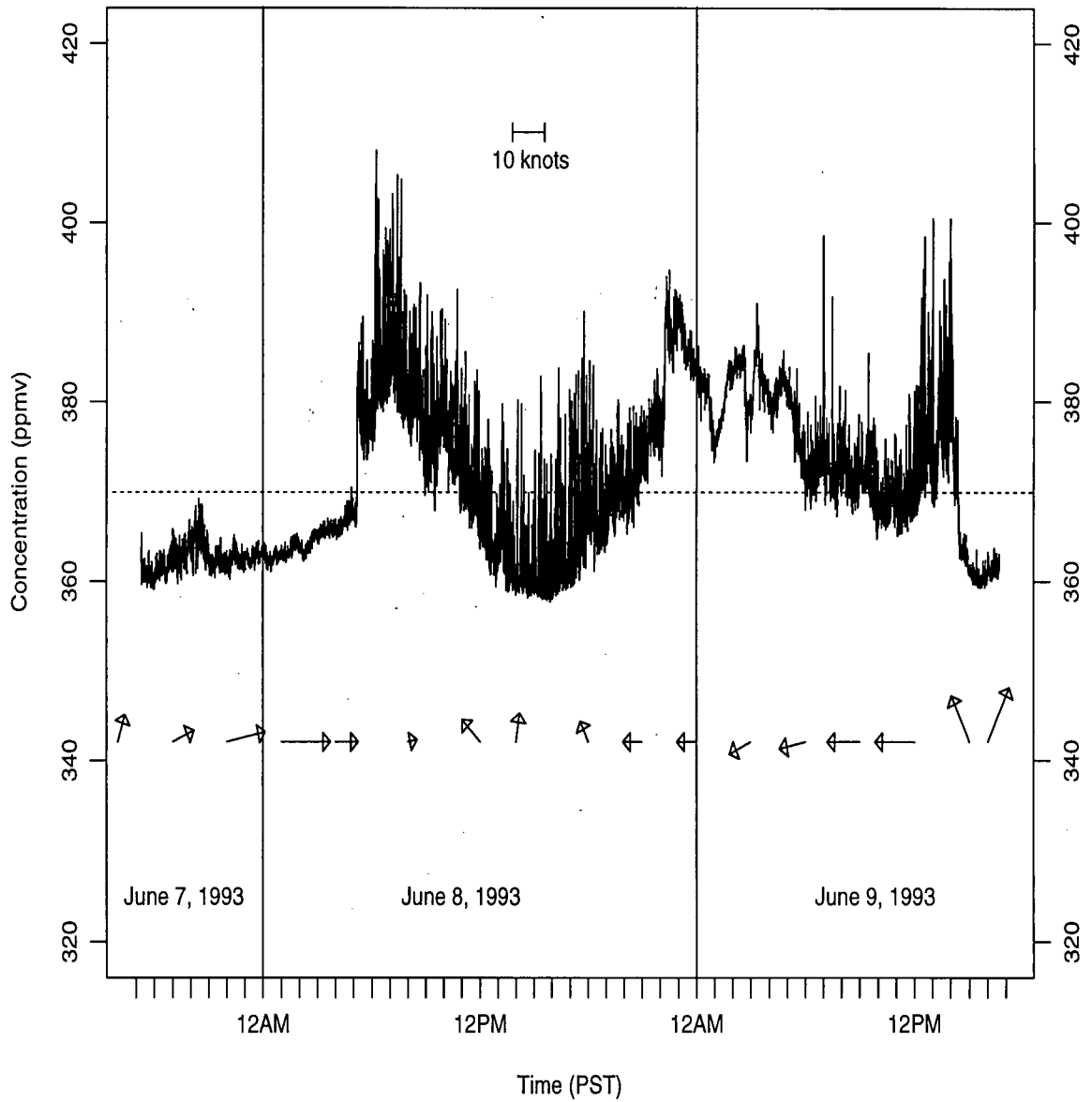
Figure B.4: Atmospheric CO_2 Concentration trace for June 7 - 9, 1993, with continuous sampling every 20 seconds. The background concentration (369.4 ppmv) is shown as a dotted line.
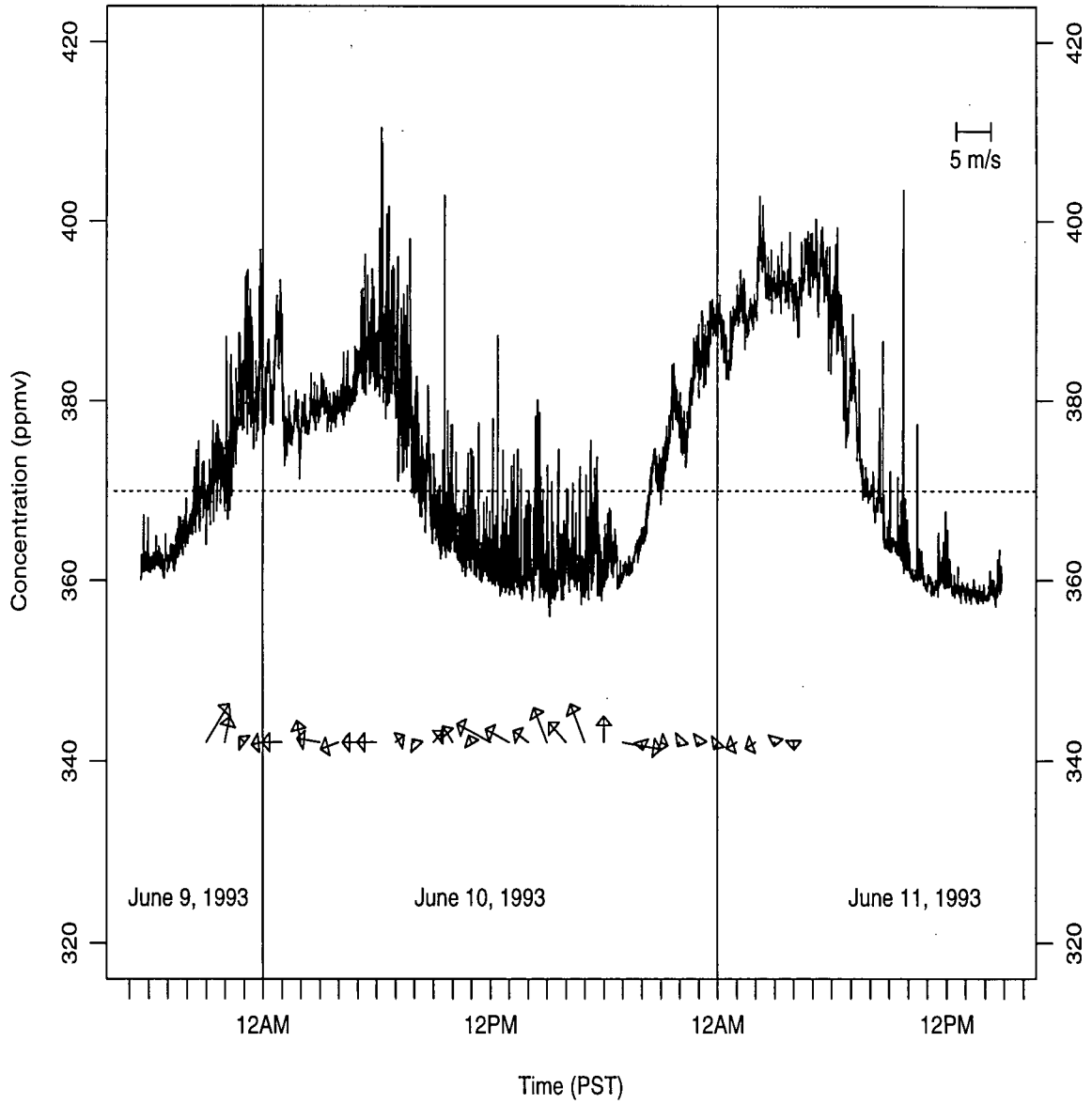
Figure B.5: Atmospheric CO_2 Concentration trace for June 9 - 11, 1993, with continuous sampling every 20 seconds. The background concentration (369.4 ppmv) is shown as a dotted line.
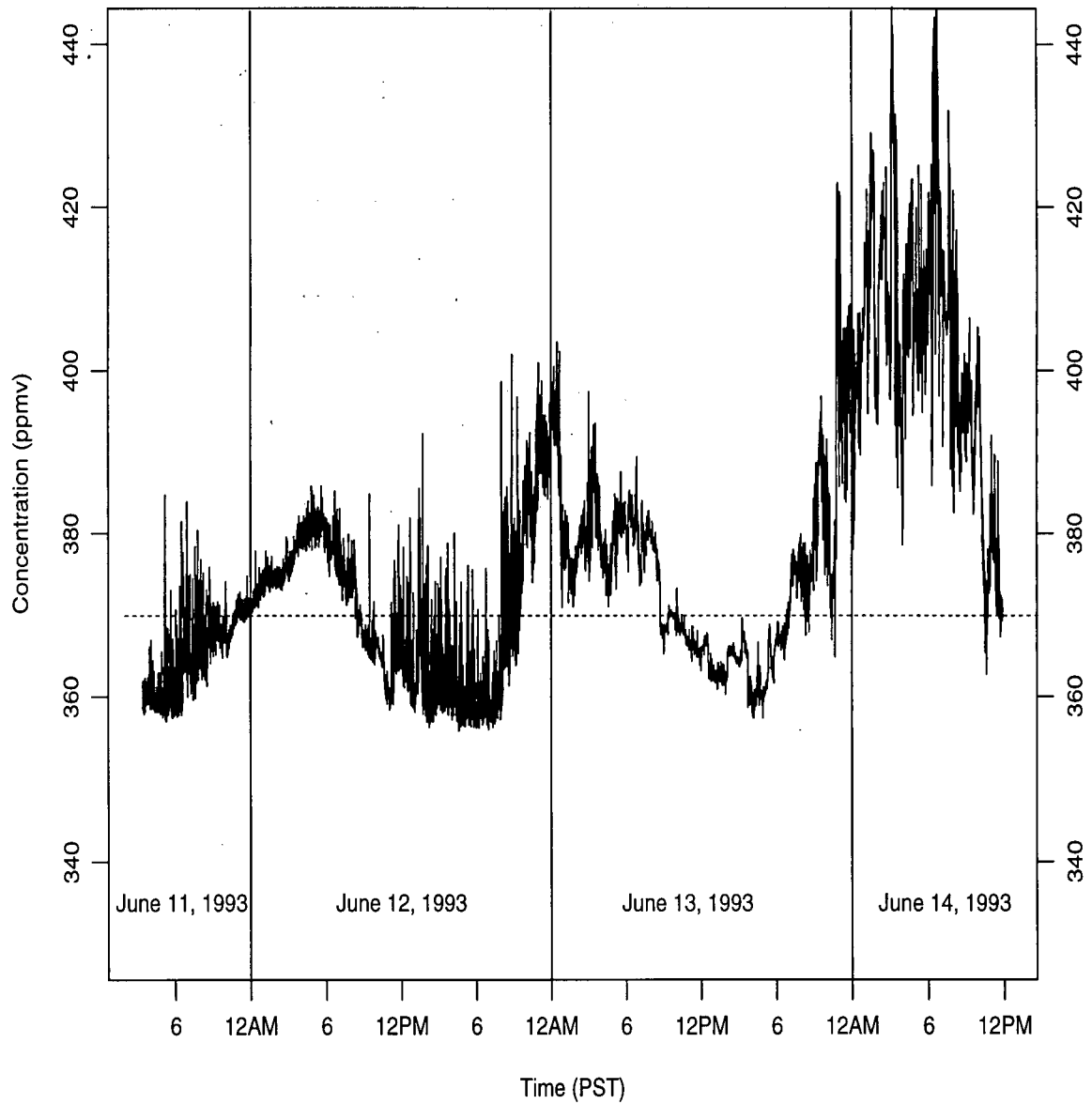
Figure B.6: Atmospheric CO_2 Concentration trace for June 11 - 14, 1993, with continuous sampling every 20 seconds. The background concentration (369.4 ppmv) is shown as a dotted line.
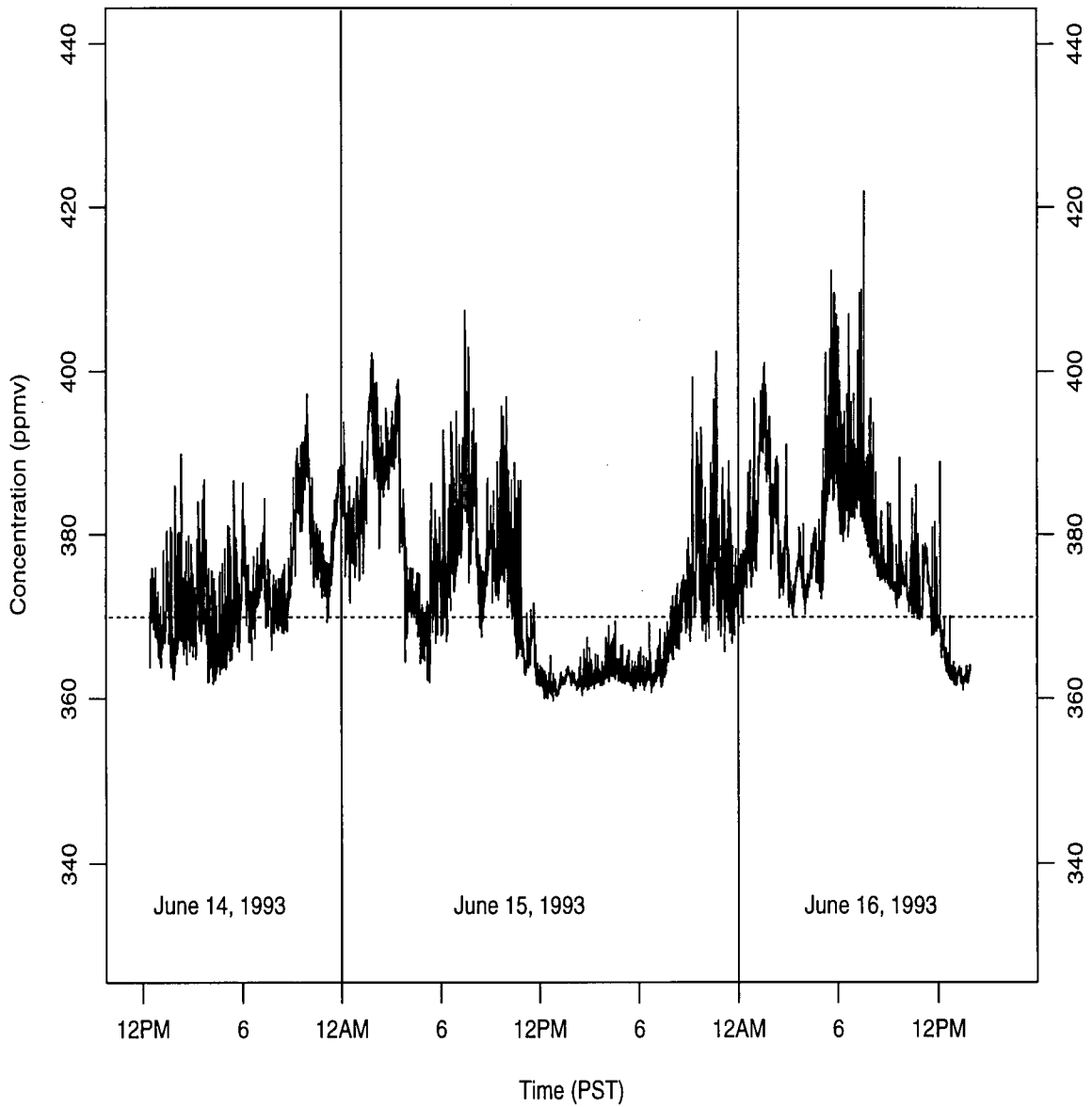
Figure B.7: Atmospheric CO_2 Concentration trace for June 14 - 16, 1993, with continuous sampling every 20 seconds. The background concentration (369.4 ppmv) is shown as a dotted line.
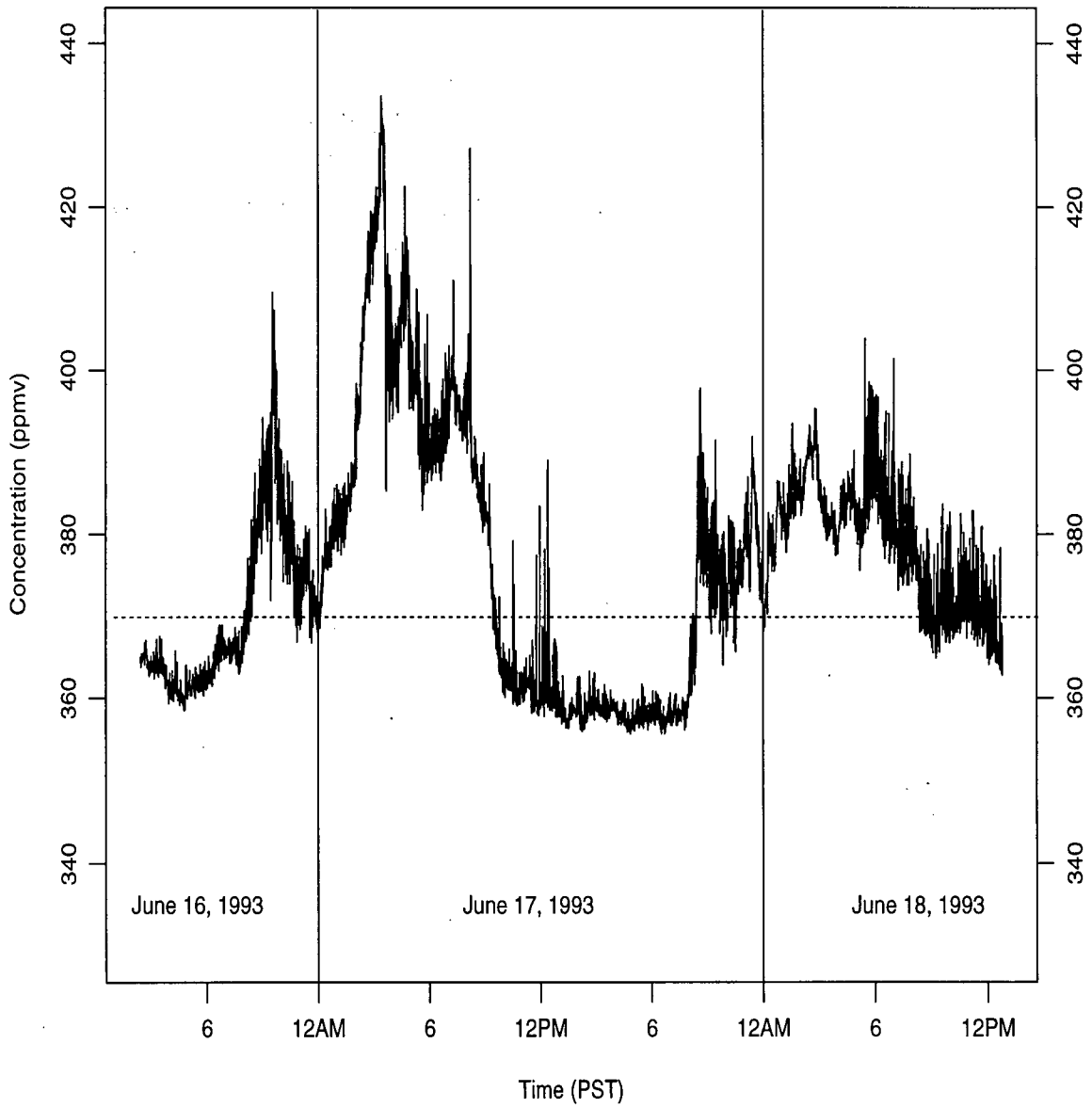
Figure B.8: Atmospheric CO_2 Concentration trace for June 16 - 18, 1993, with continuous sampling every 20 seconds. The background concentration (369.4 ppmv) is shown as a dotted line.
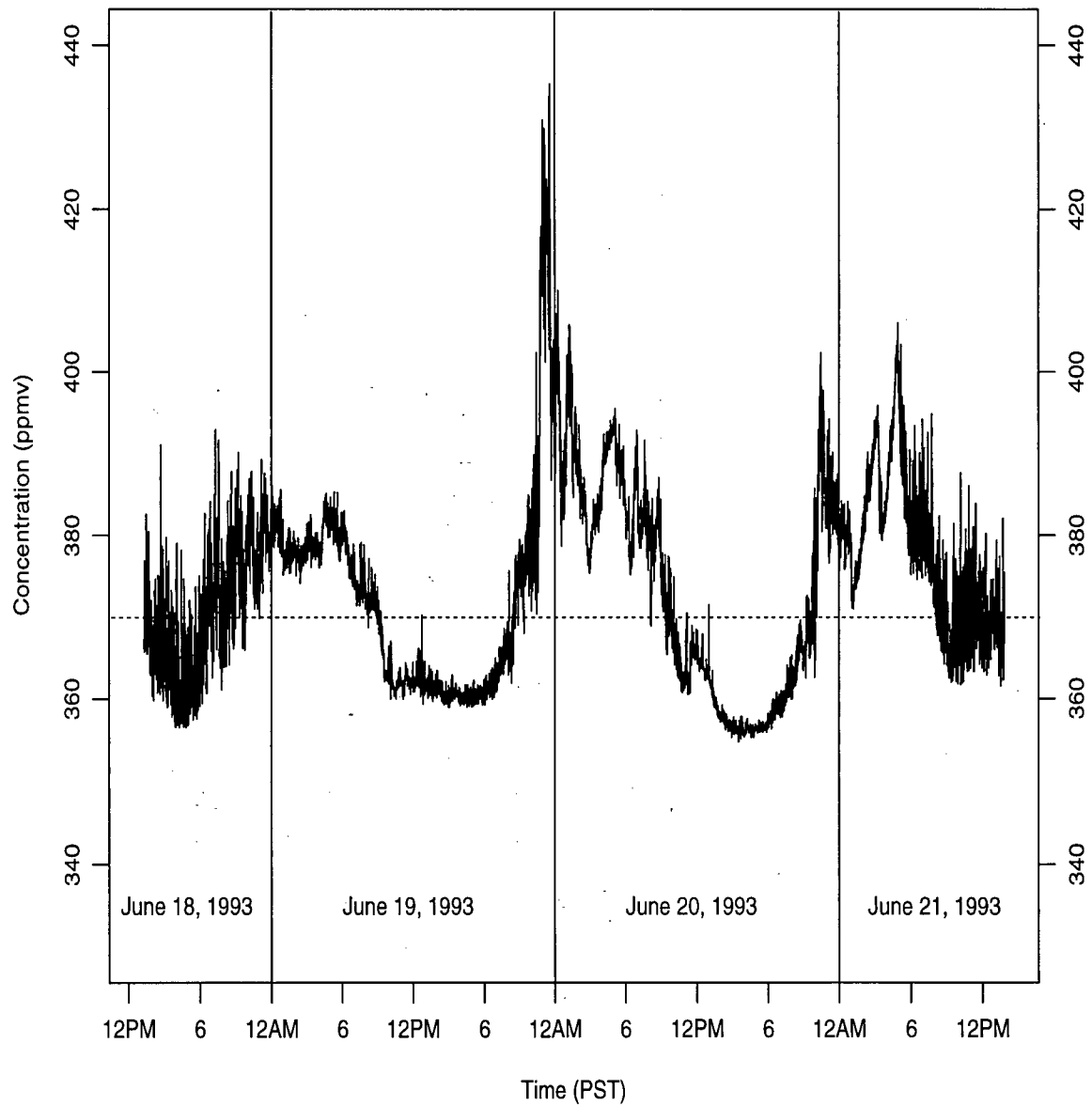
Figure B.9: Atmospheric CO_2 Concentration trace for June 18 - 21, 1993, with continuous sampling every 20 seconds. The background concentration (369.4 ppmv) is shown as a dotted line.
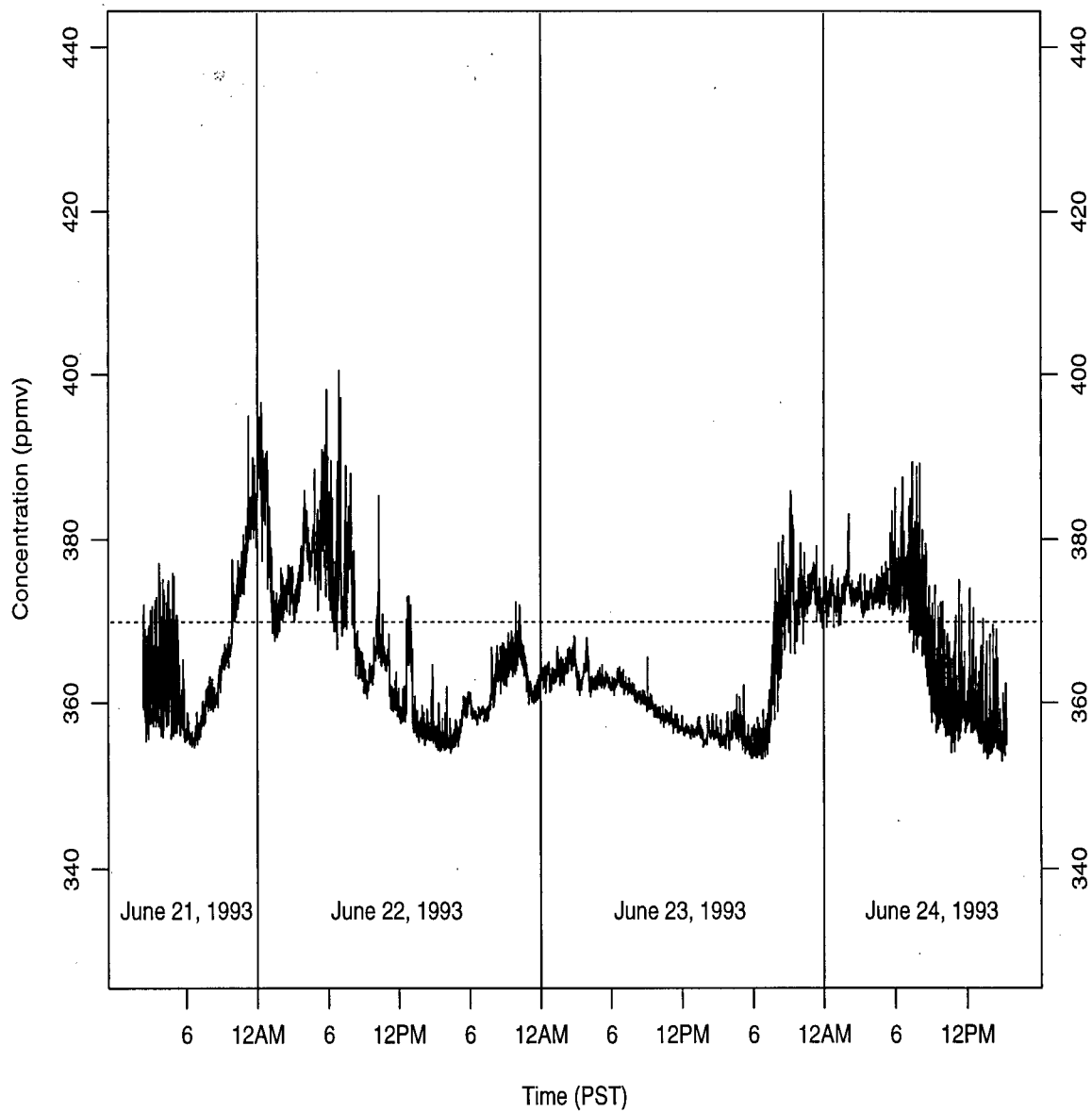
Figure B.10: Atmospheric CO_2 Concentration trace for June 21 - 24, 1993, with continuous sampling every 20 seconds. The background concentration (369.4 ppmv) is shown as a dotted line.

Appendix C

Model Variables and Constants

C.1 June 4, 1993

Table C.1: June 4, 1993: Initial model variables and model constants. Mixed layer depth (h) values are for box 8.

Initial h	Δx	C_h	$C_{background}$	h_{max}	Time (h_{max})
100 m.	1.9 km.	373 ppmv	369 ppmv	720 m.	1400 PST

Table C.2: June 4, 1993: Model variables, determined as hourly averages for box 8.

Time (PST)	h (m)	$\frac{\partial h}{\partial t}$ ($\times 10^{-2}$) (ms^{-1})	$\overline{u}$ (ms^{-1})	Wind Dir. (deg.)	Q_1 (kg km^{-2} s^{-1})	Q_2	Q_3
05-06	136	2.01	0.5	100	2.8	1.1	1.0
06-07	206	1.89	0.5	100	5.6	1.2	1.1
07-08	285	2.52	0.4	130	7.1	1.2	0.3
08-09	374	2.47	0.2	190	5.3	1.2	-2.0
09-10	451	1.80	0.6	250	5.2	1.1	-4.2
10-11	524	2.28	1.8	275	5.3	1.1	-5.3
11-12	589	1.29	3.0	275	5.4	1.0	-6.5
12-13	647	1.90	4.3	280	5.6	0.9	-7.2
13-14	701	1.09	5.5	280	6.1	0.9	-6.6
14-15	712	-0.49	6.3	280	7.5	0.8	-6.1
15-16	689	-0.78	6.0	280	7.9	0.9	-6.0
16-17	641	-1.91	5.0	280	7.9	0.9	-5.7
17-18	565	-2.29	4.0	285	6.2	1.0	-4.2
18-19	487	-2.06	3.8	290	4.7	1.1	-1.8
19-20	371	-4.39	3.0	290	3.6	1.3	-0.3
20-21	217	-2.07	1.3	320	2.5	1.4	-1.0

C.2 June 13, 1993

Table C.3: June 13, 1993: Initial model variables and model constants. Mixed layer depth (h) values are for box 8.

Initial h	Δx	C_h	$C_{background}$	h_{max}	Time (h_{max})
60 m.	1.9 km.	373 ppmv	369 ppmv	557 m.	1312 PST

Table C.4: June 13, 1993: Model variables, determined as hourly averages for box 8.

Time (PST)	h (m)	$\frac{\partial h}{\partial t}$ ($\times 10^{-2}$) (ms^{-1})	$\overline{u}$ (ms^{-1})	Wind Dir. (deg.)	Q_1	Q_2	Q_3 (kg km^{-2} s^{-1})
05-06	94	1.88	0.4	100	2.8	1.1	1.0
06-07	198	3.91	0.5	125	5.6	1.2	1.1
07-08	335	3.96	1.1	195	7.1	1.2	0.3
08-09	452	2.74	1.8	270	5.3	1.2	-2.0
09-10	520	1.05	2.8	265	5.2	1.1	-4.2
10-11	538	-0.04	3.5	250	5.3	1.1	-5.3
11-12	535	-0.11	3.3	270	5.4	1.0	-6.5
12-13	544	0.60	3.0	280	5.6	0.9	-7.2
13-14	540	-0.84	3.3	280	6.1	0.9	-6.6
14-15	493	-1.78	3.3	280	7.5	0.8	-6.1
15-16	436	-1.39	3.3	260	7.9	0.9	-6.0
16-17	396	-0.84	3.3	275	7.9	0.9	-5.7
17-18	355	-1.43	2.3	305	6.2	1.0	-4.2
18-19	325	-0.20	1.8	285	4.7	1.1	-1.8
19-20	246	-4.22	2.3	280	3.6	1.3	-0.3
20-21	173	0.19	2.5	280	2.5	1.4	-1.0

C.3 June 16, 1993

Table C.5: June 16, 1993: Initial model variables and model constants. Mixed layer depth (h) values are for box 8.

Initial h	Δx	C_h	$C_{background}$	h_{max}	Time (h_{max})
100 m.	1.9 km.	373 ppmv	369 ppmv	674 m.	1200 PST

Table C.6: June 16, 1993: Model variables, determined as hourly averages for box 8.

Time (PST)	h (m)	$\frac{\partial h}{\partial t}$ ($\times 10^{-2}$) (ms^{-1})	$\overline{u}$ (ms^{-1})	Wind Dir. (deg.)	Q_1	Q_2	Q_3
					(kg km^{-2} s^{-1})		
05-06	119	1.07	1.5	115	2.8	1.1	1.0
06-07	155	0.94	1.3	120	5.6	1.2	1.1
07-08	210	2.11	1.0	105	7.1	1.2	0.3
08-09	300	2.86	0.9	115	5.3	1.2	-2.0
09-10	416	3.57	0.4	125	5.2	1.1	-4.2
10-11	559	4.37	0.3	95	5.3	1.1	-5.3
11-12	656	1.01	1.8	200	5.4	1.0	-6.5
12-13	626	-2.65	3.8	240	5.6	0.9	-7.2
13-14	559	-1.10	3.5	240	6.1	0.9	-6.6
14-15	528	-0.61	2.8	250	7.5	0.8	-6.1
15-16	500	-0.93	2.5	250	7.9	0.9	-6.0
16-17	467	-0.91	2.3	260	7.9	0.9	-5.7
17-18	439	-0.65	1.8	250	6.2	1.0	-4.2
18-19	418	-0.54	1.3	250	4.7	1.1	-1.8
19-20	253	-8.60	0.6	260	3.6	1.3	-0.3
20-21	78	-1.13	0.3	260	2.5	1.4	-1.0